Computation of Gradually Varied Flow in Channel Networks with Hydraulic Structures

by

Félix Luis Santiago Collazo

A thesis submitted in partial fulfillment of the requirements for the degree of

MASTER OF SCIENCE
in
CIVIL ENGINEERING

UNIVERSITY OF PUERTO RICO
MAYAGÜEZ CAMPUS
2018

Approved by:

_____	_____
Walter F. Silva Araya, Ph. D. President, Graduate Committee	Date
_____	_____
Jorge Gustavo Gutiérrez, Ph. D. Member, Graduate Committee	Date
_____	_____
Jorge Rivera Santos, Ph. D. Member, Graduate Committee	Date
_____	
Eric Harmsen, Ph. D. Representative of Graduate Studies	_____ Date
_____	
Ismael Pagán Trinidad, M.S.C.E Chairperson of the Department	_____ Date

ABSTRACT

Irrigation canals transport water from a source, such as a natural river or a reservoir, to a crop field or a community, making them vital for agriculture. This research develops a computer model to determine the water levels and discharges in complex irrigation channel networks with hydraulic structures to control water distribution. The proposed algorithm, Simultaneous Solution Method (SSM), solves simultaneously the mass and energy equations for gradually varied flow as well as equations to analyze and/or design lateral weirs, sluice gates, and inverted siphons. The scope of this research is limited to subcritical flow conditions. Four case studies are analyzed, from which three are idealized channel systems and one is a real-life channel system located on a segment of the Lajas Valley Irrigation District Channel System (LVIDS). These were analyzed using the SSM. Two of the proposed case studies were also solved using the Standard Step Method (StdSM), which is used on the HEC-RAS software. Two numerical solvers, the Bi-Conjugate Gradient Stabilizer Method (BiCGSTAB) and the Gauss Elimination Method (GEM), were used to find the solution of the nonlinear system of equations. Results based on a percentage error analysis, computed with the Direct Step Method, showed that the SSM had a less significant degree of error when compared to the StdSM. In addition, the BiCGSTAB solved the numerical system faster than the GEM and converged successfully in all the case studies proposed. The SSM proved to be excellent for determining water depths, flow velocity, and diverted lateral flow through weirs and sluice gates, and proved to be comparatively easier to execute than the other available models.

Keywords: gradually-varied flow; lateral weir; sluice gate; inverted siphon; simultaneous solution; irrigation channel network; analysis; design.

RESUMEN

Los canales de irrigación transportan agua desde la fuente, ya sea un río o una reserva, hasta una comunidad o un campo de cosecha, haciéndolos vitales para la agricultura. Esta investigación desarrolla un modelo computacional para determinar los niveles de agua y las descargas en una red compleja de canales con estructuras hidráulicas utilizadas para controlar la distribución de agua. El algoritmo propuesto, "Simultaneous Solution Method" (SSM, por sus siglas en inglés), resuelve la ecuación de energía y de masa simultáneamente para el flujo gradualmente variado, en adición a las ecuaciones requeridas para el análisis y/o diseño de vertedores laterales, compuertas y sifones invertidos. El alcance de esta investigación se limitó para condiciones de flujo subcrítico. Se evaluaron cuatro estudios de caso para la investigación utilizando el SSM; tres de estos casos son sistemas de canales idealizados y uno de ellos es un sistema real obtenido del Distrito de Riego del Valle de Lajas en Puerto Rico. Dos de los casos propuestos fueron también evaluados utilizando el "Standard Step Method" (StdSM, por sus siglas en inglés), el cual es utilizado en el programa comercial HEC-RAS. Se utilizaron dos métodos numéricos para resolver el sistema no-lineal de ecuaciones, el "Bi-Conjugate Gradient Stabilizer Method" (BiCGSTAB, por sus siglas en inglés) y el "Gauss Elimination Method" (GEM, por sus siglas en inglés). Los resultados de un análisis de porcentaje de error basado en el "Direct Step Method" demuestran que el SSM obtuvo menor porcentaje de error que el StdSM. También el BiCGSTAB solucionó el sistema más rápido que el GEM y convergió exitosamente en todos los casos propuestos. El SSM demostró que es excelente para determinar niveles de

agua, descargas y flujos divergidos por vertedores y compuertas. Además, este es más fácil de utilizar que otros modelos disponibles.

Palabras claves: flujo gradualmente variado; vertedores laterales; compuertas; sifones invertidos; solución simultánea; análisis; diseño.

Dedicated to:

God above all things.

My lovely wife, Taryan Santana, for being at my side every moment and for supporting all my decisions.

My parents, Felix and Lissette, for all the unconditional support provided.

My mentor, Dr. Walter Silva, for believing in me and for all the support, guidance and teaching provided in my studies.

Dedicado a:

Dios sobre todas las cosas.

Mi amada esposa, Taryan Santana, por estar a mi lado en cada momento y apoyarme en todas mis decisiones.

Mis padres, Felix y Lissette, por todo su apoyo incondicional provisto.

Mi mentor, Dr. Walter Silva, por creer en mí y por todo el apoyo, enseñanza, y guiarme en mis estudios.

ACKNOWLEDGMENTS

The author thanks every member of his graduate committee for all the help and support provided through the entire research. Especially, Dr. Walter F. Silva for his patience, support, and guidance since the beginning of this research. Also, thanks for the different opportunities given to be part of various research projects at the Puerto Rico Water Resources and Environmental Research Institute. These opportunities motivated the author to continue graduate studies and pursue a doctoral degree.

Thanks to Dr. Jorge Gustavo-Gutiérrez and Mr. Michael Chavez for their support and advice on numerical solution techniques. Support from the Puerto Rico Water Resources and Environmental Research Institute is appreciated. Thanks to Mr. Jaime Ramírez, Geotechnical and Soil Laboratory technician from the Civil Engineering and Surveying Department at the UPRM, for access to the equipment required to perform the granulometric analysis.

Special thanks to Mr. Benjamín Negrón, PE and Ms. Karla Santiago, EIT, from the Lajas Valley Irrigation District at the Puerto Rico Electric Power Authority, for access to the Lajas Valley Irrigation District and for providing all the required construction plans about the system. Thanks to Mr. Victor Vargas, Mr. Jesús Otero and Mr. Francisco Rodríguez for the help provided during the field trip visit to the Lajas Valley Irrigation District.

TABLE OF CONTENTS

LIST OF TABLES

LIST OF FIGURES

NOTATION LIST

a	sluice gate opening
A	flow area
$[A]$	Jacobian matrix
b	sluice gate length
B	bottom width of the channel
C	Strickler coefficient for computing Manning's channel roughness
C_{bend}	head loss coefficient for siphon bends
C_{elbows}	head loss coefficient for siphon elbows
C_{in}	head loss coefficient for siphon inlets
C_{out}	head loss coefficient for siphon outlets
C'_d	sluice gate discharge coefficient
C_d	discharge coefficient for lateral weirs
C_e	effective discharge coefficient for lateral weirs
C_f	unit system coefficient for the friction slope of siphon equation
C_o	unit system coefficient of Manning's equation
C_s	unit system coefficient for initial diameter of siphon equation
d_0	initial siphon diameter
D_x	particle diameter in which the x% of the soil is passing through
D_{up}	hydraulic depth for the channel section upstream of the weir
E_L	percent of error for the reach length of each channel
Fr	Froude number
$\{F\}$	vector of energy and continuity equation
g	acceleration due to gravity
h_f	energy loss due to boundary friction in the reach
h_{seal}	hydraulic seal at the siphon
H	head above the lateral weir
i	subscript that refers to the number of the channel
j	subscript that refers to the section number of the channel i
jn_1	upstream junction of the loop channel system
jn_2	downstream junction of the loop channel system
k	subscript that refers to the equation number on the matrix system
k_b	contraction/expansion coefficient
k_s	effective surface roughness height
K	conveyance factor for the Manning's equation
L	distance between the two sections or between one reach
L_w	length of the lateral weir
m	lateral slope (m horizontal to 1 vertical)
n	Manning's roughness coefficient
n_e	equivalent Manning's channel roughness,
N	number of reaches for each channel

P	wetted perimeter of a channel cross-section
P_w	height of the lateral weir crest
Q	rate of discharge
Q_s	sluice gate discharge
Q_u	specified discharge at the upstream end channel *i*
Q_w	flow through the lateral weir
R	hydraulic radius
s_k	Strickler coefficient
S	friction slope
S_0	channel bottom slope
$\overline{S_f}$	average of the friction slope between two sections
T	top width of flow area
V	flow velocity in the channel or in the siphon
V_{ave}	average flow velocity at the upstream section of the weir
x	horizontal distance
y	water depth
y_0	upstream water depth of the sluice gate
y_2	tailwater depth of the sluice gate
y_u	Specified flow depth at the upstream end channel *i*
Y_w	average flow depth between the upstream and downstream section of the lateral weir
z	elevation of the channel bottom above a specified datum
α	velocity-head coefficient
ϰ	head-loss coefficient
$\{\Delta\}$	vector of water depth and discharge corrections
Δh	difference in water surface elevation at the two sections
Δh_v	difference in velocity head at the two sections
Δx	computed distance between two successive water depths for a specific discharge
$\emptyset$	dimensional coefficient for the Direct Step Method equation

LIST OF ACRONYMS

AOI	Area of Interest
BiCG	Bi-Conjugate Gradient algorithm
BiCGSTAB	Bi-Conjugate Gradient Stabilizer Method
CGS	Conjugate Gradient Squared method
cfs	cubic feet per second
cms	cubic meters per second
DSM	Direct Step Method
ft	feet
GEM	Gauss Elimination Method
GVF	Gradually-varied flow
GUI	Graphical user interface
in	inches
iLU	incomplete LU factorization
km^2	squared kilometers
LVIDS	Lajas Valley Irrigation District System
LW	Lateral Weir
m	meters
mi^2	squared miles
mm	millimeters
NRSM	Newton-Raphson Solution method
NaN	Not a Number
SSM	Simultaneous Solution Method
SAM	Slope Area Method
StdSM	Standard Step Method
PR	Puerto Rico
PRDNR	Puerto Rico Department of Natural Resources
PREPA	Puerto Rico Electric Power Authority
SI	International System (Metric System)
s	seconds
UPRM	University of Puerto Rico at Mayagüez
USACE	U.S. Army Corps of Engineers
USBR	U. S. Bureau of Reclamation
USGS	U.S. Geological Survey
UTD	Utah Department of Transportation
WSE	water surface elevation

1 CHAPTER – INTRODUCTION

The first major irrigation system was built during Egypt's First Dynasty, close to 3100 B.C. as a diversion of flood waters of the Nile River (Irrigation Museum 2015). Irrigation canals transport water from a source, such as a natural river or a reservoir, to a crop field or a community. Irrigation canals are vital for agriculture. One-sixth of irrigated cropland produces one-third of the world's harvest of food crops (Michael 2008). Food production is a global concern in a world of growing population and limited resources. Sustainability of food production depends on sound and efficient water use and conservation practices consisting mainly of irrigation development and management (United Nations Sustainable Development 1992). It is of utmost importance for farmers to control the water distribution in irrigation systems. Hydraulic structures such as weirs and gates must be set at specific levels to distribute the correct amount of water for crop production and water conservation.

This research developed a computer model to determine the water levels and discharges in complex irrigation channel networks with hydraulic structures to control water distribution. The solution algorithm solves the continuity and energy equations for gradually varied flow as well as equations to analyze and/or design lateral weirs, sluice gates and/or inverted siphons. After conducting a thorough literature review on the subject, the analysis and/or design of hydraulic structures for irrigation systems as part of a simultaneous solution has not been proposed before. The scope of this research was to model complex channel networks, as well as series and loop channel systems. The flow conditions are limited to subcritical flow on the entire system.

Analysis and/or design of hydraulic structures in irrigation system, such as lateral weirs, inverted siphon and/or sluice gate were included. The computer design tool has the capacity of modeling any channel configuration, including series, parallel and complex network channel systems and solving for flow and water levels simultaneously. As part of the objectives of this research, a graphical user interface (GUI) was developed to allow a user-friendly interaction with the numerical model. Finally, the numerical model was tested on the Lajas Valley Irrigation District System as a case study, in addition to different idealized channel systems that were also used as case studies.

Hydraulic structures are commonly found in real-life irrigation channel scenarios. An example of a hydraulic engineering application is the Lajas Valley Irrigation District System (LVIDS), located on the southwest of Puerto Rico (PR). According to PR Department of Natural Resources (2008), this system impacts approximately 100,000 people in its high season of tourism and vacation periods (more details of this system will be given in Chapter 5). Irrigation districts are vital for sustainability in Puerto Rico and other countries.

Even though most irrigation channel systems are artificial, parallel systems frequently occur in nature; for example, flow around an island (Chaudhry 2008). On the other hand, channel networks are less frequent in nature than parallel systems and tend to occur in braided river systems, such as in deltas. According to Chaudhry (2008), a frequent design problem is to provide cutoff channels in a meandering stream for flood control, in which the allowable flow rate and water levels in the original stream dictate the design of the new channel. By using the proposed algorithm, different designs may be modeled efficiently. In addition, the proposed algorithm may be used to determine the roughness properties of the channel, if the water depth is

known, for a specific discharge. The literature review realized for this research is presented on Chapter 2. Followed by the methodology of this research, which is presented in the Chapters 3 to 6. The examples and case study selected are presented in Chapter 7. The results, analysis and discussion are presented in Chapter 8 and the conclusion are presented in Chapter 9.

2 CHAPTER- LITERATURE REVIEW

Gradually varied flow (GVF) has been studied and researched since the 19th century. Chaudhry and Schulte (1986) were the first pioneers to develop an algorithm for parallel channels during the 1980's. Their algorithm solves for water depths and discharges at different sections for steady-state and GVF conditions based on two fundamental equations, the energy equation and the continuity equation, forming a system of non-linear equations. The nonlinear system of equations is solved simultaneously using the Newton-Raphson method. To increase accuracy and reduce computer time and storage, they transformed the resulting Jacobian matrix into a banded matrix for series and parallel channels. Similarly, Chaudhry and Schulte (1987) extended their algorithm to solve GVF conditions in a channel network, however, the matrix became sparse and more difficult to solve. This channel network algorithm is based on the same methodology as the parallel-channel algorithm; but can solve for multiple channel configurations, such as series, parallel and channel networks. The two models were applied to an idealized channel network. Results were compared with those obtained by the fourth-order Runge-Kutta method for each channel, providing excellent results.

Naidu et al. (1997) presented an algorithm for GVF computations in tree-type channel networks. This algorithm computes the water surface profile under the same flow conditions as Chaudhry and Schulte. The solving technique for this algorithm decomposes the channel network into smaller units that are solved using the fourth-order Runge-Kutta method, and connects all the solutions using the Shooting Method. This technique does not involve solving a large matrix system simultaneously and is computationally more efficient than the simultaneous

solution procedure by an order of magnitude. However, it cannot be applied to looped networks. The model was applied to an idealized tree-type channel network (as Chaudhry and Schulte's study).

Reddy and Bhallamudi (2004) developed an algorithm to compute water surface profiles in channel networks. Their algorithm is based on three principles: classify the computations in an individual channel as an initial value problem or a boundary value problem, determine the path for linking the solution from individual channels, and obtain a network solution through the Newton-Raphson iterative technique. Therefore, it does not have to solve large matrix systems. However, one of their main assumptions is that there are no hydraulic structures within the system. The model was tested with the idealized channel network presented in Chaudhry and Schulte (1987) and Naidu et al. (1997). The efficiency of their algorithm compared with the efficiency of Naidu et al.'s (1997) technique and is computationally more efficient than Sen and Garg's (2002) method as discussed herein.

The studies discussed in this literature review have the following common characteristics: (1) assume that flow conditions are steady-state, subcritical, gradually-varied flow; (2) do not consider any hydraulic structure within the channel system; and (3) were only tested on idealized channel networks (Chaudhry and Schulte 1986; Chaudhry and Schulte 1987; Naidu et al. 1997; Reddy and Bhallamudi 2004).

Sen and Garg (2002) developed a model for steady and unsteady flow in channel networks using the St. Venant equations. Their algorithm uses the finite difference method to solve the system of equations for all branches of the network simultaneously. In addition, their model was

applied to two idealized channel networks, one looped network, and one branched network. Similarly, Islam et al. (2005) conducted a comparison of two-channel network algorithms. The two algorithms had different techniques for separating end-node variables for each branch, which are the forward-elimination and branch-segment transformation equations. Both algorithms model steady and unsteady flows in branched and looped channel networks, in which the St. Venant equations were discretized. Extending his previous effort (Islam et al. 2005), Islam et al. (2008) developed a hydraulic simulation model for irrigation channel networks. The model uses the same discretization technique for the St. Venant equations, as his previous work (Islam et al. 2005), but solves the nonlinear matrix system using sparse matrix solution techniques.

Zhu et al. (2011) developed an algorithm for unsteady, subcritical flow channel networks. This algorithm simulates the gradually-varied flow conditions using the St. Venant equations for one-dimension, and solves the system using the same techniques as Islam et al.'s (2008) first algorithm. The algorithm treats backwater effects at the junction points based on junction-point water stage prediction and correction method. This method does not require any specific node-numbering strategy or the need to form and solve the global branch equation. The model was applied to two hypothetical channel networks (Islam et al. 2005; Sen and Garg 2002) and a river network in South China. Their results compared well with those from literature (Islam et al. 2005; Sen and Garg 2002) and measurements from the real-life case study in China.

At the time of this research, Islam et al. (2008) presents the only algorithm that includes analysis of different hydraulic structures, such as weirs, sluice gates, drops/falls, pipe outlet, and imposed discharge. Also, it is the only algorithm to include a user-friendly graphical user interface for entering and editing channel network description and boundary conditions. Even

though Islam et al. affirm that their algorithm can solve complex channel networks, the results presented are only for four channels connected in series from the Kangsabati irrigation project at West Bengal, India. Their results were similar to the ones computed with the HEC-RAS model, as well as a satisfactory for most of the irrigation event at the irrigation project. This case does not represent a challenging example for other solution procedures.

3 CHAPTER- METHODOLOGY

This section consists of describing the proposed methodology for the research. First, the governing equations for gradually varied flow in open channels are presented with their assumptions. Second, the Simultaneous Solution Method (SSM), proposed by this research, is explained for a system of equations of a channel network with the required boundary conditions. Third, the Direct Step Method (DSM) is explained for a simple channel in series. The DSM was used for comparing the results of water depth and discharge from the SSM and StdSM methods. Finally, the Standard Step Method (StdSM) is presented for a simple case of a channel in series. The HEC-RAS software, from the U.S. Army Corps of Engineers (USACE), was used for solving the water depths and discharges using the StdSM (Brunner 2016).

3.1 Governing Equations

Gradually varied flow (GVF) occurs when the rate of variation of depth with respect to distance is small. The analysis of GVF is usually done for long channels; therefore, friction losses must be considered. The following assumptions are incorporated in the GVF model described here. They are commonly studied in GVF theory (Chaudhry 2008):

1. The slope of the channel bottom is small; therefore, the flow depth measured vertically or normal to the bottom are approximately the same.
2. The channel could have lateral outflows through lateral weirs or other structures.
3. The pressure distribution is hydrostatic at all channel sections. The streamlines are straight and parallel.

4. The head loss is determined by using Manning's equation.

Similar to a pipe network, channel networks require specialized solution techniques that are not available in many commonly used hydraulic solvers. Incorporation of hydraulic structures in channel networks represents additional complexities both for analysis and design.

The design or analysis of channel networks with hydraulic structures is accurately done by the simultaneous solution procedure. However, it requires the simultaneous solution of a large number of non-linear equations plus verification of channel regimes. Additional equations are required to describe the flow across hydraulic structures. The governing equations are the energy equation between two consecutive sections of the same channel and the continuity equation between two consecutive channels or junctions. Equation 3.1 and Equation 3.2 are the discretized energy and continuity equations, respectively, between two channel's cross-sections. The notation is presented in Figure 3.1.

$$F_{i,k} = z_{i,j+1} - z_{i,j} + y_{i,j+1} - y_{i,j} + \alpha_i \frac{Q_{i,j+1}|Q_{i,j+1}|}{2gA_{i,j+1}{}^2} - \alpha_i \frac{Q_{i,j}|Q_{i,j}|}{2gA_{i,j}{}^2} + \frac{1}{2}(x_{i,j+1} - x_{i,j})\left(\frac{Q_{i,j+1}|Q_{i,j+1}|n_i{}^2}{C_o{}^2 A_{i,j+1}{}^2 R_{i,j+1}{}^{1.33}} + \frac{Q_{i,j}|Q_{i,j}|n_i{}^2}{C_o{}^2 A_{i,j}{}^2 R_{i,j}{}^{1.33}}\right) = 0 \quad (3.1)$$

$$F_{i,k+1} = Q_{i,j+1} - Q_{i,j} = 0 \quad (3.2)$$

where:

Q = rate of discharge (L^3/t),

z = elevation of the channel bottom above a specified datum (L),

y = water depth (L),

α = velocity-head coefficient (dimensionless),

g = acceleration due to gravity (L/t^2),

x = horizontal distance (L),

A = flow area (L^2),

n = Manning's roughness coefficient (dimensionless),

R = hydraulic radius (L),

C_o = unit system coefficient of Manning's equation, where for SI units equals 1.0 and for English units is 1.486 (Dimensionless),

i = subscript that refers to the number of the channel,

j = subscript that refers to the section number of the channel *i*, and

k = subscript that refers to the equation number on the matrix system.

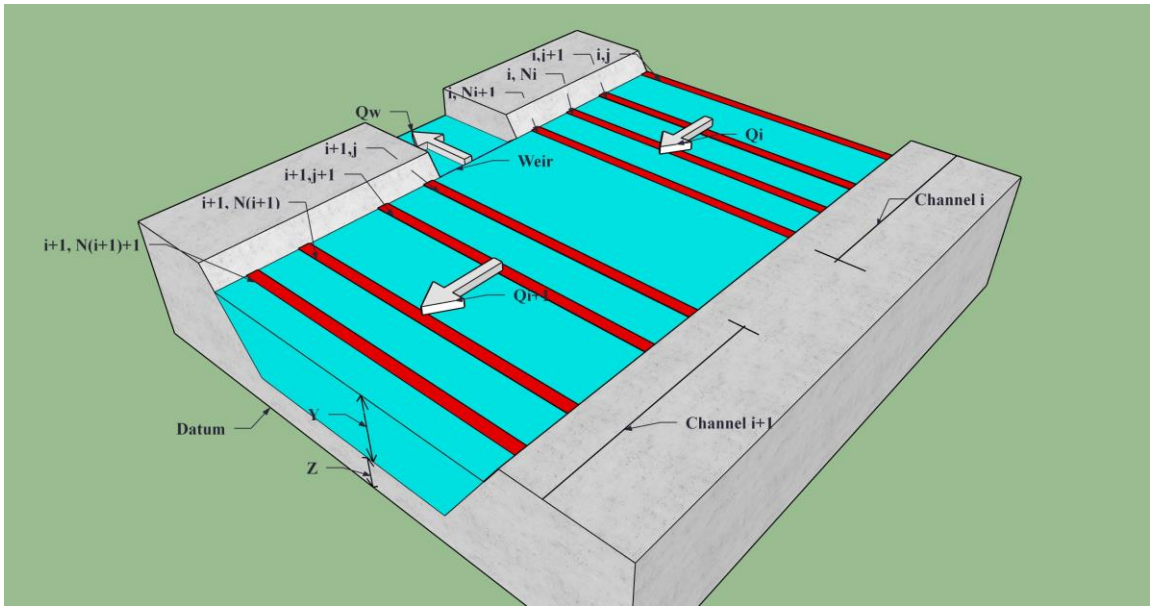

Figure 3.1. Definition sketches for the governing equations. The red bars represent a channel cross-section. The number of reaches that each channel has is represented with the variable N.

The last term on the right side of Equation 3.1 approximates the head loss, which may be computed by the average of the friction slopes. To account for reverse flow, the discharge term on the energy equation must be expressed as $Q_{i,j}|Q_{i,j}|$ instead of ${Q_{i,j}}^2$.

The energy equation (Equation 3.1), the continuity equation (Equation 3.2), and the equations for hydraulic structures within the irrigation system were solved simultaneously for each cross-section. The system is formed by a large number of non-linear equations solved by the Newton-Raphson procedure (Burden and Faires 2005). The new simultaneous solution method (SSM) computes GVF in complex channel systems with the capability for lateral weir design and analysis. The model efficiently solves large systems of equations using the Bi-conjugate Gradient Stabilizer method (BiCGSTAB) (Saad 2004). This solver is suitable for non-symmetric positive definite systems with large, sparse matrices. To better understand the concept, the SSM will be explained for a simple looped channels system on the following section.

3.2 Simultaneous Solution Method

A major difference between the algorithm for series and for looped channel networks is that, in looped networks, the discharge in each individual channel is unknown. In a generalized channel network model, the continuity equation (Equation 3.2) for each reach must be included to obtain the necessary number of equations to solve the system. A reach is the segment between two successive channel sections. A channel could have several reaches between two junctions. The SSM for GVF in any channel network, such as the one shown in Figure 3.2, can be mathematically represented as a matrix system given by Equation 3.3.

$$[A]\{\Delta\} = \{F\} \qquad 3.3$$

where:

$[A]$ = Jacobian matrix,

$\{\Delta\}$ = vector of water depth and discharge corrections, and

$\{F\}$ = vector of energy and continuity equation.

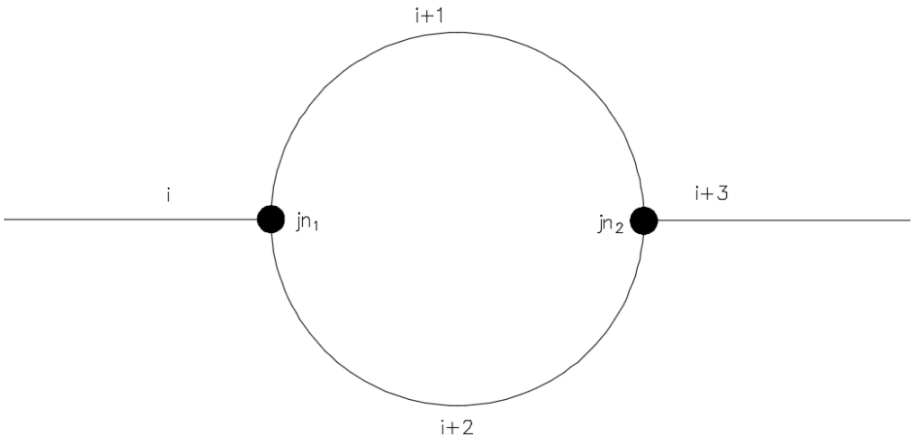

Figure 3.2. Representation of a looped channel network.

To produce a Jacobian matrix that has a minimum bandwidth, the energy and continuity equations were assembled following the recommendations from Chaudhry and Schulte (1986) for looped channel networks, which is explained in the next two paragraphs. For the channels that are before and after the looped channels, considered as channels in series, (channel *i* and *i+3* in Figure 3.2), the energy equation (Equation 3.1) is written first for each reach, followed by the continuity equation (Equation 3.2) for the same reach. This is then repeated for all the reaches (N_i) of channel *i* or *i+3* in a consecutive manner. For the looped channels, considered as channels

in parallel, (channel *i+1* and *i+2* on Figure 3.2), the energy equation for the first reach of channel *i+1* is written, followed by the continuity equation for the same reach of channel *i+1*. Then, the energy equation for the first reach of channel *i+2* is written, followed by the continuity equation for the same reach of channel *i+2*. This process is repeated in the same manner for all the reaches on both channels. It is crucial that the channels in parallel have the same number of reaches.

The Jacobian matrix $[A]$ consists of the partial derivatives of the energy and continuity equations with respect to water depth and discharge. The assembly of this matrix follows the same pattern as the vector of energy and the continuity equation $\{F\}$. First, the partial derivative of the energy equation with respect to water depth is written for section *j* of channel *i*. The second term in the same row will be the derivative of the energy equation with respect to discharge for the section *j* of the same channel *i*. Next, on the same row, the partial derivative of the energy equation with respect to water depth is written for section *j+1* of channel *i*. The last term of this row will be the partial derivative of the energy equation with respect to the discharge for section *j+1* of the same channel *i*. The following row of the Jacobian matrix will consist of the partial derivatives of the continuity equation with respect to discharge, since the partial derivative with respect of the water depth is zero. These partial derivatives are shown in Equation 3.4 and Equation 3.5 for the energy and continuity equation, respectively. The vector of flow depth and discharge corrections $\{\Delta\}$ provides the corrections of the flow depth and discharge for all the sections of all channels. This vector of solutions will be updated at each iteration until the corrections are smaller than a certain tolerance.

$$\frac{\partial F_{i,k}}{\partial y_{i,j}} = -1 + Q_{i,j}|Q_{i,j}|\left(\frac{\alpha_i T_{i,j}}{g{A_{i,j}}^3} - \frac{2{n_i}^2\left(x_{i,j+1} - x_{i,j}\right)}{3{C_o}^2{A_{i,j}}^2{R_{i,j}}^{2.33}} \times \frac{dR_{i,j}}{dy_{i,j}} - \frac{{n_i}^2 T_{i,j}\left(x_{i,j+1} - x_{i,j}\right)}{3{C_o}^2{A_{i,j}}^3{R_{i,j}}^{1.33}}\right)$$

$$\frac{\partial F_{i,k}}{\partial Q_{i,j}} = 2Q_{i,j}\left(-\frac{\alpha_i}{2g{A_{i,j}}^2} + \frac{{n_i}^2\left(x_{i,j+1} - x_{i,j}\right)}{2{C_o}^2{A_{i,j}}^2{R_{i,j}}^{1.33}}\right)$$

$$\frac{\partial F_{i,k}}{\partial y_{i,j+1}} = 1 - Q_{i,j+1}|Q_{i,j+1}|\left(\frac{\alpha_i T_{i,j+1}}{g{A_{i,j+1}}^3} - \frac{2{n_i}^2\left(x_{i,j+1} - x_{i,j}\right)}{3{C_o}^2{A_{i,j+1}}^2{R_{i,j+1}}^{2.33}} \times \frac{dR_{i,j+1}}{dy_{i,j+1}} - \frac{{n_i}^2 T_{i,j+1}\left(x_{i,j+1} - x_{i,j}\right)}{3{C_o}^2{A_{i,j+1}}^3{R_{i,j+1}}^{1.33}}\right)$$

$$\frac{\partial F_{i,k}}{\partial Q_{i,j+1}} = 2Q_{i,j+1}\left(-\frac{\alpha_i}{2g{A_{i,j+1}}^2} + \frac{{n_i}^2\left(x_{i,j+1} - x_{i,j}\right)}{2{C_o}^2{A_{i,j}}^2{R_{i,j}}^{1.33}}\right) \quad 3.4$$

$$\frac{\partial F_{i,k+1}}{\partial Q_{i,j}} = -1$$

$$\frac{\partial F_{i,k+1}}{\partial Q_{i,j+1}} = 1 \quad 3.5$$

where:

T = top width of flow area (L).

The energy and continuity equations for all the N_i reaches of the four channels of the looped network, give a total of $2(N_i + N_{i+1} + N_{i+2} + N_{i+3})$ equations (Chaudhry and Schulte 1987). Since the flow depth and discharge are unknowns at each reach, a total of $2(N_i + N_{i+1} + N_{i+2} + N_{i+3} + 4)$ unknowns must be solved. Therefore, for obtaining a unique solution for the system, eight additional equations are needed, which can be obtained by the boundary and end conditions. The upstream or the downstream end condition provides two equations, one for flow depth and

another for discharge. For this procedure, the upstream end condition will be selected (Equation 3.6).

$$F_{i,1} = y_{i,1} - y_u = 0$$

$$F_{i,2} = Q_{i,1} - Q_u = 0 \qquad 3.6$$

where:

y_u = specified water depth at the upstream end channel *i* (L), and

Q_u = specified discharge at the upstream end channel *i* (L).

The remaining six equations are provided by boundary conditions at both junctions of the looped network. The upstream junction (jn_1) provides three equations, one from the continuity equation and two from the energy equations (Equation 3.7). See Figure 3.3a for more details. In a similar manner, the downstream junction (jn_2) provides the last three equations needed (Equation 3.8), as shown in Figure 3.3b.

$$F_{jn_1,1} = Q_{i,N_i+1} - Q_{i+1,1} - Q_{i+2,1} = 0$$

$$F_{jn_1,2} = z_{i,N_i+1} - z_{i+1,1} + y_{i,N_i+1} - y_{i+1,1} + \frac{Q_{i,N_i+1}\left|Q_{i,N_i+1}\right|}{2gA_{i,N_i+1}{}^2}$$

$$- (\alpha_{i+1} + \kappa)\frac{Q_{i+1,1}\left|Q_{i+1,1}\right|}{2gA_{i+1,1}{}^2} = 0$$

$$F_{jn_1,3} = z_{i,N_i+1} - z_{i+2,1} + y_{i,N_i+1} - y_{i+2,1} + \frac{Q_{i,N_i+1}\left|Q_{i,N_i+1}\right|}{2gA_{i,N_i+1}{}^2}$$

$$- (\alpha_{i+2} + \kappa)\frac{Q_{i+2,1}\left|Q_{i+2,1}\right|}{2gA_{i+2,1}{}^2} = 0 \qquad 3.7$$

$$F_{jn_2,1} = Q_{i+3,1} - Q_{i+1,N_{i+1}+1} - Q_{i+2,N_{i+2}+1} = 0$$

$$F_{jn_2,2} = z_{i+1,N_{i+1}+1} - z_{i+3,1} + y_{i+1,N_{i+1}+1} - y_{i+3,1} + \frac{Q_{i+1,N_{i+1}+1}\left|Q_{i+1,N_{i+1}+1}\right|}{2gA_{i+1,N_{i+1}+1}{}^2} - (\alpha_{i+3} + \kappa)\frac{Q_{i+3,1}\left|Q_{i+3,1}\right|}{2gA_{i+3,1}{}^2} = 0$$

$$F_{jn_2,3} = z_{i+2,N_{i+2}+1} - z_{i+3,1} + y_{i+2,N_{i+2}+1} - y_{i+3,1} + \frac{Q_{i+2,N_{i+2}+1}\left|Q_{i+2,N_{i+2}+1}\right|}{2gA_{i+2,N_{i+2}+1}{}^2} - (\alpha_{i+3} + \kappa)\frac{Q_{i+3,1}\left|Q_{i+3,1}\right|}{2gA_{i+3,1}{}^2} = 0 \qquad 3.8$$

where:

κ = head-loss coefficient (dimensionless).

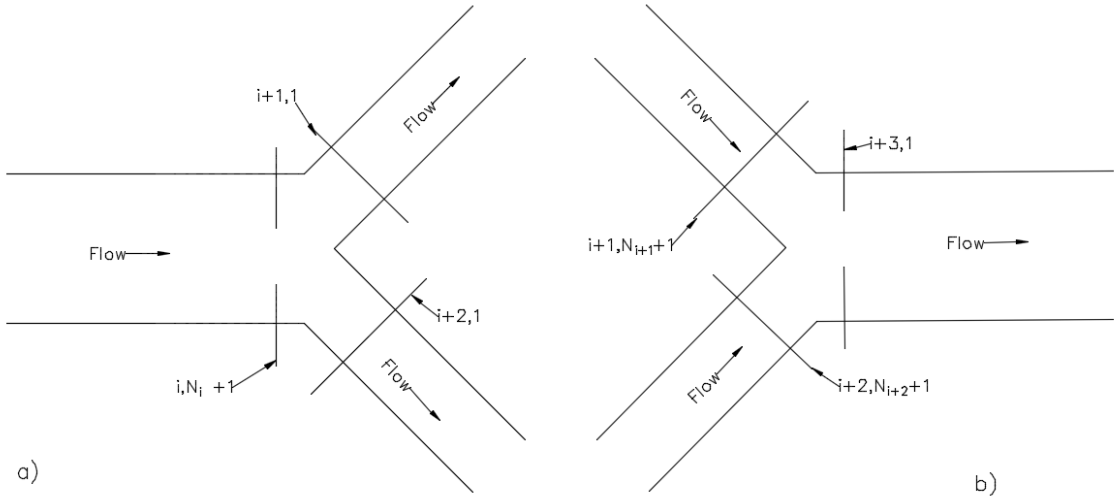

Figure 3.3. Definition sketch of channel junctions in a looped network. a) Upstream junction (jn1); and b) downstream junction (jn2).

For a parallel channel system with *M* parallel channels, the arrangement of equations results in a Jacobian of bandwidth 3*M* + 1 (Chaudhry 2008). However, in more complex

networks, additional equations must be included for branch junctions of three or more channels. Consequently, there is not a generalized procedure for complex channel networks that allows an arrangement of equations that produces a Jacobian matrix of minimum bandwidth. In general, the system will be asymmetric.

The numerical solution of the system of non-linear equations is based on the Newton-Raphson Solution method (NRSM). The procedure requires an initial guess of the unknown variables, flow depths and discharges, in all the sections of the channel network. Then, the matrix system, given by Equation 3.3, will be assembled and solved using a numerical solver. The results will be used for correcting the water depths and discharges, previously assumed. The corrected water depths and discharges will be used on the second iteration for computing the new values of the matrix system, and so on. This iterative procedure is repeated until the water depths and discharge corrections are less than a given tolerance.

The following subsections explains in more detail the two numerical solvers used for the system. The Gauss Elimination Method will be explained first. This method is categorized as a direct solution technique. The Bi-Conjugate Gradient Stabilizer Method is presented next. This method is categorized as an iterative solution technique.

3.2.1. Gauss Elimination Method

The Gauss Elimination Method (GEM) is the most important and most useful elimination method for solving system of linear algebraic equations (Hoffman 2001). According to Hoffman (2001), pivoting is an essential element of GEM, since pivoting to avoid zero pivot elements is always required. Pivoting can be described as a process where the coefficients on the matrix are

interchanged to put the coefficient of largest magnitude on the diagonal of the matrix, in order to guarantee a nonzero divisor if there is a solution to the set of equations (Gerald and Wheatley 1992). To improve the accuracy of the solution, scaled pivoting is recommended to decrease round-off errors (Hoffman 2001). Scaled pivoting introduces a normalization (i.e., scaling) of a column by the largest element on the corresponding row before applying the pivoting. Some modifications or extensions of the GEM are the Gauss-Jordan Elimination, the matrix inverse method, the LU factorization method, and the Thomas algorithm (Hoffman 2001).

3.2.2. Bi-Conjugated Gradient Stabilizer Method

The Bi-conjugated Gradient Stabilizer with Preconditioner method (BiCGSTAB) was selected for solution of the system of equations in complex channel networks. BiCGSTAB is a variation of the Conjugate Gradient Squared method (CGS), which is based on squaring the residual polynomial, and was developed to remedy the difficulty presented by the CGS, which may lead to substantial build-up of rounding errors and possibly even overflow (Saad 2003). The BiCGSTAB can solve non-symmetric positive definite systems with large sparse matrices, similar to the conditions that are produced for the channel network systems. This algorithm introduces a new polynomial which is defined recursively at each step with the goal of "stabilizing" or "smoothing" the convergence behavior of the original algorithm, Bi-Conjugate Gradient algorithm (BiCG) (Saad 2003). According to Babaoğlu (2003), BiCGSTAB often converges twice as fast as the BiCG, and the convergence behavior is considerably smoother, since the residual vector is minimized. The convergence ability of the method strongly depends

on the condition number of the interaction matrix. The number of iterations to reach a desired level of error varies with the properties of the matrix (Babaoğlu 2003).

The system of equations representing a channel network forms an ill-conditioned non-diagonally dominant system, hence, a preconditioner was used with BiCGSTAB. According to Yuvashankar et al. (2016), preconditioning is a key factor in solving iterative methods and its purpose is to make solvers converge faster, resulting in less iterations. A good preconditioner should meet the following requirements: the preconditioned system should be easy to solve, and should be cheap to construct and apply (Yuvashankar et al. 2016). The preconditioner selected for the solver is the incomplete LU factorization (iLU) with threshold and pivoting. iLU produces a unit lower triangular matrix and, an upper triangular matrix, in which the zeros on the original matrix are preserved on the produced matrices; preserving the sparsity of the system. The pivoting of the iLU prevents zeros in the main diagonal.

3.3 Direct Step Method

The Direct Step Method (DSM) is commonly used to determine the distance between two successive water depths for a specific discharge; usually, the selected water sections are called the “upstream” and “downstream” section. The DSM is only suitable for prismatic channels, since the same cross-sectional geometric relationships are used for all the sections along the channel (Chaudhry 2008). It is suggested that for subcritical flow, the computations begin at the downstream end section and progress upstream, one section at a time (Chaudhry 2008; Gupta 2008; Houghtalen et al. 2013). In this case, the water depth at the upstream and downstream

section will be known for a specific discharge. Equation 3.9 determines the distance between two predetermined flow depths, where $\overline{S_f}$ is the average of the energy slope at the upstream and downstream cross-sections as expressed by Equation 3.10.

$$\Delta x = \frac{\left(y_2 + {\alpha_2 V_2^2}/{2g}\right) - \left(y_1 + {\alpha_1 V_1^2}/{2g}\right)}{S_0 - \overline{S_f}} \tag{3.9}$$

$$\overline{S_f} = \frac{1}{2}\left(\frac{n_2^2 V_2^2}{\emptyset R_2^{4/3}} + \frac{n_1^2 V_1^2}{\emptyset R_1^{4/3}}\right) \tag{3.10}$$

where:

Δx = computed distance between two successive water depths for a specific discharge (L),

y_1 = water depth at the upstream section (L),

y_2 = water depth at the downstream section (L),

V_1 = flow velocity at the upstream section (L),

V_2 = flow velocity at the downstream section (L),

S_0 = slope of the channel bottom (Dimensionless),

$\bar{S_f}$ = average of the energy slope between two sections (Dimensionless),

R_1 = hydraulic radius at the upstream section (L),

R_2 = hydraulic radius at the downstream section (L), and

$\emptyset$ = unit system coefficient; 1 for SI unit system and 2.22 for English unit system (dimensionless).

According to Chaudhry (2008), the DSM has two disadvantages: (1) water depths cannot be computed at specified locations, requiring the use of interpolation techniques, which may not yield accurate results; (2) it is unwieldy to apply to non-prismatic channels.

3.4 Standard Step Method

The Standard Step Method (StdSM) is commonly used to compute water depths at specified locations, even if the channel is non-pristmatic, which occurs when the channel cross-section and/or the bottom slope changes with distance. For example, if the water depth and location is known at the downstream section, the upstream water depth can be computed if the upstream

location of the section is known. It is suggested that for subcritical flow conditions, the StdSM computes the solution one reach at a time, starting from the downstream end section until reaching the upper limit of the channel (Chaudhry 2008; Gupta 2008; Houghtalen et al. 2013). The StdSM is derived from an energy balance between two successive cross-sections (See Figure 3.1) that are separated by a sufficiently short distance so that the water surface can be approximated by a straight line (Houghtalen et al. 2013). The energy relationship between the two successive sections may be written as:

$$\left(z_1 + y_1 + \frac{\alpha_1 {V_1}^2}{2g}\right) = \left(z_2 + y_2 + \frac{\alpha_2 {V_2}^2}{2g}\right) + \Delta x\, \bar{S_f} \qquad 3.11$$

The computation procedure yields the correct depth at a cross-section that is a distance Δx away from a section with a known depth. Equation 3.11 cannot be solved directly for the unknown depth (e.g., y_1), since V_1 and $\bar{S_f}$ depend on y_1. Therefore, an iterative procedure is required using successive approximations of y_1 until the downstream and upstream energies balance. Some iterative procedures used are the trial-and-error procedure, Newton-Raphson or the bisection method (Chaudhry 2008).

4 CHAPTER – ANALYSIS AND DESIGN OF HYDRAULIC STRUCTURES

This section consists of describing the analysis and/or design of the hydraulic structures selected for this research. First, the incorporation of the lateral weir is explained. Followed by the design/analysis procedure for an inverted siphon within the channel system. Finally, the sluice gate analysis/design procedure is presented in detailed.

4.1 Lateral Weir

Lateral weirs (LW) are commonly found in irrigation systems as a structure to divide flow in a controlled manner to provide water to crop parcels (Silva-Araya and Vargas, 2014). Two cases are possible when a lateral weir is within the channel: 1) determine the length of the crest necessary to provide a pre-determined discharge to a parcel or 2) determine the amount of water that an existing structure is distributing into a parcel. Case 1 is the "design" problem and Case 2 is the "analysis" problem.

The head at the crest of a lateral weir is obtained by subtracting the height of the crest from the flow depth in Equation 4.1. For the SSM, the flow depth at the weir is the average flow depth between its preceding and following sections. This head of water above the crest is related to the discharge; therefore, a higher head of water means an increase in the flow throughout the weir. The discharge through the weir is computed with the following equations proposed by Hager (1986):

$$H = Y_w - P_w \tag{4.1}$$

$$Q_w = C_e L_w H^{3/2} \tag{4.2}$$

$$C_e = \frac{2}{3} C_d \sqrt{2g} \tag{4.3}$$

$$C_d = 0.485 \sqrt{\frac{2 - Fr^2}{2 + 3Fr^2}} \tag{4.4}$$

where:

L_w = length of the weir (L),

H = head above the lateral weir (L),

C_e = effective discharge coefficient (dimensionless),

C_d = discharge coefficient (dimensionless),

Fr = Froude number (dimensionless),

Q_w = flow through the lateral weir (L^3/t)

P_w = height of the weir crest (L), and

Y_w = average flow depth between the upstream and downstream section of the lateral weir (L).

The Froude number is defined as:

$$Fr = \frac{V_{ave}}{\sqrt{g D_{up}}} \qquad 4.5$$

where:

V_{ave} = average flow velocity at the upstream section of the weir (L/t), and

D_{up} = hydraulic depth for the channel section upstream of the weir (L).

The lateral weir design depends on the flow depth at the weir location. To determine the appropriate height of the crest (P_w) an initial estimate for this value is set equal to the ratio of the wetted area to the top width ($P_w = A_w/T_w$) (May et al. 2003). Also, it is recommended that the height of the crest of a suppressed rectangular weir should be at least equal to three times the maximum head (H_{max}) at the weir (U. S. Bureau of Reclamation 2001). Also, the sidewalls of the weir must extend at least a distance of 0.3 H_{max} (U. S. Bureau of Reclamation 2001). Figure 4.1 shows the schematic of a lateral weir.

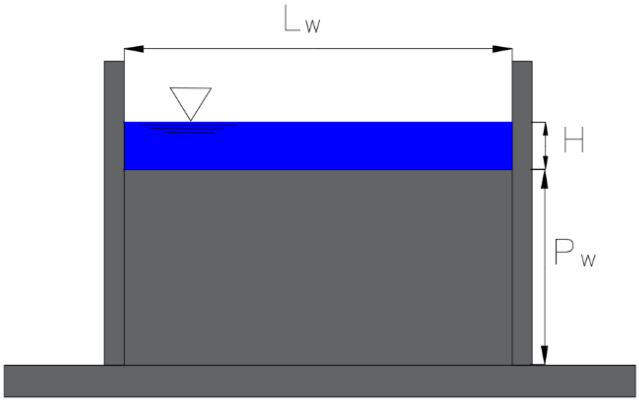

Figure 4.1. Cross-section of a suppressed rectangular weir (Adapted from U. S. Bureau of Reclamation 2001).

A lateral weir produces a division of the existing channel into two new channels, usually with the same geometric properties. This new junction is modeled as a series junction adding the weir equation to the continuity equation. The design criterion for the lateral weir consists of determining the necessary crest length to evacuate a pre-determined discharge throughout the weir. The desired weir flow will be provided to the model as a percent of the discharge upstream of the weir location. An initial estimate of the height of the crest is also given as input. The proposed solution is verified according to the criterion proposed by the U.S. Bureau of Reclamation (2001). The effective coefficient and the discharge coefficient are computed. Finally, the length of the weir is obtained from Equation 4.2. If the proposed solution does not meet the USBR criterion, then the initial height of the crest should be changed, and the process should be repeated.

The analysis of an existing lateral weir consists of determining the amount of flow that goes through the weir. Therefore, the height of the crest, the discharge coefficient and the length of

the weir will be given to the algorithm as an input. Finally, the flow through the weir can be computed using Equation 4.2.

4.2 Inverted Siphon

The inverted siphons (sometimes called sag culverts or siphons) are used to convey water by gravity under roads, railroads, other structures, various types of drainage channels and depressions. It is defined as a closed conduit designed to run full and under pressure (UDT 2004). The siphon profile (see Figure 4.2) is designed to satisfy certain requirements of cover, siphon slopes, bend angles and submergence of inlet and outlet. One of the most important design criteria is the siphon velocities. According to the Utah Department of Transportation (2004), these velocities should range between 3.5 ft/s to 10 ft/s and depend on the available head, economic considerations and siphon length (UDT 2004). The siphon velocity criteria will determine the minimum siphon diameter in the following manner (UDT 2004):

1. 3.5 ft/s or less for a short siphon not located under a highway with only earth transitions provided at entrance and exit,
2. 5 ft/s or less for a short siphon located under a highway with a concrete transition provided at the inlet and a concrete transition provided at the outlet, and
3. 10 ft/s or less for a siphon longer than 200 ft with a concrete transition provided at the inlet and a concrete transition provided at the outlet.

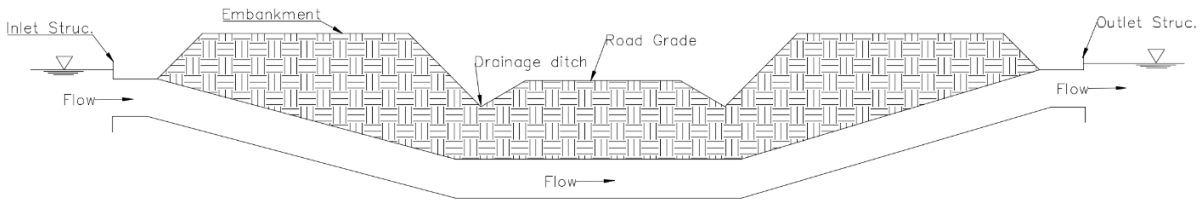

Figure 4.2. Typical siphon profile (Adapted from UDT 2004).

The head losses that should be included in the syphon design are (UDT 2004):

1. convergence loss in the inlet transition,
2. friction and bend losses in the siphon,
3. divergence loss in the outlet transition,
4. transition friction only in special or very long transitions, and
5. convergence and divergence head losses in earth transitions are required between an unlined canal and concrete transition. These are usually small and are ignored.

The first step in the design procedure of an inverted siphon, provided by the UDT (2004), is to determine the inlet and outlet structures and approximate the siphon size. Next, select a preliminary transition geometry and create an initial siphon profile. Then, compute the siphon head losses and compare them with the available head. If the computed losses are greater than the difference in upstream and downstream canal water surface, the siphon will probably cause backwater in the canal upstream from the siphon, and therefore, the siphon size should be increased or the canal profile should be changed. If the computed losses are appreciably less than the difference in upstream and downstream water surfaces, it may be possible to decrease the size of siphon so that the available head is approximately the same as the head losses. Finally,

determine the final transition geometry, compute actual head losses and prepare the final siphon profile.

An inverted siphon is a type of inline structure commonly found on irrigation channel systems. Since the siphon does not remove any discharge from the system, the continuity equation remains constant upstream and downstream of the siphon. Therefore, the subroutine for the analysis/design of the siphon structure is implemented after the algorithm has converged to a final water depth and discharge solution. The objective of the design procedure is to determine the required siphon diameter that meets the standards of the region or country where the siphon is located. As an example, the siphon diameter should meet the standards of the UDT. The UDT is required to comply with five standards: flow velocity, friction slope, hydraulic seal, head loss, and Froude number. To compute an initial estimate of the siphon diameter, a variation of the Manning's equation is used (Equation 4.6), in which the siphon roughness coefficient and an initial slope are given as an input to the algorithm. This initial diameter is rounded to the next commercial diameter. The siphon commercial diameter selected is used to compute the flow velocity through the siphon. If the flow velocity is less than 3.5 ft/s, the siphon diameter must decrease, and if the flow velocity is greater than 10.0 ft/s, the siphon diameter must increase. With the selected diameter, the friction slope is computed using Equation 4.7. The initial siphon slope given to the algorithm and the computed friction slope are compared, and the maximum of both slopes is selected as the siphon design slope. To compute the hydraulic seal in the siphon, Equation 4.8 is used to verify that the computed hydraulic seal is greater than the minimum required by the UDT (2004), which is 3 in, if not, the flow velocity on the siphon must increase. To compute the total head loss produced by the siphon, Equation 4.9 is used (Ankum 2002).

Typical values for transition head losses of inlets and outlets and head loss coefficients in bends and elbows are presented by Ankum (2002). The available head is computed from the drop in the water surface elevation at the upstream and downstream section of the siphon. If the total head loss is greater than the available head, the siphons' inlets, outlets, bends and/or elbows should be changed. In subcritical flow conditions, the Froude number should be limited to 0.5 to avoid standing waves at the water surface and to avoid flow to become critical because of decreased channel roughness (Ankum 2002). The Froude number can be computed using Equation 4.5. If the Froude number is greater than 0.5, the flow velocity in the siphon must be decreased.

$$d_0 = C_s \times \frac{Q^{0.375} n^{0.375}}{{S_0}^{0.1875}} \quad 4.6$$

$$S_f = \frac{n^2 V^2}{C_f \, R^{4/3}} \quad 4.7$$

$$h_{seal} = 1.5 \times \left(\frac{V^2}{2g} - \frac{{V_{up}}^2}{2g} \right) \quad 4.8$$

$$h_{loss} = \left(C_{in} + C_{out} + C_{bend} + C_{elbow} + \frac{2g \, L_s}{{s_k}^2 R^{4/3}} \right) \times \frac{V^2}{2g} \quad 4.9$$

where:

d_0 = initial siphon diameter (L),

Q = discharge through the siphon (L^3/t),

n = Manning's roughness coefficient of the siphon (dimensionless),

C_s = unit system coefficient for initial diameter of siphon equation; where for SI units equals 5.0797 and for English units is 1.3346 (dimensionless),

S_0 = initial siphon bottom slope (L/L),

R = hydraulic radius within the siphon (L),

V = flow velocity in the siphon (L/t),

S_f = computed siphon friction slope (L/ L),

C_f = unit system coefficient for the friction slope of siphon equation; where for SI units equals 0.9964 and for English units is 2.2 (dimensionless),

V_{up} = flow velocity upstream the siphon (L/t),

h_{seal} = hydraulic seal at the siphon (L),

s_k = Strickler coefficient; which may have values of 50 $m^{1/3}/s$ for stone masonry, up to values of 70 $m^{1/3}/s$ for concrete,

C_{in} = head loss coefficient for siphon inlets (dimensionless),

C_{out} = head loss coefficient for siphon outlets (dimensionless),

C_{bend} = head loss coefficient for siphon bends (dimensionless), and

C_{elbow} = head loss coefficient for siphon elbows (dimensionless).

The objective of the analysis procedure is to determine if the operational discharge is less than or equal to the design discharge of the siphon. Similar to the design procedure, the five standards proposed by the UDT (2004) for siphon design are verified. The design discharge is computed from Equation 4.6 for the design siphon diameter. The operational discharge of the siphon equals the discharge at the upstream section of the siphon. If the operational discharge is greater than the design discharge, the siphon diameter should be increased to accommodate the incoming discharge and avoid choking at the siphon inlet. The siphon flow velocity, the friction

slope, the head loss, and the Froude number are verified in a similar manner as the design procedure.

4.3 Sluice Gates

A sluice gate is another type of lateral structure commonly found on irrigation channel systems. The sluice gate is an opening used for controlling discharge (Swamee 1992). Figure 4.3 shows the definition sketch for free flow and submerged flow sluice gate. Downstream free flow occurs at a (relatively) large ratio of upstream depth to the gate-opening height. However, submerged flow at the downstream would occur for low values of this ratio (Swamee 1992). The conventional sluice gate discharge equation is written in the following form:

$$Q_s = C'_d ab\sqrt{2gy_0} \qquad 4.10$$

where:

Q_s = sluice gate discharge (L^3/t),

C'_d = sluice gate discharge coefficient (depends on the flow condition) (dimensionless),

a = sluice gate height (L),

b = sluice gate length (L), and

y_0 = upstream water depth (L).

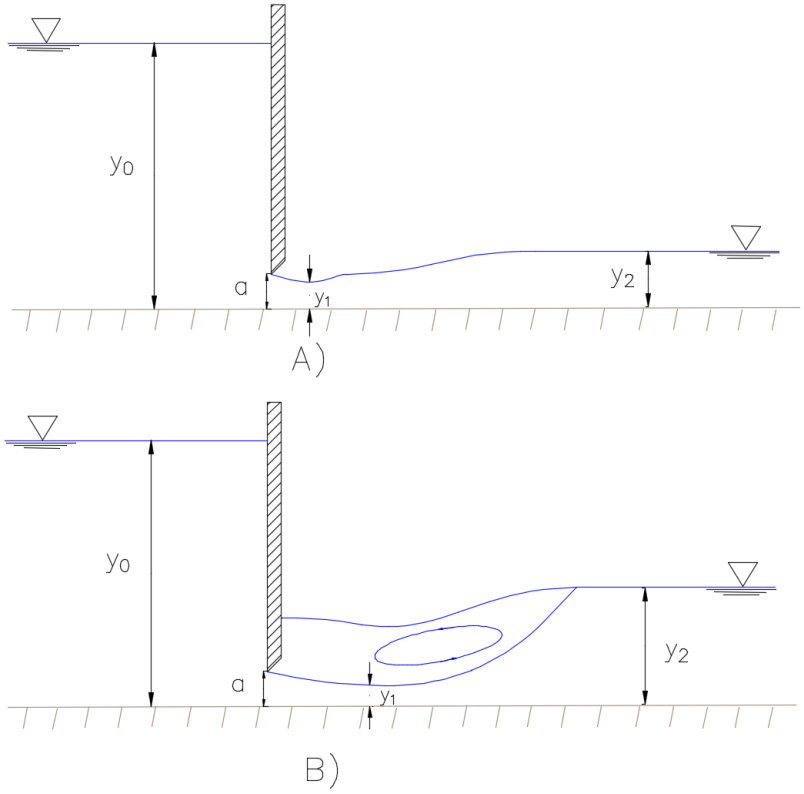

Figure 4.3. Sluice gate definition sketch. A) Free flow condition; B) Submerged flow condition.

The free flow condition can be defined as Equation 4.11 and the submerged flow conditions can be defined as Equation 4.12 (Swamee 1992). Depending on the flow conditions the sluice gate discharge coefficient can be defined as Equation 4.13 or Equation 4.14 for free flow and submerged flow conditions, respectively.

$$y_0 \geq 0.81 y_2 \left(\frac{y_2}{a}\right)^{0.72} \tag{4.11}$$

$$y_2 \leq y_0 \leq 0.81 y_2 \left(\frac{y_2}{a}\right)^{0.72} \tag{4.12}$$

$$C'_d = 0.611\left(\frac{y_0 - a}{y_0 + 15a}\right)^{0.072} \quad 4.13$$

$$C'_d = 0.611\left(\frac{y_0 - a}{y_0 + 15a}\right)^{0.072}(y_0 - y_2)^{0.7}\{0.32\left[0.81y_2\left(\frac{y_2}{a}\right)^{0.72} - y_0\right]^{0.7} + (y_0 - y_2)^{0.7}\}^{-1} \quad 4.14$$

where:

y_2 = tailwater depth (L).

The analysis/design of a sluice gate is similar to the lateral weir procedure described in the previous sections. The objective of the design procedure is to determine the necessary gate length to provide a pre-determined discharge to a parcel. The desired gate flow will be provided to the model as a percent of the discharge upstream of the weir location. An initial estimate of the sluice gate opening, as well as the tailwater depth, given as a percent of the upstream water depth, is fed to the algorithm as an input. This is necessary to determine the flow condition at the sluice gate and compute the required sluice gate discharge coefficient. Finally, the length of the gate is obtained from Equation 4.10.

The objective of the analysis procedure is to determine the amount of water that an existing structure is distributing into a parcel. Therefore, the sluice gate opening, the discharge coefficient and, the length of the sluice gate will be given to the algorithm as an input. Finally, the flow through the sluice gate can be computed using Equation 4.10.

5 CHAPTER – FIELD MEASUREMENTS

A field reconnaissance trip was coordinated to the Lajas Valley Irrigation District System (LVIDS) on March 2017. The purpose of this trip was to determine a possible segment of the LVIDS that could be modeled using the Simultaneous Solution Method (SSM). More detail on the importance and characteristics of the LVIDS is presented next. The selected segment for modeling is presented in the following sections of this chapter and is explained in more detail on Section 7.4. On May 24, 2017, a field survey trip was performed on the selected segment of the LVIDS. The objective of this trip was to record the required information for modeling the selected segments using the SSM. The data collected at the LVIDS for the area of interest (AOI) can be divided into three categories: water levels, channel cross-sections, and sediments samples that were deposited in the concrete channel bottom. A granulometric analysis was performed to the sediment samples taken and are explained in the following section. In addition, the Slope-Area Method (SAM) was used to estimate the discharge through the channel. This method was developed by the U.S. Geological Survey (USGS) and is presented in the last section of this chapter, in addition to other techniques to compute the discharge.

5.1 Description of the System

The Lajas Valley Irrigation District System (LVIDS) is located on the southwest region of Puerto Rico. It begins on the Loco Reservoir, located in the municipality of Yauco, and flows through the municipalities of Guánica, Sabana Grande, and Lajas, ending on the Boquerón Bay, located in the municipality of Cabo Rojo. Figure 5.1 illustrates the complete LVIDS, in which the red line represents the main irrigation channel and the blue line represents the branches or

laterals from the main system. The AOI selected is shown in a black box. The LVIDS was constructed by the USACE and the River Source Authority ("Autoridad de las Fuentes Fluviales" in Spanish) from 1950 to 1955. Most of the system consists of a concrete trapezoidal channel. The water that runs through the LVIDS comes from three main watersheds: Yauco River, Loco River, and Añasco River (WRPR 2017). In addition to these watersheds, the Lajas Valley watershed contributes from accidental surface runoff that falls directly to the channels. This irrigation system is maintained and operated by the Puerto Rico Electric Power Authority (PREPA). The Yauco River watershed has a catchment area of approximately 119.39 km^2 (46.1 mi^2), while the Loco River watershed has 63.97 km^2 (24.7 mi^2) of catchment area (WRPR 2017). The Lajas Valley coastal watershed is one of the biggest on the island, with a superficial area of 216.25 km^2 (83.5 mi^2) (WRPR 2017).

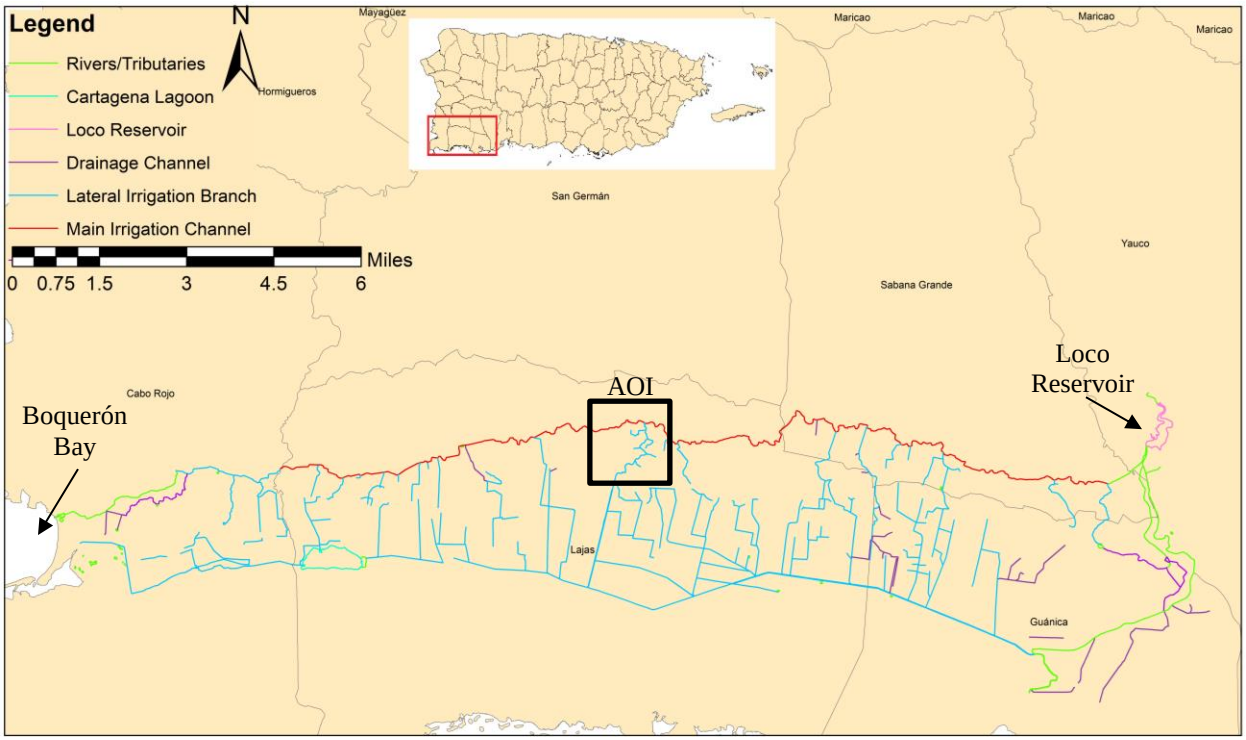

Figure 5.1. Lajas Valley Irrigation District System map with its main and lateral irrigation channel, river and tributaries, reservoirs and lagoons, and drainage channels (PRDNR 2008). The area of interest (AOI) selected is shown in a black box.

The topography of the Lajas Valley is relatively flat, with maximum elevations of 80-ft above mean sea level (WRPR 2017). According to Water Resources of PR (2017), the LVIDS feeds approximately 330 agricultural intakes and 4 water treatment plants, which serve potable water to the residents of Sabana Grande, Guánica, Lajas, San Germán and Cabo Rojo. Therefore, the LVIDS is the most important irrigation system on the island.

5.2 Granulometric Analysis

Three sediment samples were collected at the AOI, all at the downstream portion of the junction between the main channel and the lateral M-63. The sample labeled MC1 denotes the sample obtained at the downstream portion of the main channel closest to the junction between

the lateral M-63 and the main channel (Cross-section MC-BU in Figure 5.4), while the sample labeled MC3 represents the sample obtained at the downstream portion of the main channel closest to the upstream portion of the inverted siphon #14 named “Ramón Toro” (Cross-section MC-CU in Figure 5.4). The sample labeled MC2 represents the sample obtained at a segment between the MC1 and MC3. A granulometric analysis, also known as sieve analysis, was performed to the sediment sample that was collected from the channel bottom, at the Geotechnical and Soil Laboratory from the Civil Engineering and Surveying Department at UPRM. The purpose of the sieve analysis is to find the particle-size distribution of the sediment collected (Das and Sobhan 2014). This analysis consists of shaking the sediment sample through a set of sieves that have progressively smaller openings (Das and Sobhan 2014). The U. S. standard sieve number and the openings sizes are given in Table 5.1. The following paragraph briefly explains the sieve analysis procedure performed at the laboratory for the sediment samples obtained. Details are given by the standard ASTM F-11 (Das and Sobhan 2014):

1. The collected sample is oven dried for at least 24 hours, to eliminate any moisture. The lumps of the sediment sample are broken manually, and the sample weight is recorded. Figure 5.2 illustrate the sediment sample MC1. On samples MC1 and MC3, organic material was found in the shape of shells.

Figure 5.2. Sediment Sample MC1 obtained at the main channel of the Lajas Valley Irrigation Channel System.

2. The sieves are cleaned up and weighted individually. Then, they are stacked up from the biggest to the smallest (from top to bottom) opening until reaching the pan. The soil is placed on the top of the stack of sieves, as shown in Figure 5.3.

Figure 5.3. Soil sample MC2 placed on the stack of sieve prior to shacking of the sample.

3. The stack of sieves with the soil is placed on a vibrator machine for 5 minutes.

4. The weight of each pan with the sample soil is recorded and the weight of the soil retained at each pan is computed.

5. The percent of soil retained at each sieve is calculated and the percent accumulated at each sieve is also computed.

6. The percent passing through each sieve is computed from the percent accumulated at each sieve. The percent passing and the sieve opening, which is a measure of the particle size, are used to create the particle-size distribution curve.

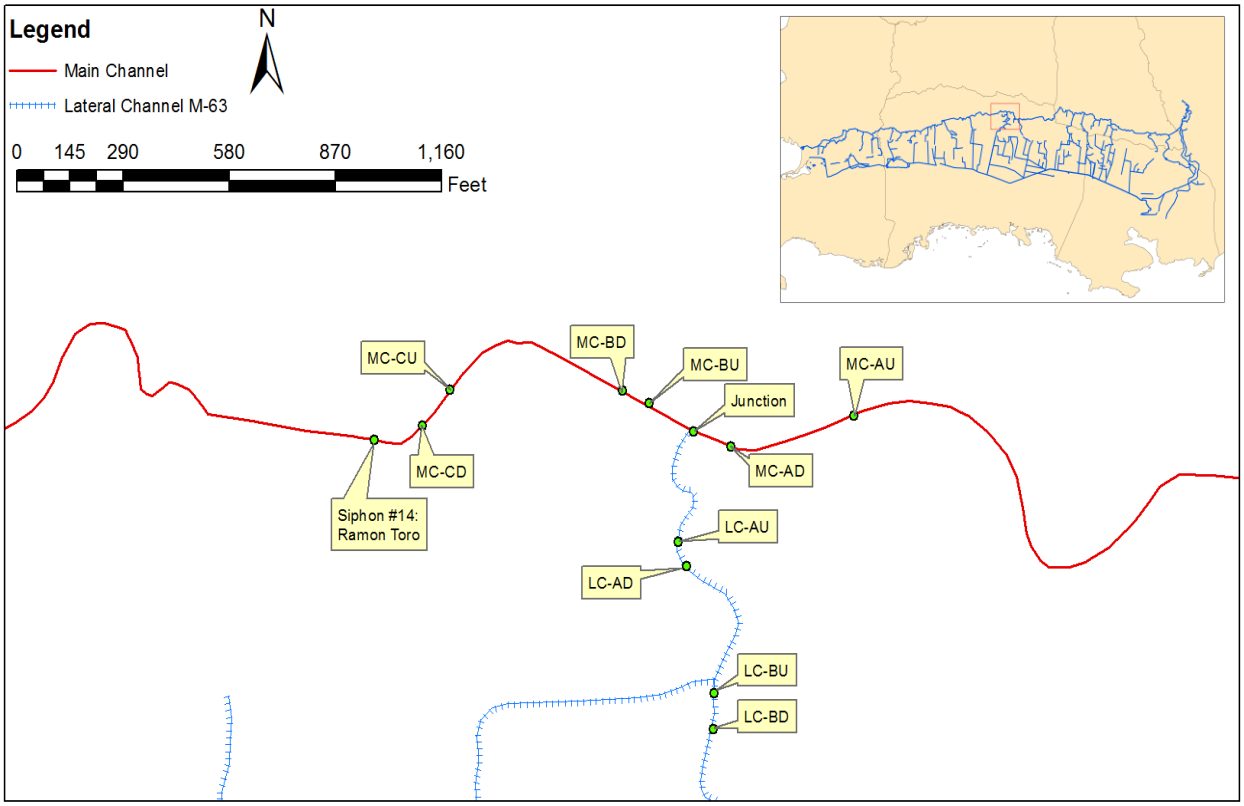

Figure 5.4. Location of the survey data for the area of interest at the Lajas Valley Irrigation District System.

Table 5.1 presents the granulometric analysis for the three samples obtained at the field, including the soil weight retained, the sieve weight, and the amount of soil passing through the sieve. The values in Table 5.1 were used to create the particle-size distribution curve, which is presented in Figure 5.5. The amount of soil lost for each sample MC1, MC2, and MC3 was

0.32%, 0.20%, and 0.43%, respectively. The amount of gravel that a sediment sample has is defined as the amount of soil retained at the sieve #4, with an opening of 4.75 mm (Das and Sobhan 2014). The amount of sand that a sediment sample has is defined as the amount of soil that passes sieve #4 and is retained at sieve #200 (Das and Sobhan 2014). The amount of fines, namely clay and silt that a sediment sample has is defined as the amount of soil that passes sieve #200 and is retained at the pan (Das and Sobhan 2014). Table 5.2 summarizes the percent of gravel, sand and fines for the three samples obtained at the LVIDS. The sample with the greatest amount of gravel was MC1, while the MC3 sample had the greatest amount of both of sand and fines.

Table 5.1. Granulometric analysis performed to the three samples obtained at the Lajas Valley Irrigation District System.

U.S. Sieve #	Sieve Opening (mm)	Sieve Weight (g)	Sieve Weight + Soil (g)			Soil Weight at Sieve (g)			Percent Retained at Sieve (%)			Percent Retained Cumulative (%)			Percent Passing (%)		
			MC1	MC2	MC3	MC1	MC2	MC3	MC1	MC2	MC3	MC1	MC2	MC3	MC1	MC2	MC3
4	4.75	461.0	892.2	863.4	613.7	431.2	402.4	152.7	73.5	58.9	25.6	73.5	58.9	25.6	26.5	41.1	74.4
10	2	427.2	471.7	489.2	487.0	44.5	62.0	59.8	7.6	9.1	10.0	81.0	67.9	35.6	19.0	32.1	64.4
20	0.85	382.6	430.6	447.4	477.1	48.0	64.8	94.5	8.2	9.5	15.8	89.2	77.4	51.5	10.8	22.6	48.5
40	0.425	346.4	380.1	409.7	442.0	33.7	63.3	95.6	5.7	9.3	16.0	95.0	86.7	67.5	5.0	13.3	32.5
60	0.25	326.0	341.1	372.1	413.3	15.1	46.1	87.3	2.6	6.7	14.6	97.5	93.4	82.1	2.5	6.6	17.9
100	0.15	316.4	323.2	340.1	378.8	6.8	23.7	62.4	1.2	3.5	10.5	98.7	96.9	92.6	1.3	3.1	7.4
200	0.075	306.4	310.0	317.5	334.3	3.6	11.1	27.9	0.6	1.6	4.7	99.3	98.5	97.3	0.7	1.5	2.7
Pan	----	360.4	364.5	370.5	376.7	4.1	10.1	16.3	0.7	1.5	2.7	100.0	100.0	100.0	0.0	0.0	0.0
					total	587.0	683.5	596.5									

Table 5.2. Percent of gravel, sand and fines for the three samples obtained at the Lajas Valley Irrigation District System.

Sample	Gravel (%)	Sand (%)	Fines (%)
MC1	73.5	25.8	0.7
MC2	58.9	39.6	1.5
MC3	25.6	71.7	2.7

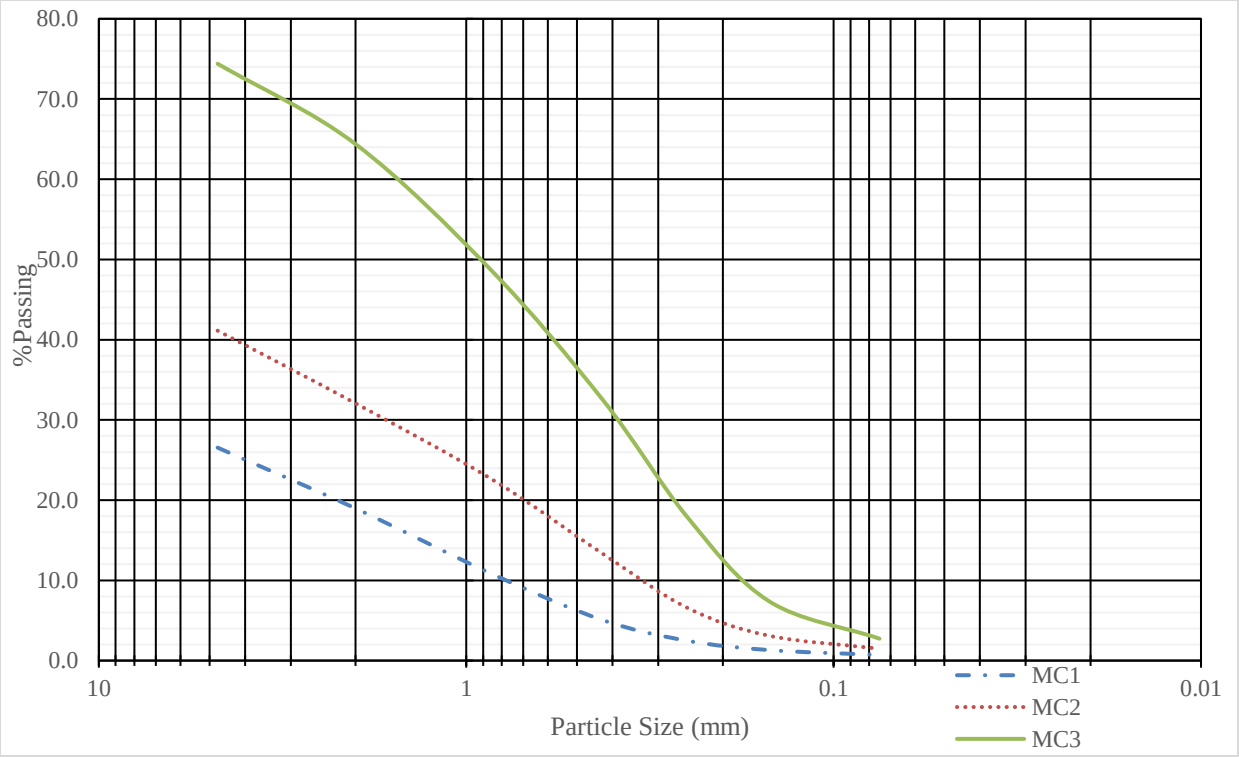

Figure 5.5. Particle-size distribution curve for the three sediment samples obtained at the Lajas Valley Irrigation District System.

The granulometric analysis was used to compute the Manning's roughness coefficient for the channel bottom using the Strickler equation (Equation 5.1). The Strickler equation (Equation 5.1) requires the particle size of the sediment, depending if the sediment is part of a riprap system or if it is a natural sediment (Chow 1959).

$$n = C\, k_s{}^{1/6} \qquad 5.1$$

where:

C = Strickler coefficient for computing Manning's channel roughness (equal to 0.034 for riprap size calculations and natural sediments and equal to 0.038 for discharge capacity of riprap channels), and

k_s = effective surface roughness height (L); equal to D_{90} for riprap size calculation and equal to D_{50} for natural sediment.

The D_{50} represents the particle diameter in which 50% of the soil is passing (Das and Sobhan 2014). In a similar manner, the D_{90} represents the particle diameter in which 90% of the soil is passing (Das and Sobhan 2014). This particle diameter (D_x) can be obtained through the particle-size distribution curve attained from the granulometric analysis. In the case of the sample obtained at the LVIDS, the Strickler equation for computing the Manning's channel roughness (Equation 5.1) will be used for natural sediment; therefore, the D_{50} was computed from Figure 5.5 and is presented in Table 5.3 for each of the samples. In addition, Table 5.3 presents the computed Manning's roughness coefficient for the natural sediment (denoted as n_{bed}).

The conditions presented at the main channel of the LVIDS during the field trip visit were similar to the schematic presented in Figure 5.6, in which the channel has a natural sediment bottom and concrete lateral slopes. Therefore, an equivalent Manning's channel roughness was computed for a channel cross-section that does not have the same roughness through the entire wetted perimeter and is divided in *M* subareas. See Equation 5.2 (Chaudhry 2008).

$$n_e = \left(\frac{\sum P_i {n_i}^{3/2}}{\sum P_i} \right)^{2/3} \qquad 5.2$$

where:

n_e = equivalent Manning's channel roughness,

P = wetted perimeter (L), and

i = 1, 2, 3, …, *M*.

The wetted perimeter for the lateral slope and channel bottom were computed from the field surveying data and are explained in more detail on the next section. The Manning's channel roughness for the lateral slopes was assumed to have a value of 0.015, which represent the value of a concrete float finish surface (Chow 1959). Table 5.3 presents the computed values of the equivalent Manning's channel roughness for the three sediment samples obtained at the field trip, in addition to all the required parameters to convey these results. The section with the largest and least equivalent Manning's channel roughness was MC1 and MC3, respectively. The progressive decrease of the Manning's channel roughness obtained from the sediment sample at the first (i.e., MC1) and the last sites (i.e., MC3) in the direction of flow can be attributed to a reduction in flow velocities in the main channel. High flow velocities carry coarser sediment than lower flow velocities, and the Manning's roughness coefficient is a function of the particle size, therefore, the section at MC1 should have a higher Manning's coefficient. This change in flow velocities, within the main channel, can be attributed to the presence of an inline weir located upstream where the MC1 sample was collected. The arithmetic average of the equivalent Manning's channel roughness for the three samples was 0.047. The conditions at the channel were assumed to be the same in the entire channel segment considered at the AOI, including the characteristics of the sediment samples obtained. Therefore, the equivalent Manning's channel roughness for the entire segment of the AOI is equal to the arithmetic average of this value, which is 0.047.

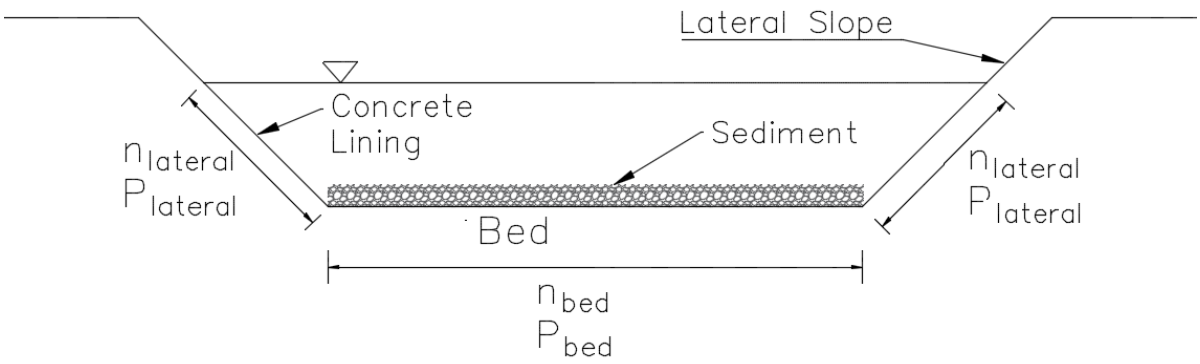

Figure 5.6. Main channel conditions during the field trip visit at the Lajas Valley Irrigation District System.

Table 5.3. Manning's roughness coefficient for natural sediment and equivalent value for the sections at which the three sediment samples were obtained at the Lajas Valley Irrigation District System.

Sample	D_{50} (mm)	n_{bed}	$n_{lateral}$	P_{bed} (m)	$P_{lateral}$ (m)	$\sum n_i P_i$	n_e
MC1	57.50	0.067	0.015	1.48	0.71	0.120	0.059
MC2	10.67	0.050	0.015	1.48	0.71	0.096	0.047
MC3	0.90	0.033	0.015	1.64	0.73	0.077	0.036

5.3 Survey Data

Part of the field trip at the LVIDS was to survey the channel cross-section at specific sections of the AOI for the numerical model, including the water surface depth at the sections. This data was used to compute the discharge using the USGS Slope-Area Method, to compute the equivalent Manning's roughness coefficient, and to calibrate the numerical model (Simultaneous Solution Method). Five pairs of cross-sections were surveyed including the water depth at each section. Each pair consists of an upstream and a downstream section that are separated by a straight segment of the channel. The location of this survey data is presented in Figure 5.4 for the

main channel and the lateral channel M-63 of the LVIDS. Three pairs of cross-sections were obtained at the main channel, one upstream and two downstream of the junction between the main channel and the lateral channel M-63. The other two pairs of cross-sections were obtained at the lateral channel M-63. The pair of cross-sections located upstream of the junction at the main channel were labeled with the prefix MC-A. The pair of cross-sections located closest to the downstream segment of the junction at the main channel were labeled with the perfix MC-B. The pair of cross-sections located at the downstream portion of the main channel closest to the upstream portion of the inverted siphon #14 named "Ramón Toro" was labeled as MC-C. The pair of cross-sections located closest to upstream segment at the lateral channel M-63 were labeled with the prefix LC-A. The pair of cross-sections located closest to downstream segment at the lateral channel M-63 was labeled as LC-B. All the labels for the cross-sections will be followed by a U or by a D, which represents the upstream and downstream section, respectively. For example, the label LC-AU refers to the upstream section that is closest to the upstream segment at the lateral channel M-63.

The channel cross-section was surveyed by placing the prism rods above the sediment layer that the channel bed has, primarily on the main channel; the same was done for measuring the water depth. All the elevations of the channel cross-sections are referenced to the WGS84-EGM96. Due to the high-water depth, the MC-AD cross-section could not be measured. For this, the water depth was recorded, and it was assumed that the channel cross-section at MC-AD was equal to the cross-section at MC-AU. Table 5.4, on page 56, illustrates the recorded water depth at each of the cross-sections surveyed, denoted by *y*. Figure 5.7 illustrates the surveyed channel cross-section at MC-AU, while Figure 5.8 illustrates the surveyed channel cross-sections at both

the upstream and downstream sections of MC-B. Also, Figure 5.9 illustrates the surveyed channel cross-section at both the upstream and downstream sections of MC-C. Figure 5.10 illustrates the surveyed channel cross-sections at both the upstream and downstream sections of LC-A. Figure 5.11 illustrates the surveyed channel cross-sections at both the upstream and downstream sections of LC-B.

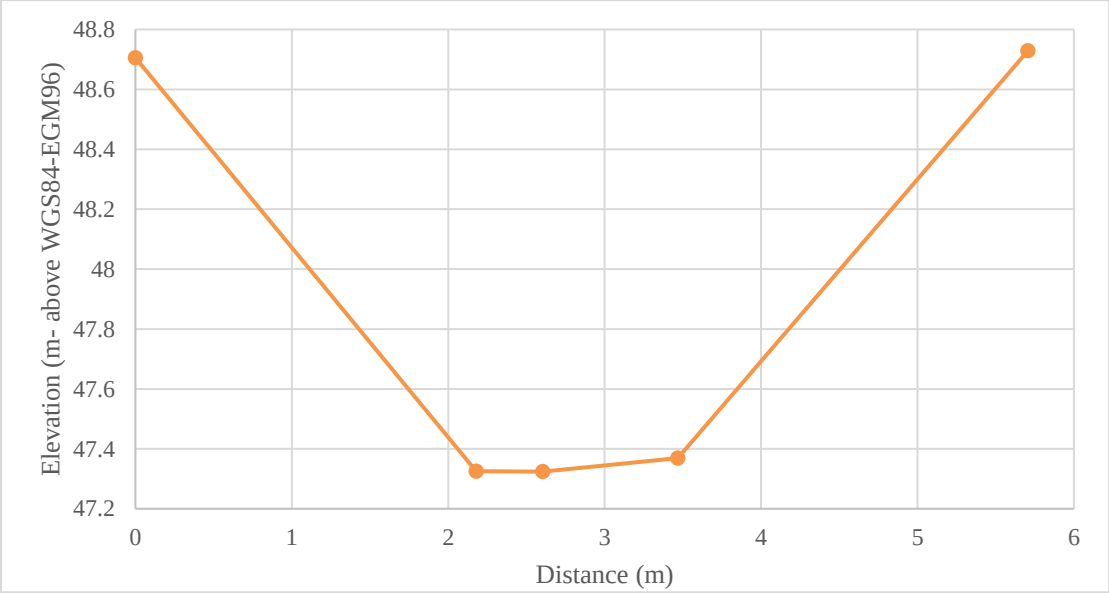

Figure 5.7. Surveyed channel cross-section at MC-AU.

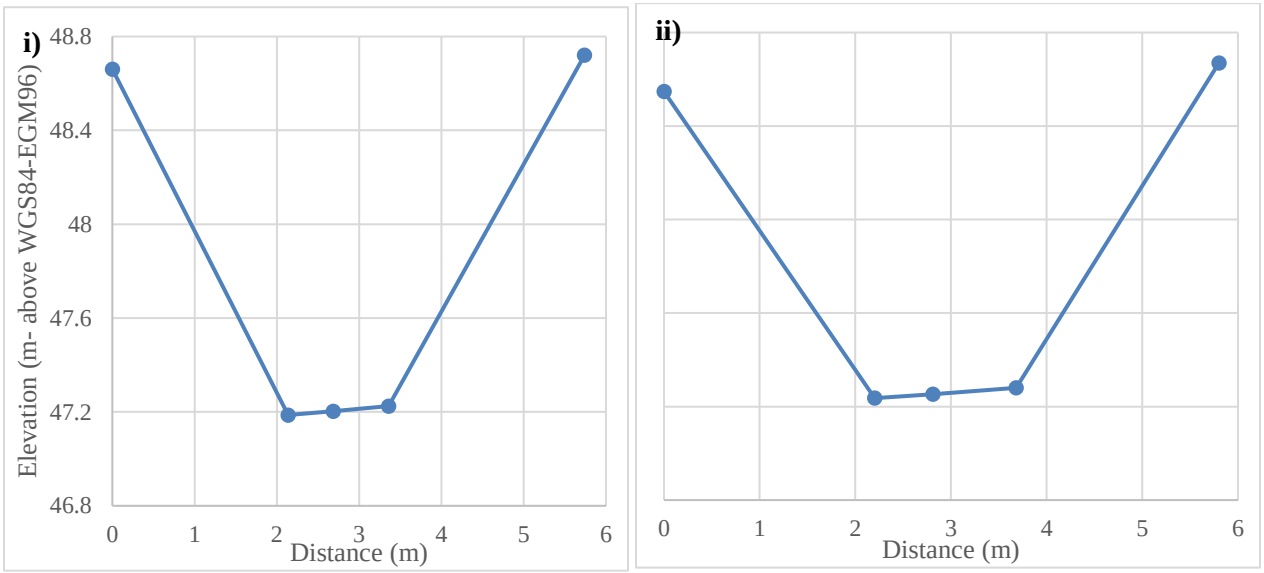

Figure 5.8. Surveyed channel cross-section at MC-B. i) upstream section of MC-B. ii) downstream section of MC-B.

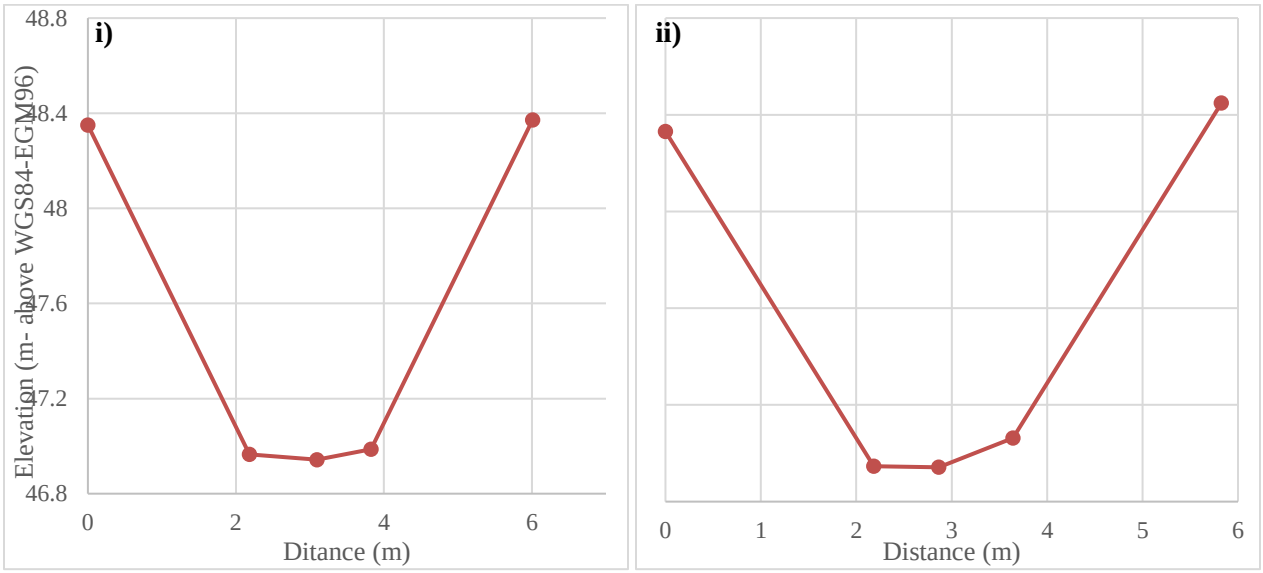

Figure 5.9. Surveyed channel cross-section at MC-C. i) upstream section of MC-C. ii) downstream section of MC-C.

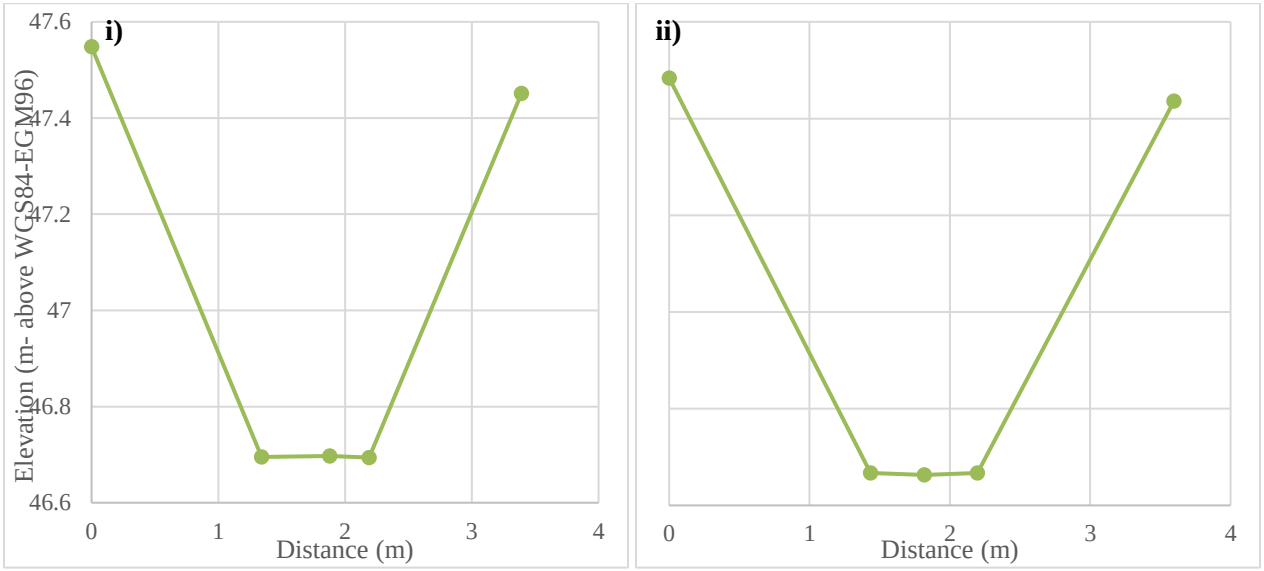

Figure 5.10. Surveyed channel cross-section at LC-A. i) upstream section of LC-A. ii) downstream section of LC-A.

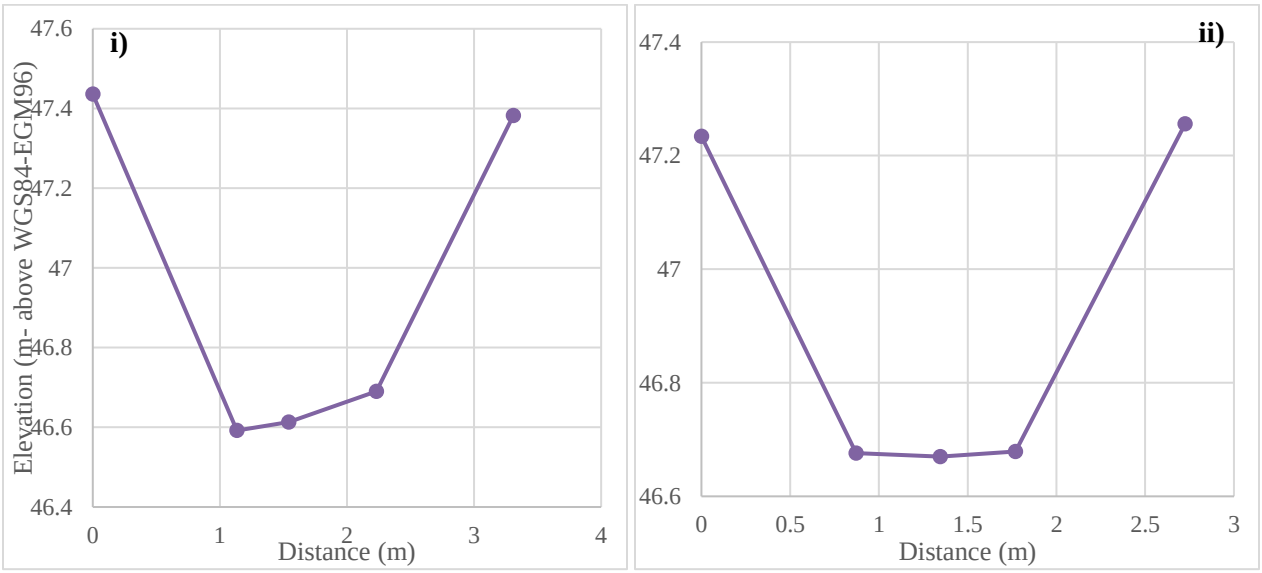

Figure 5.11. Surveyed channel cross-section at LC-B. i) upstream section of LC-B. ii) downstream section of LC-B.

5.4 Computation of Discharge

Two methodologies were used to compute the discharge on the day of the field visit to the LVIDS: (1) USGS Slope-Area Method (SAM), and (2) inline weir equations. The SAM is the most commonly used form of indirect measurement of discharge (Dalrymple and Benson 1967). In this method, the discharge is computed using Manning's equation (Equation 5.3) as the basis, assuming uniform flow conditions (Dalrymple and Benson 1967). Manning's equation can be expressed in terms of the conveyance factor (K), in which the mean conveyance in the reach is computed as the geometric mean of the conveyance at the two sections (Equation 5.4). The subscript 1 and 2 on the equation refers to the upstream and downstream sections that compose the reach, respectively. The friction slope on Manning's equations (Equation 5.3 and Equation 5.4) can be determined as the ratio between the energy loss due to boundary friction in the reach, h_f, and the length of the reach, L (Equation 5.5). The difference in velocity heads, Δh_v, can be computed using Equation 5.6; but first, the velocity head coefficient must be determined. The velocity head coefficient is assumed to be 1.0 if the section is not subdivided, but if not, it may be computed using Equation 5.7 (Dalrymple and Benson 1967). In Equation 5.7, the subscripts s and T refer to the individual subsections and to the total section, respectively.

$$Q = \frac{C_o}{n} A\, R^{2/3} S^{1/2} \tag{5.3}$$

$$Q = \sqrt{K_1 K_2 S} \tag{5.4}$$

$$S = \frac{h_f}{L} = \frac{\Delta h + \Delta h_v - (k_b \Delta h_v)}{L} \tag{5.5}$$

$$\Delta h_v = \frac{\alpha_1 {V_1}^2}{2g} - \frac{\alpha_2 {V_2}^2}{2g} \quad 5.6$$

$$\alpha = \frac{\sum {K_s}^3 / {A_s}^2}{{K_T}^3 / {A_T}^2} \quad 5.7$$

where:

Q = flow discharge (L^3/t)

S = friction Slope (L/L),

K = conveyance factor; which is $K = \frac{C_o}{n} A\, R^{2/3}$,

h_f = energy loss due to boundary friction in the reach (L),

L = distance between the two sections (L),

Δh = difference in water surface elevation at the two sections (L), and

k_b = contraction/expansion coefficient; which equals 0.5 if Δh_v is positive and 0 if Δh_v is negative.

One of the most important elements of the SAM is probably the selection of a suitable reach (Dalrymple and Benson 1967). The selection of the reach may depend on several factors: availability of water marks, geometry of the channel in the reach, channel bends, and length of the reach. The channel should be as uniform as possible, but compound channels can be used if they are properly subdivided. In addition, straight channel is preferred, and the accuracy of the SAM will improve as the length of the reach is increased (Dalrymple and Benson 1967). The difference in water surface elevation (Δh) can be computed as the arithmetic average of the elevations on both banks at each cross-section. To compute the discharge using the SAM,

Dalrymple and Benson (1967) recommend using Equation 5.8 when two reaches have been surveyed at the field. Results for the peak discharge computed using the SAM are presented in Table 5.4 for all the five pairs of cross-sections surveyed at the field, which includes all the required parameters for the SAM.

$$Q = K_2 \left(\frac{\Delta h}{\frac{K_2}{K_1} L + \frac{{K_2}^2}{2g{A_2}^2} \left[-\alpha_1 \left(\frac{A_2}{A_1} \right)^2 (1 - k_b) + \alpha_2 (1 - k_b) \right]} \right)^{1/2} \quad 5.8$$

The results from the SAM demonstrates that the segment with the greatest amount of discharge is the segment upstream from the junction at the main channel (MC-A). The peak discharges computed for the two reaches downstream from the junction at the main channel (MC-B and MC-C) are relatively similar, since no water is being diverted from the system between those two reaches. If the continuity equation (Equation 3.7) is applied at the junction with the discharges computed using the SAM, the equation is not satisfied (i.e., the equation is not equal to zero). The outflow discharges at the junction (MC-B and LC-A) are similar, but the inflow is much higher, violating the continuity law. This can be attributed to the fact that just downstream from the junction, an inline weir is located within the main channel, with the purpose of raising the water level at the main channel in order to increase the amount of flow diverting to lateral channel M-63. Therefore, a backwater effect is produced and the difference in water surface elevation of the reach MC-A is of one order of magnitude in comparison to the other reaches. The discharge computations for the reach MC-A are presented in Table 5.4, but were not used since they are not reliable due to the backwater effect produced by the inline weir.

The difference in discharges between the two segments at lateral channel M-63 (LC-A and LC-B) can be attributed to the fact that a diversion channel exists between both reaches. But, this outflow discharge can be neglected since, as observed in the field, the head of water about the weir crest was almost zero.

Table 5.4. Discharge computations for the Slope-Area Method at the five pairs of cross-section surveyed at the Lajas Valley Irrigation District System*.

Reach ID	Section	L (m)	B (m)	m_{rigth}	m_{left}	y (m)	A (m^2)	P (m)	R (m)	n_e	K	α	Δh (m)	S_o	Q_{mean} (m^3/s)	V_{mean} (m/s)	h_v (m)	Δh_v (m)	h_f (m)	S	k_b	Q_{peak} (m^3/s)
MC-A	1	89.68	1.289	1.578	1.646	0.610	1.386	3.603	0.385	0.0361	20.313	1.1426	0.621	0.00692	2.334	1.684	0.1651	0.101	0.722	0.0081	0.5	2.435
	2		1.289	1.578	1.646	0.842	2.227	4.482	0.497	0.0361	38.714					1.048	0.0639					
MC-B	1	19.48	1.223	1.449	1.592	0.457	0.877	2.887	0.304	0.0590	6.707	1.1434	0.026	0.00133	0.225	0.257	0.0038	-0.001	0.025	0.0013	0	0.222
	2		1.479	1.681	1.525	0.381	0.796	2.918	0.273	0.0590	5.670					0.283	0.0047					
MC-C	1	31.78	1.641	1.577	1.577	0.432	1.003	3.254	0.308	0.0361	12.686	1.1426	0.014	0.00044	0.247	0.246	0.0035	-0.001	0.013	0.0004	0	0.238
	2		1.459	1.577	1.577	0.419	0.888	3.023	0.294	0.0361	10.874					0.278	0.0045					
LC-A	1	21.26	0.848	1.571	1.590	0.305	0.406	1.989	0.204	0.0150	9.374	1	0.015	0.00071	0.259	0.639	0.0208	0.003	0.018	0.0008	0.5	0.272
	2		0.761	1.758	1.820	0.324	0.434	2.089	0.208	0.0150	10.166					0.597	0.0182					
LC-B	1	31.20	1.097	1.344	1.556	0.298	0.456	2.147	0.212	0.0150	10.814	1	0.107	0.00343	0.288	0.631	0.0203	-0.169	-0.062	-0.0012	0	0.179
	2		0.897	1.563	1.656	0.134	0.149	1.405	0.106	0.0150	2.229					1.928	0.1895					

*See the notation list to define the symbols used at the table.

The second method used to measure the discharge was the inline weir equations. Two inline weirs were found. One inline weir was located downstream from the junction at the main channel. The schematic of the characteristics of this trapezoidal-rectangular weir are illustrated in Figure 5.12. The measurements of the weir and the water depth at the weir were surveyed during the field trip. A photo of this weir is shown in Figure 5.13. This weir can be simulated as two half-trapezoidal weirs with a crest length of 4.3 ft (1.31 m), which is the same as one full-trapezoidal weir with a crest length of 4.3 ft (also known as a Cipoletti weir). The water depth measurement at the center of the weir was 41.5 in (1.054 m) for the flow conditions during the field visit. The effective discharge coefficient for a Cipolleti (trapezoidal) weir is commonly taken as 3.367 (USBR 2001), and the weir length and head above the weir are input in feet. Using a crest length of 4.3 ft and a head above the weir of 0.669 ft (0.204 m), the discharge through the weir was computed using Equation 4.2, resulting in 7.93 cfs (0.225 cms). This value is very similar to the discharge obtained for this same segment (MC-B) using the SAM (i.e., it only varies at the third decimal value).

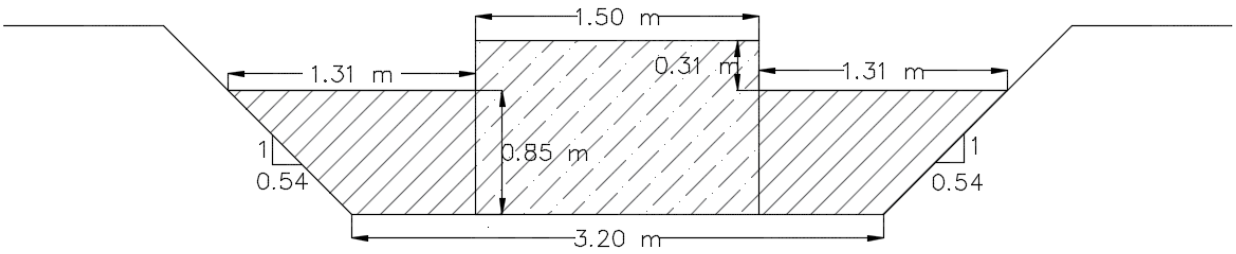

Figure 5.12. Characteristic and measurements of the weir located immediately downstream of the junction at the AOI main channel of the Lajas Valley Irrigation District System.

Figure 5.13. Inline weir located at the main channel downstream from the junction between the main channel and the lateral channel M63 at the Lajas Valley Irrigation District System.

The second inline weir is located at the upstream portion of lateral channel M-63. This weir is preceded by a stilling basin, as shown in Figure 5.14. The weir has a trapezoidal shape with a crest length of 6 ft (1.829 m). A calibrated ruler placed on the stilling basin was used to determine the water depth preceding the weir. Along with the crest height, the head above crest weir was computed as 0.32 ft (9.75 cm). Using the same effective discharge coefficient as the previous weir (3.367) and Equation 4.2, the discharge through the weir that flows downstream lateral channel M-63 was computed as 3.66 cfs (0.104 cms). Using the continuity equation (Equation 3.7), the inflow discharge at the main channel upstream from the junction was computed as 11.59 cfs (0.329 cms).

Figure 5.14. Stilling basin and trapezoidal weir located at lateral channel M-63 at the Lajas Valley Irrigation District System.

6 CHAPTER – MODELING ENVIRONMENT

The Simultaneous Solution Method (SSM) algorithm was programmed using the MATLAB computer language (Moler 2004). MATLAB started as a simple matrix laboratory in 1979. It was mostly employed as a teaching aid for students at Stanford University. This first version was based on the Fortran computing language, but was not particularly powerful (Moler 2004). According to Moler (2004), in 1981 MATLAB was reprogrammed in the C computing language and became a commercial product, with more stored programmed functions, toolboxes and more powerful graphics. Now, it is a full-featured technical computing environment. The next section describes the SSM algorithm and how it was divided into different subroutines. Finally, the graphical user interface (GUI) that was developed to aid the user interaction with the algorithm is explained in more detail.

6.1 Simultaneous Solution Method Algorithm

The SSM algorithm was divided into 5 subroutines. The first subroutine is the principal script that reads the input variables, calls the other subroutines, performs the Newton-Raphson Solution method (NRSM), creates graphs, and writes the results. The second subroutine is responsible for assembling the nonlinear system of equations, expressed by Equation 3.3. This subroutine assigns the initial discharge and water depth at the system, computes the geometric parameters of the channel (i.e., flow area, hydraulic radius, etc.), and applies the required boundary conditions of the system, including the boundary conditions produced by lateral weirs and sluice gates found in the system. The third subroutine is the numerical solver algorithm for the system. The numerical solver could be either the Gauss Elimination Method or the Bi-conjugated Gradient Stabilizer with Preconditioner method. The solution of the numerical solver is the correction of the discharge and water depth at each section of the system. The fourth subroutine computes the water depth and discharge for the next iteration of the NRSM. This subroutine adds the corrections (i.e., solution of the numerical solver) to the corresponding values of water depth and discharge (i.e., current iteration values) to produce the modified values of water depth and discharge. The first subroutine (i.e., principal script) evaluates if the corrections produced by the third script (i.e., numerical solver) are less than a specified tolerance. If these corrections are less than the tolerance, the NRSM is finished and the modified water depth and discharge are the final values for the systems, if not, the NRSM is repeated using the corrected water depth and discharge as the initial values for the next iteration. The fifth, and last, subroutine was created to include the analysis/design of the inverted siphon hydraulic structure. This script is called after the system has converged to a final solution through the first subroutine. The five subroutines of

the SSM algorithm have been programed by the author and are self-contained, which means that they do not contain any function exclusive to MATLAB that could limit the use of the algorithm on different versions of MATLAB.

6.2 Graphical User Interface

A graphical user interface (GUI) was developed by the author to allow a user-friendly interaction with the numerical model. A screen-shot of the principal GUI for the algorithm is presented in Figure 6.1. The main features of the principal GUI are: 1) input the main characteristics and description of the system, 2) specify the channel properties, 3) describe the hydraulic structures within the system, 4) run the algorithm, and 5) graph the results using another GUI. Therefore, the user can input parameters, run the program, and plot the results without leaving the principal GUI. The following paragraphs explain every function of the main GUI.

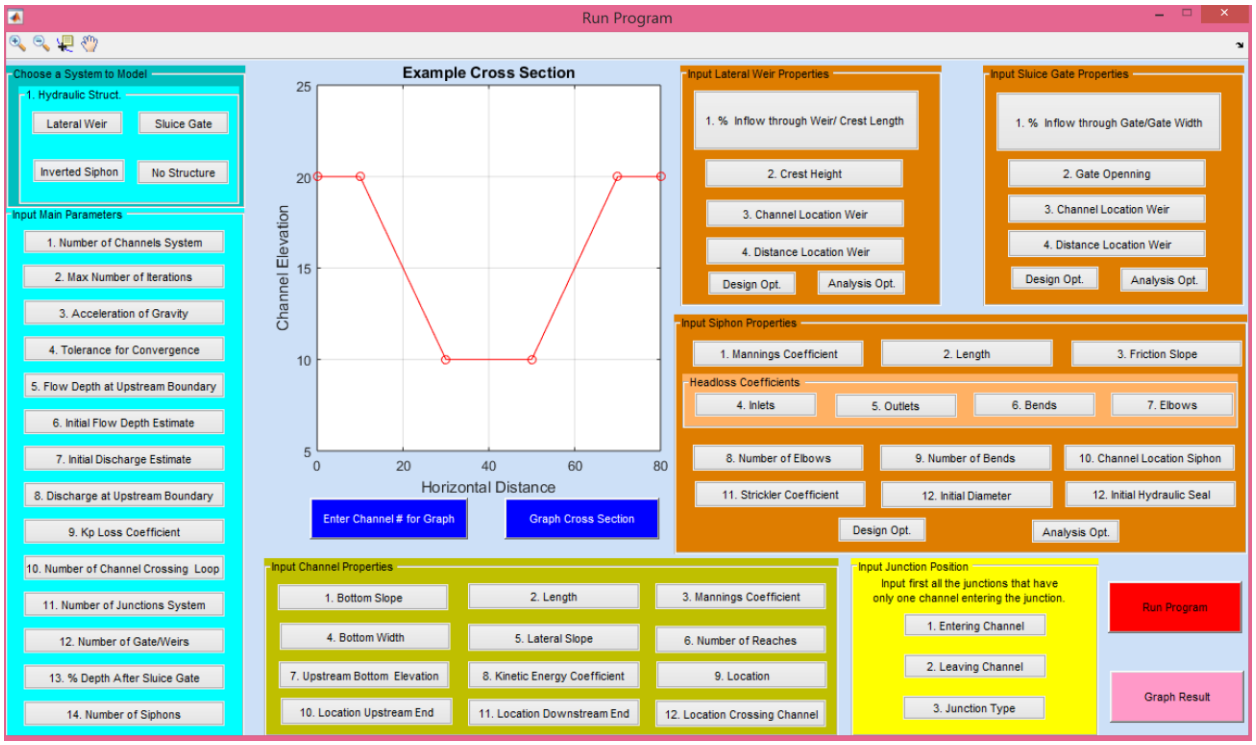

Figure 6.1. Screen-shot of the principal graphical user interface developed for the Simultaneous Solution Method algorithm.

Almost every function at the main GUI has a push button that opens a message box that requires the user to introduce the required value. Some examples of this are the "*Input Main Parameters*" menu, the "*Input Channel Properties*" menu, "*Input Junction Position*" menu, and the input of hydraulic structure properties (see Figure 6.1 for more details). The rest of the functions are classified as push buttons that performs some procedures in the background. The user must input the required information at the principal GUI from left to right and from top to bottom. The following order must be used to input the required information by the user: 1) "*Hydraulic Struct.*" box, 2) "*Input Main Parameters*" box, 3) "*Input Channel Properties*" box, 4) plot the desired cross-sections, 5) "*Input Junction Position*" box, 6) input the properties of the hydraulic structures within the system, 7) "*Run Program*" button, and 8) "*Graph Results*" button,

which opens a secondary GUI. The "Hydraulic Struct." Box was developed to specify to the algorithm the hydraulic structures that are present on the channel system. The user must select, by pressing the corresponding push button, the hydraulic structures within the system, no matter the amount.

The "*Input Main Parameters*" box specifies the main features of the system, which must be input in the numerical order of the box (from top to bottom). The following briefly explains the function of each button on this input box:

1. "*Number of Channels System*": input the total number of channels within the system.
2. "*Max Number of Iteration*": input the maximum number of iteration allowed for convergence of the NRSM. The algorithm has a default value of 100. But, the user can change the default value by choosing a value from 20 to 100.
3. "*Acceleration of Gravity*": input the constant of gravitational acceleration. This value indicates the algorithm the system of units being used. For example, if 9.81 is input as the acceleration of gravity, the algorithm establishes that the SI unit system (Metric System) will be used.
4. "*Tolerance for Convergence*": input the tolerance for convergence, which is used to compare with the corrections of the water depth and discharge values produced by the numerical solver. The algorithm has a default value of 0.0001. But, the user can change the default value by choosing a value from 0.01 to 0. 0001.
5. "*Flow Depth at Upstream Boundary*": input the water depth at the upstream boundary. This value is used in the upstream boundary equation (Equation 3.6).

6. "*Initial Flow Depth Estimate*": input the initial water depth estimate. The initial water depth is assumed to be the same in the entire system.

7. "*Initial Discharge Estimate*": input the initial discharge estimate. The initial discharge is distributed by the algorithm to each channel by satisfying the continuity equation at each junction. This depends on the channel configuration.

8. "*Discharge at Upstream Boundary*": input the discharge at the upstream boundary. This value is used at the upstream boundary equation (Equation 3.6).

9. "K_p *Loss Coefficient*": input the form loss coefficient for all junctions. Most of the time, this coefficient is assumed to be zero, but alternate values can be found in the literature.

10. "*Number of Channel Crossing Loop*": input the number of channels that are crossing between the upper and lower branch of the loop in a channel network (see Section 7.3 for an example).

11. "*Number of Junctions System*": input the total amount of junctions within the system. A junction is defined as a node that has three or more channels.

12. "*Number of Gate/Weirs*": input the total amount of lateral weir and sluice gates within the system.

13. "*% Depth After Sluice Gate*": input the percent of water depth from the water depth upstream the sluice gate, only if sluice gates are present on the system. This value

represents the tailwater depth after the sluice gate and is used to determine the flow conditions at the sluice gate (See Section 4.3 for more details).

14. "*Number of Siphons*": input the total amount of inverted siphons within the system.

The "*Input Channel Properties*" box specifies the main properties of each channel of the system. For a single channel, the following order of input properties must be followed. These properties should be input for one channel at a time. If more than one channel exists on the system, the channel properties should be input in the same manner and repeated, as necessary. If any of the properties vary along the channel, the channel must be divided into channels that have different properties along its length. The following briefly explains the function of each button on this input box:

1. "*Bottom Slope*": input the bottom slope of the channel in decimal form (i.e., 0.0005).
2. "*Length*": input the total length of the channel.
3. "*Manning's Coefficient*": input the Manning's roughness coefficient given to the entire channel.
4. "*Bottom Width*": input the channel bottom width.
5. "*Lateral Slope*": input the lateral slope. This input refers only to the horizontal component (*m*); the vertical component equals one (i.e., 1: *m*).
6. "*Number of Reaches*": input the number of desired reaches for the channel. A reach is defined by two successive sections separated by some distance. The total number of sections in a channel will be equal to the number of reaches in the channel plus

one. These sections will be separated by an equal distance between them, which will depend on the amount of reaches and the total channel length.

7. "*Upstream Bottom Elevation*": input the upstream bottom elevation, specified to compute the water surface elevation along the entire channel.

8. "*Kinetic Energy Coefficient*": input the kinetic energy coefficient, also known as the velocity-head coefficient (α).

9. "*Location*": input the id for the location of the channel within the system. For example, if the channel is located upstream from the first junction (i.e., from left to right) of a loop channel (See Figure 3.2), a value of 1 is given. If the channel is located downstream from the last junction of a loop channel, a value of 4 is given. On the other hand, a value of 2 is given if the channel is located on the upper branch of the loop channel. But, if the channel is located on the lower branch of the loop channel, a value of 3 is given. Finally, if the channel is crossing between the upper and lower branch of the loop channel, a value of 5 is given. This is necessary for the arrangement of the elements on the Jacobian Matrix (See Equation 3.3).

10. "*Location Upstream End*": input the junction id for the location of the upstream end of the channel. The value input for this parameter is with respect to the junction numbers. Therefore, if junction #1 is located at the upstream end of a channel, then the input value will be 1. If the channel does not connect to a junction (node with three or more channels) on the upstream end, a value of 0 is given.

11. "*Location Downstream End*": input the junction id for the location of the downstream end of the channel. The value input for this parameter is with respect to the junction numbers. Therefore, if junction #1 is located at the downstream end of a channel, then the input value will be 1. If the channel does not connect to a junction on the upstream end, a value of 0 is given.

12. "*Location Crossing Channel*": input the id for the location of the crossing channel. A value of 1 is given if downstream of the corresponding channel, another channel is crossing both branches of a loop channel. If the corresponding channel is crossing both branches of a loop channel, a value of 2 is given. If the corresponding channel has a downstream channel that can be considered as a series for both channels, a value of 3 is given. If none of these conditions are satisfied, a value of 0 should be input.

To plot a channel cross-section, the user selects the channel to graph, by pressing the button "*Enter Channel # for Graph*" and input the channel number of the desired channel. By pressing the button "*Graph Cross Section*", the channel cross-section will be plotted on the designated area.

The "*Input Junction Position*" box specifies the properties of each junction. The junctions that will be input first are the junctions classified as "outflow junction", which is defined as a junction that has more channels leaving than channels entering the junction. An "inflow junction" is defined as a junction that has more channels entering than channels leaving the junction. A "neutral junction" is defined as a junction that has the same number of channels

entering and channels leaving the junction. First, all the numbers of the channels that are entering the junction are input. Next, all the numbers of the channels that are leaving the junction are input. For example, if a junction has Channel #2 and Channel #3 as leaving channels and Channel #1 as an entering channel, the "*Entering Channel*" button is pressed and the value of 1 should be given. In addition, the "*Leaving Channel*" button is pressed twice, and the values given for each press is 2 and 3, respectively. Finally, the junction type is input, in which a value of 100 is given for an "outflow junction", -100 for an "inflow junction", and 200 for "neutral junction". Then, this input information is repeated for all the inflow junctions of the system, followed by all the junctions that are classified as neutral junction.

The "*Input Lateral Weir Properties*" and "*Input Sluice Gate Properties*" boxes are used to provide the features of these hydraulic structures. If the design option is desired for a lateral weir, the percent of inflow that will go through the weir (in decimal format) is input first. But, if the analysis option is desired, the effective crest length of the lateral weir should be given. In a similar manner, if the design option is desired for a sluice gate, the percent of inflow that will go through the gate (in decimal format) is input first. On the other hand, if the analysis option is desired, the gate width of the sluice gate should be given. Next, the crest height of a lateral weir or the gate opening of a sluice gate is specified, followed by the channel location of the weir or gate. This value represents the channel number where the gate or weir is located. Next, the distance from the beginning of the channel until the weir or gate location is specified. Finally, the "*Design Opt.*" or "*Analysis Opt.*" button is pressed, according to the desired procedure. This should be repeated for all the lateral weirs and sluice gates that the system may have. It is

important to input all the features of a sluice gate or a lateral weir before moving to another structure.

If any inverted siphon is located at the system, the "*Input Siphon Properties*" box must be filled. This box includes all the required properties for an analysis or design of an inverted siphon. The parameters should be input on the following order: 1) Manning's roughness coefficient, 2) length of the siphon, 3) friction slope (also known as siphon bottom slope), 4) head loss coefficient for the different form losses (i.e., inlet, outlet, bend and elbows), 5) number of elbows within the siphon, 6) number of bends within the siphon, 7) channel number upstream the location of the siphon, 8) Strickler coefficient, 9) initial estimate of the siphon diameter, and 10) initial estimate of the hydraulic seal. Finally, the "Design Opt." or "Analysis Opt." button is pressed, according to the desired procedure.

After all the input parameters are given to the algorithm through the GUI, the button "*Run Program*" is pressed, which will run the algorithm. If the algorithm converges to a final solution successively, a message will appear on the screen confirming that the program successfully ran. If not, an error message will be displayed on the command window of MATLAB. If the user desires to plot and view the results, the button "*Graph Results*" should be pressed. This button will open a secondary GUI, which is shown in Figure 6.2. This secondary GUI was developed to aid the visualization of the results and to export the graph as pairs of coordinates. The results plotted are the water surface elevations along the longitudinal distance of the channel, also known as a water surface profile. The water surface profile can be plotted for one or more consecutive channels. First, the channel number to be plotted is specified. If the user wants to plot more than one channel, a space must be introduced between channel numbers. Second, the

number of the channel section that is being plotted is given. In a similar manner, if more than one channel is plotted, a space must be introduced between channel reaches. Third, the button "*Plot Results*" is pressed and the graph will be displayed on the designated area with its corresponding coordinates and axes limits. Finally, to export the results as pairs of coordinates, the button "*Export Results*" is pressed and a file with an extension .txt will be recorded to the working directory of MATLAB.

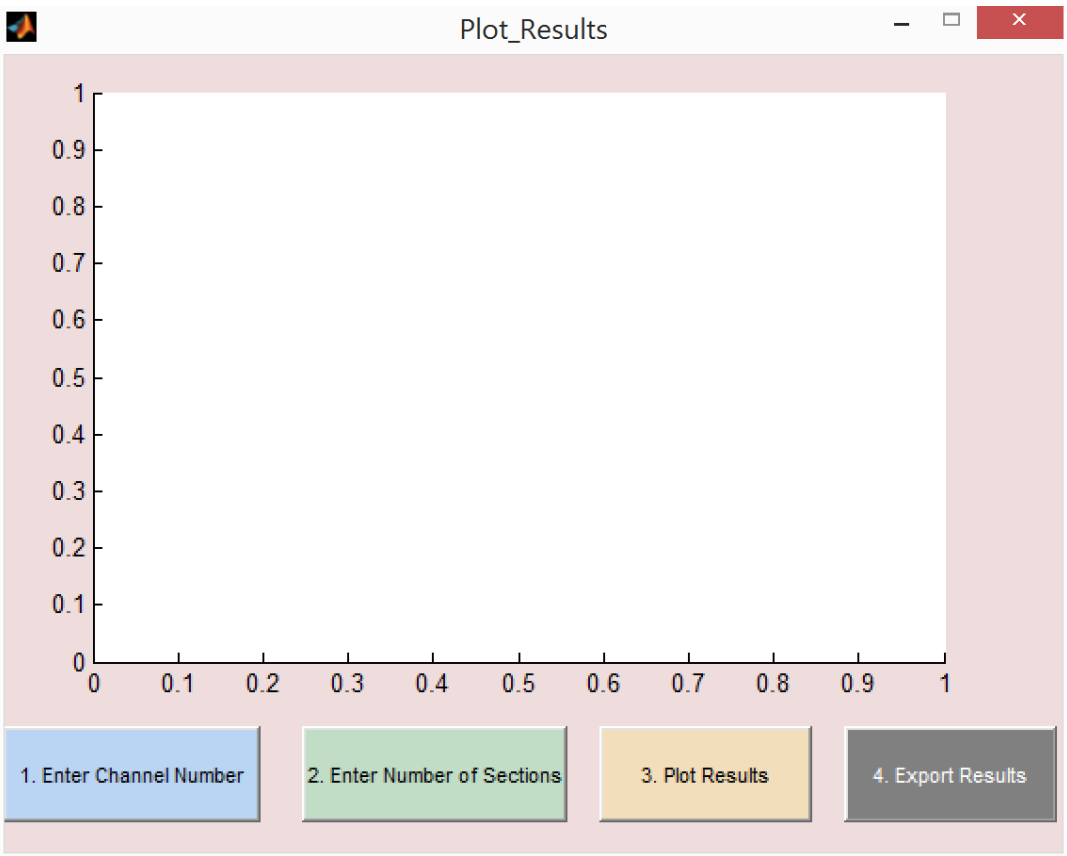

Figure 6.2. Screen-shot of the secondary graphical user interface developed to graph and export the results from the Simultaneous Solution Method algorithm.

7 CHAPTER – EXAMPLES AND CASE STUDY

Three channel systems and one case study are presented to demonstrate the capability of the new SSM algorithm. The first example is a series channel system with lateral weirs. Second, is a parallel channel system with lateral weirs. The third example is a complex channel network with lateral weirs, sluice gates and inverted siphons. Finally, a segment of the Lajas Valley Irrigation District System is presented as a real-life case study.

7.1 Series Channel System

A "series channel system" can be defined as multiple channels that are connected to each other in a successive manner. The series channel system presented here consists of three main trapezoidal concrete channels and six lateral weirs. These channels have the same geometric properties and are subdivided into a total of nine channels. At a lateral weir location, the channel is divided into two sub-channels with the same properties. Figure 7.1 illustrates the series channel system, in which the assumed flow direction is shown with arrows. Table 7.1 shows details of the geometry and roughness for each channel. Since the case study is a series of channels, the continuity equation (Equation 3.2) may be neglected because the discharge will remain constant on the entire channel. Therefore, this channel system encompasses a total of 69 unknowns to be solved. Each section of the channel system will have one unknown to be solved for, water depth. This channel system configuration produces a Jacobian matrix of 69-by-69, with a bandwidth (i.e., maximum separation between nonzero elements) of two. Each channel is identified with the letter C and a number. Lateral weirs are identified for analysis or design according to their subscript *A* and *D*, respectively. For this case, all the lateral weirs were

designed. The notation for the lateral weir refers to the channels that are located upstream and downstream from that lateral weir. For example, W3-4D refers to a weir between channels 3 and 4 that is to be designed. Table 7.2 shows the geometry and design type of each lateral weir used for this case study. Values with an asterisk are obtained from the results of the design or analysis using the SSM. The upstream boundary discharge and initial depth were 399.5 cms and 8.0 m, respectively. Also, a velocity-head coefficient of 1.0 was assumed for all the channels and the form loss coefficient was set to zero. A tolerance for convergence was specified at 0.0001 and the maximum number of iterations was established at 25. Results will be shown with four decimal places with the purpose of comparing the results.

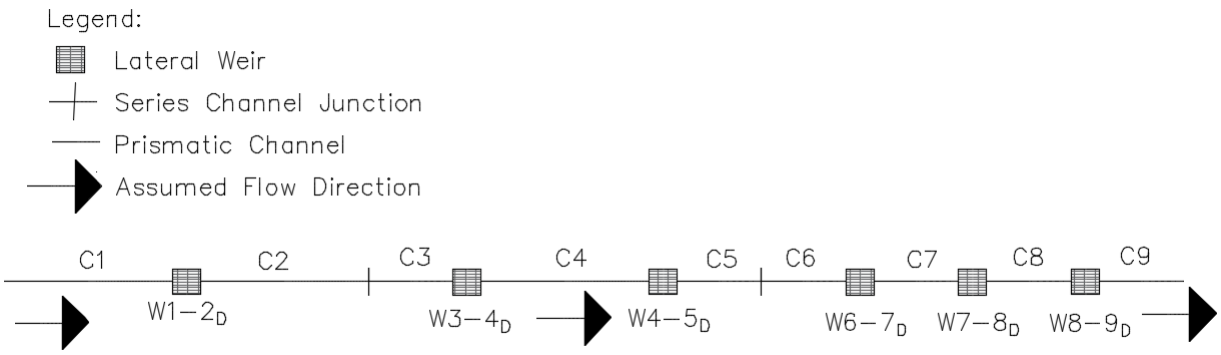

Figure 7.1. Schematic of the series channel system.

Table 7.1. Geometric and roughness properties of the series channel system.

Channel ID	Channel Length (m)	Bottom Slope (m/m)	Manning's Roughness Coefficient	Bottom Width(m)	Lateral Slope (m/m)	Number of Reaches	Upstream End Channel Bottom Elevation (m)
C1	1000	0.0001	0.020	10	1:1.5	10	100
C2	1000	0.0001	0.020	10	1:1.5	10	99.90
C3	500	0.0003	0.018	9	1:1	5	99.80
C4	1000	0.0003	0.018	9	1:1	10	99.65
C5	500	0.0003	0.018	9	1:1	5	99.35
C6	500	0.0005	0.016	8	1:0.75	5	99.20
C7	500	0.0005	0.016	8	1: 0.75	5	98.95
C8	500	0.0005	0.016	8	1: 0.75	5	98.70
C9	500	0.0005	0.016	8	1: 0.75	5	98.45

Table 7.2. Summary of the geometry and results of the lateral weirs on the series channel system.

Lateral Weir ID	Type	Crest Height (m)	Weir Length (m)	Weir Flow (m^3/s)	Flow through weir (%)
W1-2	Design	6.8	71.82*	99.88	25
W3-4	Design	6.6	34.58*	59.93	20
W4-5	Design	6.4	15.01*	43.15	18
W6-7	Design	6.8	11.78*	31.45	16
W7-8	Design	6.8	6.78*	23.11	14
W8-9	Design	6.8	4.08*	17.04	12
*Values that were output from the Simultaneous Solution Method					

7.2 Parallel Channel System

A parallel channel system contains a loop within its system. A parallel channel with 5 lateral weirs and 11 trapezoidal concrete channels with different geometries was solved. Figure 7.2 shows the parallel channel system. The assumed flow directions are shown with arrows. This channel system encompasses 80 unknowns to be solved, from which, half the variables are related to water depth and the other half to discharge. Each section of the channel system will have two unknowns to be solved for water depth and discharge. Therefore, the Jacobian matrix for this system will be 80-by-80 matrix, with a bandwidth of seven, shown in Appendix 1. Table 7.3 shows details of the geometry and roughness for each channel. Table 7.4 shows the geometry, as well as the design or analysis type for each lateral weir used on the loop channel system. The upstream boundary discharge and initial depth were 250 cms and 5.0 m, respectively. Also, a velocity-head coefficient of 1.0 was assumed for all the channels; the form loss coefficient was set to zero. A tolerance for convergence was specified at 0.0001 and the maximum number of iterations was established at 100.

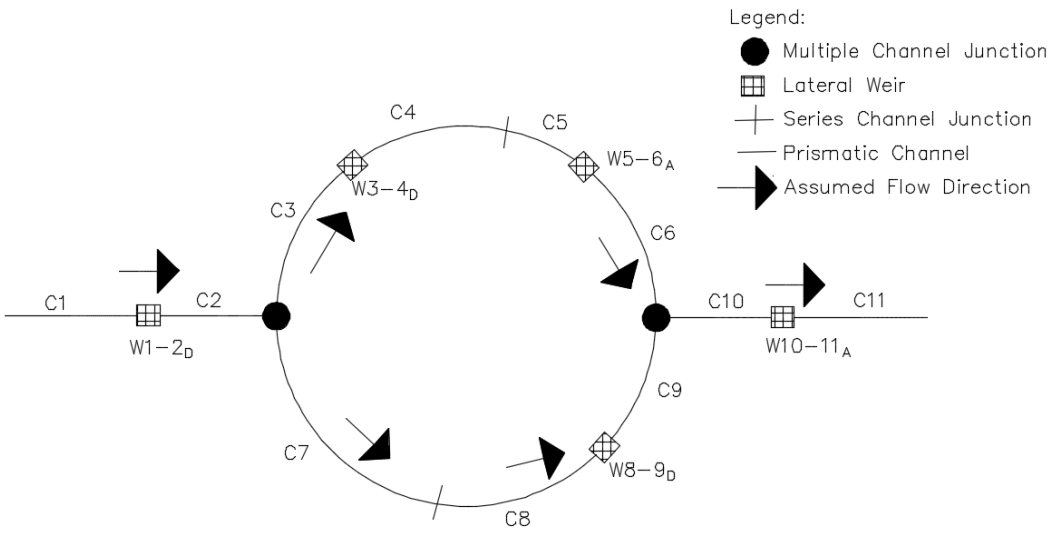

Figure 7.2. Schematic of the parallel channel system.

Table 7.3. Geometric and roughness properties of the parallel channel system.

Channel ID	Channel Length (m)	Bottom Slope (m/m)	Manning's Roughness Coefficient	Bottom Width(m)	Lateral Slope (m/m)	Number of Reaches	Upstream End Channel Bottom Elevation (m)
C1	100	0.0001	0.013	50	1:1.5	2	99.87
C2	100	0.0001	0.013	45	1:1.5	2	99.86
C3	200	0.0005	0.012	30	1:1.5	4	99.85
C4	100	0.0005	0.012	25	1:1.5	2	99.75
C5	100	0.0005	0.012	20	1:1.5	2	99.70
C6	100	0.0005	0.014	20	1:1.5	2	99.65
C7	200	0.0005	0.013	40	1:1.5	5	99.85
C8	200	0.0005	0.014	35	1:1.5	4	99.75
C9	100	0.0005	0.014	30	1:1.5	2	99.65
C10	100	0.0001	0.015	20	1:1.5	2	99.60
C11	100	0.0001	0.015	20	1:2.0	2	99.59

Table 7.4. Summary of the design and analysis of the lateral weir on the parallel channel system.

Lateral Weir ID	Type	Crest Height (m)	Weir Length (m)	Weir Flow (m^3/s)	Flow through weir (%)
W1-2	Design	4	26.2*	37.5	15
W3-4	Design	4.5	13.26*	9.67	10
W5-6	Analysis	4.5	11.51	10.32	12*
W8-9	Design	4.5	14.1*	12.74	11
W10-11	Analysis	4.5	18.22	16	9*
*Values that were output from the Simultaneous Solution Method					

7.3 Complex Channel Network System

A channel network system exists when a channel crosses the upper and lower branch of a loop channel. This example presents a complex channel network with 4 lateral weirs, 4 sluice gates, 2 inverted siphons and 10 trapezoidal concrete channels with different geometries, as shown in Figure 7.3. The assumed flow directions are shown with arrows. This channel system encompasses a total of 120 unknowns to be solved, in which half are variables of water depths and the other half are discharges. Each section of the channel system, will have two unknowns to be solved for, water depth and discharge. Therefore, the Jacobian matrix for this system will be a 120-by-120 matrix with a bandwidth of 54. Table 7.5 shows details of the geometry and roughness for each channel. Table 7.6 and

Table 7.7 show the geometry and design or analysis type of each lateral weir or sluice gate used for the channel network system, respectively. The notation for the lateral weir refers to the channel were the lateral weir is located, similarly for the sluice gates and inverted siphon location. Table 7.8 shows the geometry and design or analysis type of each inverted siphon used for the channel network system. The upstream boundary discharge and initial depth were 400 cms and 7.0 m, respectively. Also, a velocity-head coefficient of 1.0 was assumed for all the channels; the form loss coefficient was set to zero. A tolerance for convergence was specified at 0.0001 and the maximum number of iterations was established at 100. The percent of water depth from the water depth before the sluice gate (i.e., tailwater depth) was specified to be 20%. The head loss coefficients for the siphon inlet and outlet were specified at 0.1 and 0.2, respectively, and no elbows or bends were included on the siphon. In addition, the Strickler coefficient was set to 70 $m^{1/3}/s$ for both inverted siphons. This example could not be modeled using the HEC-RAS software, since it is limited to series and parallel channel systems. Therefore, a comparison between the SSM and the StdSM could not be established.

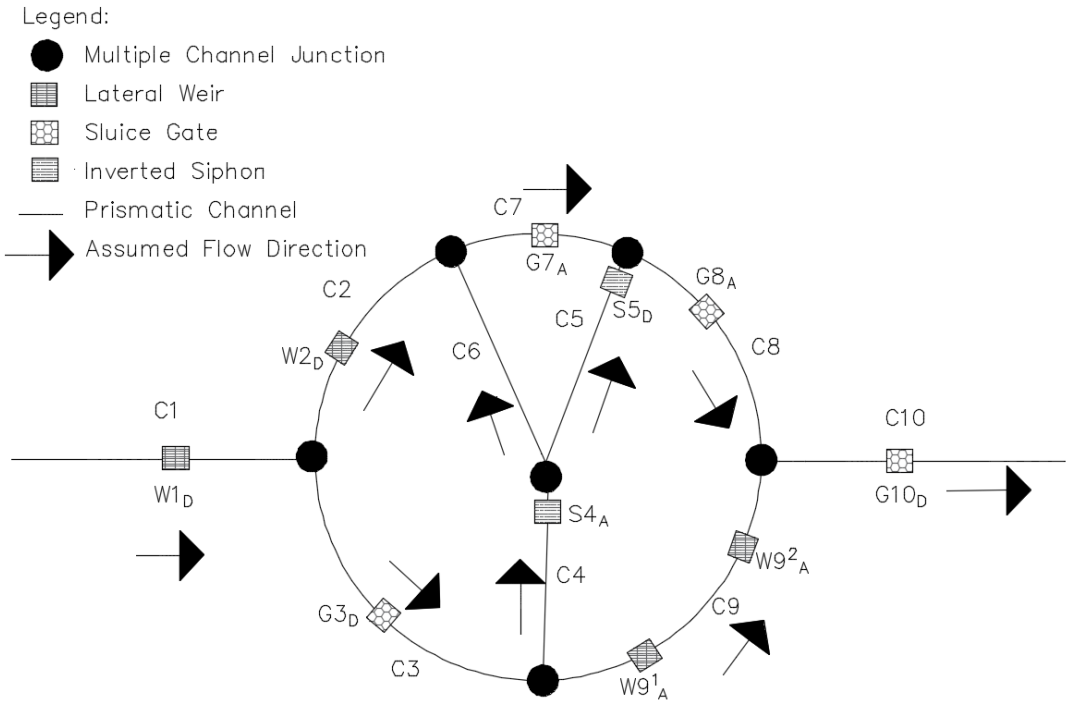

Figure 7.3. Schematic of the complex channel network system.

Table 7.5. Geometric and roughness properties of the complex channel network system.

Channel ID	Channel Length (m)	Bottom Slope (m/m)	Manning's Roughness Coefficient	Bottom Width (m)	Lateral Slope (m/m)	Number of Reaches	Upstream End Channel Bottom Elevation (m)
C1	600	0.0001	0.015	50	1:1.5	5	100.0
C2	400	0.0005	0.013	30	1:1.5	5	99.94
C3	200	0.0005	0.014	40	1:1.5	5	99.94
C4	100	0.0005	0.015	25	1:1.5	5	99.84
C5	200	0.0005	0.013	20	1:1.5	5	99.79
C6	100	0.0005	0.014	30	1:1.5	5	99.79
C7	100	0.0005	0.013	30	1:1.5	5	99.74
C8	200	0.0005	0.013	20	1:1.5	5	99.69
C9	500	0.0005	0.014	35	1:1.5	5	99.84
C10	600	0.0001	0.015	50	1:1.5	5	99.59

Table 7.6. Summary of the design and analysis of the lateral weir on the complex channel network system.

Lateral Weir ID	Type	$Dist_{Ch}$ (m)$^{+}$	Crest Height (m)	Weir Length (m)	Weir Flow (m^3/s)	Flow through weir (%)
W1	Design	360	6.0	27.15*	40.0	10
W2	Design	160	6.0	12.41*	21.66	15
W9[1]	Analysis	100	6.5	11.5	9.26	6.25*
W9[2]	Analysis	400	6.4	10.0	12.87	9.04*

*Values that were output from the Simultaneous Solution Method
$^{+}$ Distance from Upstream end of the Channel to weir location.

Table 7.7. Summary of the design and analysis of the sluice gates on the complex channel network system.

Sluice Gate ID	Type	$Dist_{Ch}$ (m)$^{+}$	Gate Opening (m)	Gate Length (m)	Gate Flow (m^3/s)	Flow through gate (%)
G3	Design	120	0.6	6.37*	25.87	12
G7	Analysis	100	0.5	5.0	17.28	15.35*
G8	Analysis	400	0.6	6.0	24.84	16.97*
G10	Design	240	0.7	8.57*	41.27	16

*Values that were output from the Simultaneous Solution Method

$^{+}$ Distance from Upstream end of the Channel to weir location.

Table 7.8. Summary of the design and analysis of the inverted siphon on the complex channel network system.

Parameter/ Inverted Siphon ID	S4	S5
Type	Analysis	Design
Manning's Roughness Coefficient	0.015	0.015
Length (m)	60	80
Bottom Slope (m/m)	0.002	0.004
Friction Slope (m/m)	0.0015*	0.0017*
Diameter (m) {ft}	4.57 {15}	4.648 {15.25} *
Hydraulic Seal (m)	0.7	0.68*
Available Head (m)	0.0010*	0.003*
Total Head loss (m)	0.20*	0.26*
Operational Flow (m^3/s)	45.86*	50.71*
Operational Flow Velocity (m/s)	2.80*	3.0*
Design Flow (m^3/s)	53.45*	50.71*
Design Flow Velocity (m/s)	3.26*	3.0*

*Values that were output from the Simultaneous Solution Method

7.4 Lajas Valley Irrigation District System

A segment of the Lajas Valley Irrigation District System (LVIDS) was selected to be modeled as a series channel. The LVIDS case study consists of two trapezoidal concrete channels joined by a lateral weir at channel M-63. However, the situation becomes complicated by the existence of an inline-weir just downstream of the lateral weir, in channel C2. Figure 7.4 presents the schematic of this junction, whereas Figure 5.4 shows the schematic of the AOI. The upper end of channel C1 is 168.36 m upstream of the junction between the main channel and lateral channel M-63. Section MC-AU was surveyed at this point (See Figure 5.4 for more details). The downstream end of channel C2 is located upstream of the inverted siphon #14, which is named "Ramón Toro", located on the main channel (See Figure 5.4). Table 7.9 shows details of the geometry and roughness for each channel. Table 7.10 shows the geometry and analysis of the lateral weir found at the junction between the main channel and lateral channel M-63. These values were obtained from field survey, granulometric analysis, and discharge calculations (See Chapter 5). The water depth measurements in the main channel downstream of the junction (Section MC-B and MC-C on Table 5.4), were used to calibrate the numerical model. Two parameters were calibrated: effective discharge coefficient for the trapezoidal inline weir and the equivalent Manning's roughness coefficient. The initial estimate of the equivalent Manning's roughness coefficient is shown in Table 7.9 and the initial effective discharge coefficient for the trapezoidal inline weir was established at 3.367 (See Section 5.4 for more details). These values will be updated during the calibration.

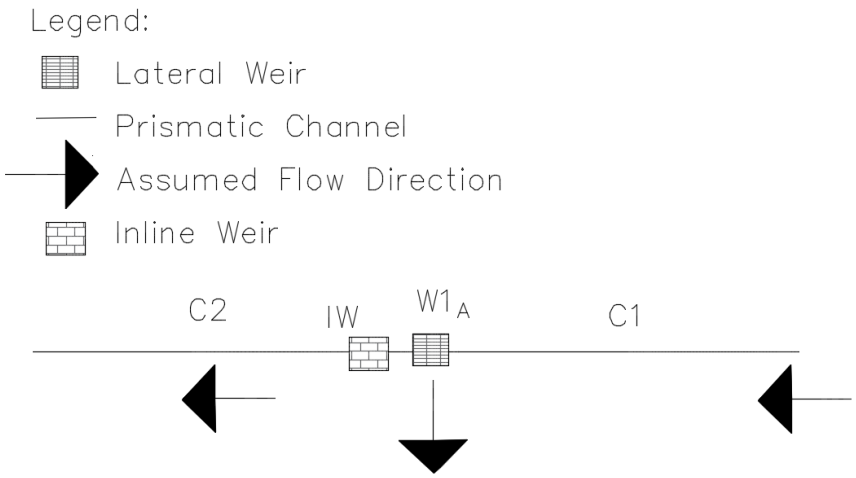

Figure 7.4. Schematic of the junction at channel M63 at the Lajas Valley Irrigation District System.

Table 7.9. Geometric and roughness properties of the channels at the Lajas Valley Irrigation District System.

Channel ID	Channel Length (m)	Bottom Slope (m/m)	Manning's Roughness Coefficient	Bottom Width (m)	Lateral Slope (m/m)	Number of Reaches	Upstream End Channel Bottom Elevation (m)
C1	168.36	0.0007	0.047	1.29	1:1.62	15	47.325
C2	310.84	0.0007	0.047	1.64	1:1.58	15	47.207

Table 7.10. Summary of the analysis and geometry of the lateral weir on the Lajas Valley Irrigation District System.

Lateral Weir ID	Type	Crest Height (m)	Weir Length (m)	Weir Flow (m^3/s)	Flow through weir (%)
$W1_A$	Analysis	0.585	1.829	0.1035*	31.5*

*Values that were output from the Simultaneous Solution Method

The inline weir creates a discontinuity in the water profile and introduces one additional unknown into the system of equations, the water depth downstream of the weir. To provide a solution, a new equation was added to the system. The equation assumes that the water depth downstream of the inline weir can be obtained from Manning's equation, while the flow discharge is governed by the weir equation (Equation 4.2). Equating the weir equation and the Manning's equation results in (Equation 7.1):

$$F_{i,k} = \left(C_e L_w H^{3/2}\right) - \left(\frac{C_o}{n_i} A_{i,j+1} {R_{i,j+1}}^{2/3} {S_i}^{1/2}\right) = 0 \qquad 7.1$$

This equation is applied between the first cross-section of channel C2 and a new cross-section added immediately downstream of the inline weir. This approximation provides the equation needed to solve the system. Two partial derivatives of Equation 7.1, one with respect to water depth and another with respect to discharge are added to the Jacobian matrix.

This channel system encompasses a total of 32 unknowns to be solved, all pertaining to water depth at each section of the channel system. The Jacobian matrix is 32-by-32, with a bandwidth of two. The upstream boundary discharge and initial depth were 0.329 cms and 0.61 m, respectively (See Chapter 5 for more details). Also, a velocity-head coefficient of 1.143 was computed for the two channels within the system. The form-loss coefficient was set to zero. A tolerance for convergence was specified at 0.0001 and the maximum number of iterations was established at 100.

8 CHAPTER – RESULTS, ANALYSIS AND DISCUSSION

A procedure to compare the results obtained between different methodologies is explained next, followed by the results obtained for the series channel system and the parallel channel system. Both examples were modeled using the Standard Step Method (StdSM) and the Simultaneous Solution Method (SSM). The complex channel network system was only modeled using the SSM. Finally, the results obtained for the Lajas Valley Irrigation District System (LVIDS) are presented.

8.1 Comparison Procedure Between Different Methodologies

The results from the SSM were verified with results obtained with a model with similar characteristics developed in HEC-RAS. HEC-RAS uses the Standard Step Method (StdSM) for solving the flow depths and discharges (Brunner 2016). HEC-RAS is suitable for series and parallel channel systems, but it cannot solve for complex channel networks. Therefore, only the series channel system and parallel channel system were modeled using this software. HEC-RAS has different calculation tolerance for parameters. For the two examples modeled, the water surface and flow tolerances in HEC-RAS were set to 0.0001, which was the same tolerance for convergence of the SSM model. In addition, it has an optimization procedure for the split flow conditions that occur in parallel channels. This optimization procedure is based on determining the flow at each loop branch that satisfies the continuity equation, and verifying that the energy grade line elevation is the same at both the upstream and downstream junctions. With the optimized flows selected for each branch, the StdSM computes the water depth at each section

on the HEC-RAS model. HEC-RAS does not design lateral weirs or any hydraulic structure, it is only coded for analysis. Therefore, the lateral weirs selected for design in the SSM model were first dimensioned using the SSM and the results were provided to HEC-RAS. Both models were run with identical lateral weir dimensions.

Another comparison was performed using the Direct Step Method (DSM). Flow depths and discharges obtained from SSM and HEC-RAS were used as input to compute the reach lengths of each channel using the DSM (Equation 3.9). Results were compared with the exact lengths, which were provided as an input to the model. The error calculations were computed using Equation 8.1. This error calculations were compared between the two model's results (SSM and HEC-RAS). Figure 8.1 illustrates a schematic of the comparison performed between the results from the StdSM and the SSM using the DSM. In other words, the results (i.e., water depth and discharge) from the two methodologies (i.e., SSM and StdSM) cannot be compared directly between them, since these models were similar, not identical. Therefore, to establish a direct comparison, a third methodology (i.e., DSM) was required. The DSM methodology is explained in the section 3.3.

$$E_L = \left(\frac{L_{comp} - L_{given}}{L_{given}}\right) \times 100 \qquad 8.1$$

where:

L_{comp} = computed reach length using the DSM for the results of the SSM and StdSM (L),

L_{given} = reach length given to both methods (SSM and StdSM) (L), and

E_L = percent error for the reach length of each channel (L/L).

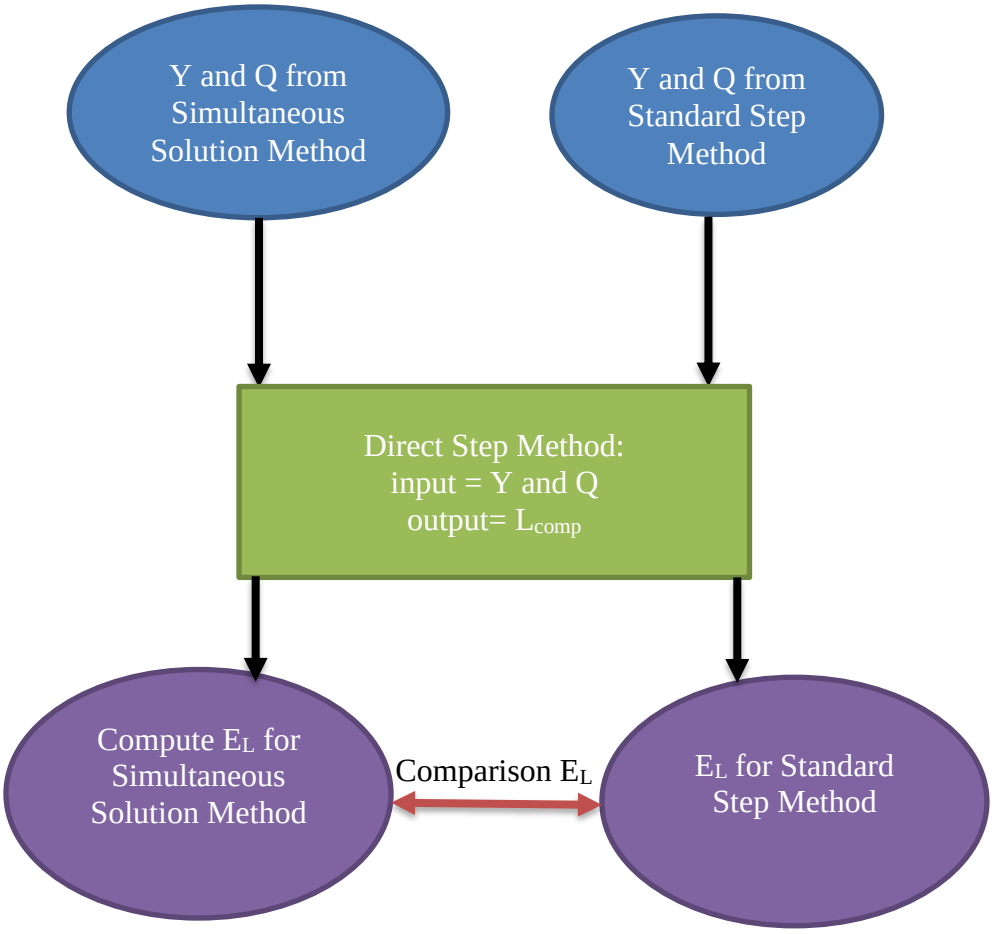

Figure 8.1. Schematic diagram showing the comparison between the results from the Simultaneous Solution Method and the Standard Step Method using the Direct Step Method.

8.2 Results for Series Channel System

The results for the series channel system were compared using water surface elevation (WSE) profiles and percent errors of reach lengths in each channel and reach. Table 8.1 presents the computed WSE at each channel section in the series system using the SSM, while Table 8.2 presents the computed WSE for the HEC-RAS model (StdSM).

Table 8.1. Computed water surface elevation and water depth for each channel of the series channel system using the Simultaneous Solution Method.

	Section	Distance (m)	Depth (m)	WSE (m)		Section	Distance (m)	Depth (m)	WSE (m)
Channel 1	1	0	8.0	108.0	Channel 2	1	0	7.9197	107.8197
Q=399.5	2	100	7.9804	107.9704	Q=299.625	2	100	7.9132	107.8032
m^3/s	3	200	7.9604	107.9404	m^3/s	3	200	7.9066	107.7866
	4	300	7.9400	107.9100		4	300	7.8999	107.7699
	5	400	7.9193	107.8793		5	400	7.8931	107.7531
	6	500	7.8982	107.8482		6	500	7.8863	107.7363
	7	600	7.8768	107.8168		7	600	7.8795	107.7195
	8	700	7.8549	107.7849		8	700	7.8726	107.7026
	9	800	7.8326	107.7526		9	800	7.8656	107.6856
	10	900	7.8098	107.7198		10	900	7.8585	107.6685
	11	1000	7.7867	107.6867		11	1000	7.8514	107.6514
	Section	Distance (m)	Depth (m)	WSE (m)		Section	Distance (m)	Depth (m)	WSE (m)
Channel 3	1	0	7.7348	107.5348	Channel 5	1	0	8.0786	107.4286
Q=299.625	2	100	7.7396	107.5096	Q=196.554	2	100	8.1002	107.4202
m^3/s	3	200	7.7445	107.4845	m^3/s	3	200	8.1218	107.4118
	4	300	7.7495	107.4595		4	300	8.1435	107.4035
	5	400	7.7545	107.4345		5	400	8.1653	107.3953
	6	500	7.7597	107.4097		6	500	8.1872	107.3872
	Section	Distance (m)	Depth (m)	WSE (m)		Section	Distance (m)	Depth (m)	WSE (m)
Channel 4	1	0	7.8637	107.5137		7	600	7.9592	107.4292
Q=239.7	2	100	7.8793	107.4993		8	700	7.9755	107.4155
m^3/s	3	200	7.8950	107.4850		9	800	7.9919	107.4019
	4	300	7.9109	107.4709		10	900	8.0085	107.3885
	5	400	7.9269	107.4569		11	1000	8.0252	107.3752
	6	500	7.9430	107.4430					
	Section	Distance (m)	Depth (m)	WSE (m)		Section	Distance (m)	Depth (m)	WSE (m)
Channel 6	1	0	8.1372	107.3372	Channel 7	1	0	8.3843	107.3343
Q=196.554	2	100	8.1778	107.3278	Q=165.105	2	100	8.4285	107.3285
m^3/s	3	200	8.2185	107.3185	m^3/s	3	200	8.4729	107.3229
	4	300	8.2595	107.3095		4	300	8.5173	107.3173
	5	400	8.3006	107.3006		5	400	8.5619	107.3119
	6	500	8.3419	107.2919		6	500	8.6065	107.3065
	Section	Distance (m)	Depth (m)	WSE (m)		Section	Distance (m)	Depth (m)	WSE (m)
Channel 8	1	0	8.6304	107.3304	Channel 9	1	0	8.8762	107.3262
Q=141.991	2	100	8.6767	107.3267	Q=124.952	2	100	8.9236	107.3236
m^3/s	3	200	8.7229	107.3229	m^3/s	3	200	8.9711	107.3211
	4	300	8.7693	107.3193		4	300	9.0186	107.3186
	5	400	8.8158	107.3158		5	400	9.0661	107.3161
	6	500	8.8623	107.3123		6	500	9.1137	107.3137

Table 8.2. Computed water surface elevation and water depth for each channel of the series channel system using the Standard Step Method (HEC-RAS model).

	Section	Distance (m)	Depth (m)	WSE (m)		Section	Distance (m)	Depth (m)	WSE (m)
Channel 1	1	0	8.0	108.0	Channel 2	1	0	7.9172	107.8172
Q=399.5	2	100	7.9806	107.9705	Q=279.5243	2	100	7.9129	107.8029
m^3/s	3	200	7.9606	107.9405	m^3/s	3	200	7.9087	107.7886
	4	300	7.9401	107.9102		4	300	7.9040	107.7742
	5	400	7.9194	107.8795		5	400	7.8997	107.7598
	6	500	7.8985	107.8485		6	500	7.8954	107.7454
	7	600	7.8770	107.8170		7	600	7.8910	107.7310
	8	700	7.8553	107.7852		8	700	7.8866	107.7165
	9	800	7.8328	107.7529		9	800	7.8820	107.7019
	10	900	7.8101	107.7202		10	900	7.8773	107.6874
	11	1000	7.7870	107.6870		11	1000	7.8727	107.6728
	Section	Distance (m)	Depth (m)	WSE (m)		Section	Distance (m)	Depth (m)	WSE (m)
Channel 3	1	0	7.7535	107.5536	Channel 5	1	0	8.1495	107.4994
Q=279.5243	2	100	7.7624	107.5323	Q=143.494	2	100	8.1751	107.4951
m^3/s	3	200	7.7711	107.5111	m^3/s	3	200	8.2008	107.4909
	4	300	7.7799	107.4900		4	300	8.2268	107.4868
	5	400	7.7890	107.4690		5	400	8.2526	107.4827
	6	500	7.7980	107.4481		6	500	8.2787	107.4786
	Section	Distance (m)	Depth (m)	WSE (m)		Section	Distance (m)	Depth (m)	WSE (m)
Channel 4	1	0	7.8958	107.5459		7	600	8.0178	107.4878
Q=202.955	2	100	7.9160	107.5359		8	700	8.0384	107.4785
m^3/s	3	200	7.9360	107.5261		9	800	8.0593	107.4692
	4	300	7.9565	107.5164		10	900	8.0801	107.4601
	5	400	7.9767	107.5067		11	1000	8.1012	107.4511
	6	500	7.9971	107.4972					
	Section	Distance (m)	Depth (m)	WSE (m)		Section	Distance (m)	Depth (m)	WSE (m)
Channel 6	1	0	8.2481	107.4480	Channel 7	1	0	8.5108	107.4608
Q=143.494	2	100	8.2935	107.4434	Q=97.147	2	100	8.5589	107.4589
m^3/s	3	200	8.3390	107.4389	m^3/s	3	200	8.6071	107.4571
	4	300	8.3844	107.4344		4	300	8.6553	107.4553
	5	400	8.4301	107.4301		5	400	8.7036	107.4536
	6	500	8.4759	107.4259		6	500	8.7519	107.4519
	Section	Distance (m)	Depth (m)	WSE (m)		Section	Distance (m)	Depth (m)	WSE (m)
Channel 8	1	0	8.7676	107.4676	Channel 9	1	0	9.0210	107.4711
Q=62.8753	2	100	8.8169	107.4670	Q=37.7451	2	100	9.0708	107.4709
m^3/s	3	200	8.8662	107.4663	m^3/s	3	200	9.1206	107.4707
	4	300	8.9155	107.4656		4	300	9.1704	107.4705
	5	400	8.9649	107.4650		5	400	9.2201	107.4702
	6	500	9.0143	107.4644		6	500	9.2701	107.4700

WSE profiles were plotted for the entire channel system length, which was 6,000 m. These profiles are presented in Figure 8.2. The continuous line are the results obtained with SSM and the dotted line are the results obtained with HEC-RAS. The WSE from both methods have similar behavior, but are slightly different in magnitude, particularly at the downstream end of the system (Channel IDs: C6, C7, C8 and C9). A water surface increase was obtained at the locations of the lateral weirs, as expected for subcritical flow (May et al. 2003). This behavior was observed on every location of the lateral weir. WSEs decreased at the junction due to changes in geometry of the two channels and local energy losses.

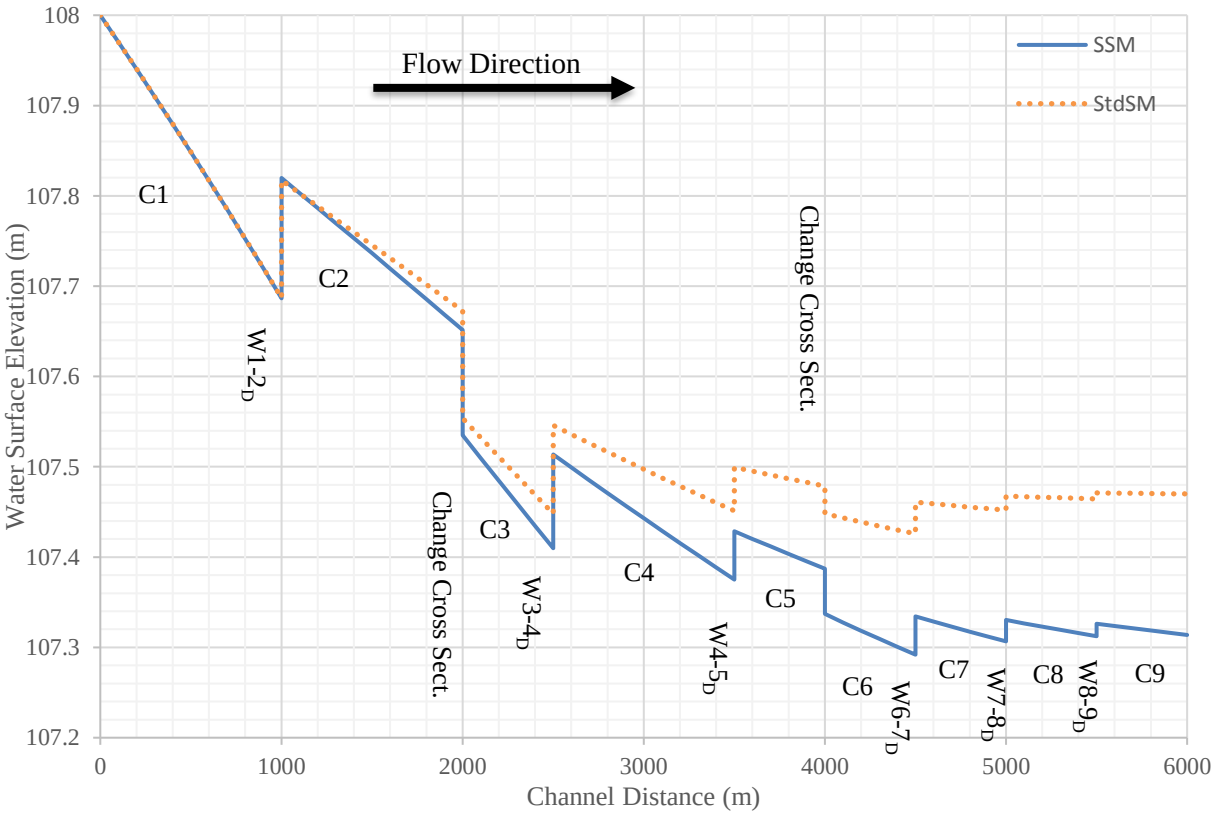

Figure 8.2. Water surface elevation profiles of the series channel system.

The relative errors in reach lengths obtained with this comparison is shown in Figure 8.3 for both models. The solid bars are the results obtained with SSM and the dotted bars are

the results obtained with HEC-RAS. This relative error in reach lengths was computed using Equation 8.1. The values of relative error for each reach and the entire channel are presented in Table 8.3

Table 8.3 for the SSM, while the values for the HEC-RAS model are illustrated in Table 8.4. The SSM had a lower percent error for the reach lengths in four of the nine channels than HEC-RAS (StdSM). SSM underestimated the reach length in 7 channels and overestimated in 2 channels, shown as negative and positive values, respectively, in Figure 8.3. On the other hand, StdSM underestimated the reach length in 5 channels and overestimated in 4 channels. The maximum percent error for the reach lengths for both models (SSM and StdSM) were found on channel #3, which was 0.158% for HEC-RAS model and -0.273% for the SSM. This channel (Channel ID: C3) has an upstream change in cross-section boundary condition and a downstream lateral weir boundary condition. The difference between errors for each channel can be as much as one order of magnitude. Since, this is a non-looped channel system, the percent error for reach length can be computed to the entire system. The percent error for the entire system using the SSM and the StdSM was -0.00077% and 0.03315%, respectively. Therefore, the SSM had less percent error for the entire length of the system than the StdSM.

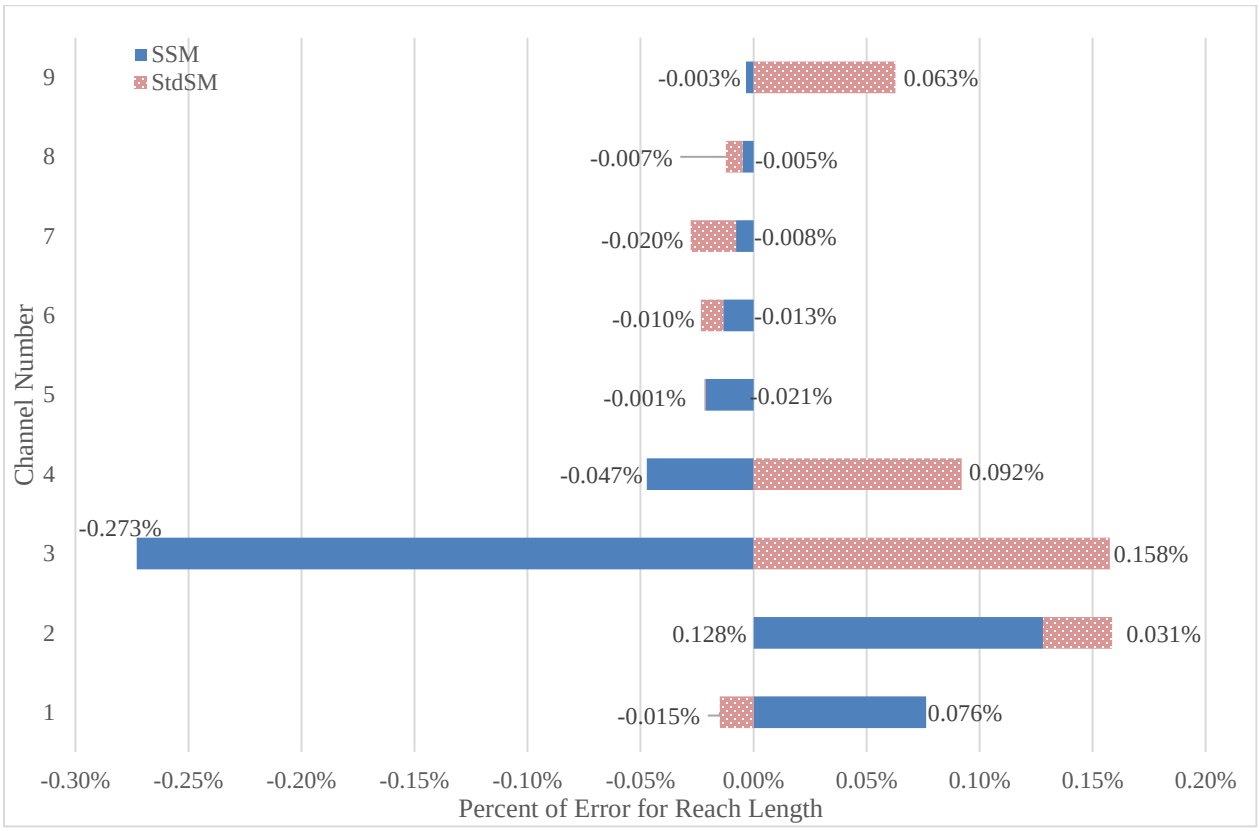

Figure 8.3. Percent error for reach lengths of both method results for the series channel system.

Table 8.3. Percent error for reach lengths of each channel for the series channel system using the Simultaneous Solution Method.

	Reach	L_{comp} (m)	E_L (%)		Reach	L_{comp} (m)	E_L (%)
Channel 1	1	100.0789	0.0789	Channel 2	1	100.1315	0.1315
	2	100.0783	0.0783		2	100.1307	0.1307
	3	100.0778	0.0778		3	100.1299	0.1299
	4	100.0772	0.0772		4	100.1292	0.1292
	5	100.0767	0.0767		5	100.1284	0.1284
	6	100.0761	0.0761		6	100.1276	0.1276
	7	100.0755	0.0755		7	100.1268	0.1268
	8	100.0750	0.0750		8	100.1260	0.1260
	9	100.0744	0.0744		9	100.1253	0.1253
	10	100.0739	0.0739		10	100.1245	0.1245
	total	1000.7638	0.0764		total	1001.2800	0.1280
	Reach	L_{comp} (m)	E_L (%)		Reach	L_{comp} (m)	E_L (%)
Channel 3	1	99.7180	-0.2820	Channel 5	1	99.9782	-0.0218
	2	99.7227	-0.2773		2	99.9785	-0.0215
	3	99.7272	-0.2728		3	99.9787	-0.0213
	4	99.7317	-0.2683		4	99.9790	-0.0210
	5	99.7361	-0.2639		5	99.9793	-0.0207
	total	498.6357	-0.2729		total	499.8937	-0.0213
	Reach	L_{comp} (m)	E_L (%)		Reach	L_{comp} (m)	E_L (%)
Channel 4	1	99.9495	-0.0505		7	99.9538	-0.0462
	2	99.9503	-0.0497		8	99.9545	-0.0455
	3	99.9510	-0.0490		9	99.9552	-0.0448
	4	99.9517	0.0483		10	99.9558	-0.0442
	5	99.9524	-0.0476		total	999.5274	-0.0473
	6	99.9531	-0.0469				
	Reach	L_{comp} (m)	E_L (%)		Reach	L_{comp} (m)	E_L (%)
Channel 6	1	99.9860	-0.0140	Channel 7	1	99.9919	-0.0081
	2	99.9863	-0.0137		2	99.9921	-0.0079
	3	99.9866	-0.0134		3	99.9922	-0.0078
	4	99.9869	-0.0131		4	99.9924	-0.0076
	5	99.9872	-0.0128		5	99.9925	-0.0075
	total	499.9330	-0.0134		total	499.9611	-0.0078
	Reach	L_{comp} (m)	E_L (%)		Reach	L_{comp} (m)	E_L (%)
Channel 8	1	99.9949	-0.0051	Channel 9	1	99.9965	-0.0035
	2	99.9950	-0.0050		2	99.9966	-0.0034
	3	99.9950	-0.0050		3	99.9967	-0.0033
	4	99.9952	-0.0048		4	99.9967	-0.0033
	5	99.9953	-0.0047		5	99.9968	-0.0032
	total	499.9757	-0.0049		total	499.9834	-0.0033

Table 8.4. Percent error for reach lengths of each channel for the series channel system using the Standard Step Method from the HEC-RAS model

	Reach	L_{comp} (m)	E_L (%)		Reach	L_{comp} (m)	E_L (%)
Channel 1	1	99.3443	-0.6557	Channel 2	1	100.2204	0.2204
	2	100.1540	0.1540		2	97.1280	-2.8720
	3	100.8679	0.8679		3	107.8098	7.8098
	4	100.0502	0.0502		4	97.8302	-2.1698
	5	99.2170	-0.7830		5	97.0715	-2.9285
	6	100.2164	0.2164		6	98.5534	-1.4466
	7	99.2865	-0.7135		7	97.7789	-2.2211
	8	101.0122	1.0122		8	101.4058	1.4058
	9	99.9564	-0.0436		9	102.7583	2.7583
	10	99.7462	-0.2538		10	99.7492	-0.2508
	total	999.8510	-0.0149		total	1000.3055	0.0306
	Reach	L_{comp} (m)	E_L (%)		Reach	L_{comp} (m)	E_L (%)
Channel 3	1	102.5458	2.5458	Channel 5	1	99.4831	-0.5169
	2	99.0523	-0.9477		2	99.6626	-0.3374
	3	99.0302	-0.9698		3	100.6170	0.6170
	4	101.2144	1.2144		4	99.6393	-0.3607
	5	98.9451	-1.0549		5	100.5954	0.5954
	total	500.7878	0.1576		total	499.9974	-0.0005
	Reach	L_{comp} (m)	E_L (%)		Reach	L_{comp} (m)	E_L (%)
Channel 4	1	100.6812	0.6812		7	99.6408	-0.3592
	2	99.1711	-0.8289		8	100.6099	0.6099
	3	101.1326	1.1326		9	99.6574	-0.3426
	4	99.1517	-0.8483		10	100.6253	0.6253
	5	99.6403	-0.3597		total	1000.9208	0.0921
	6	100.6106	0.6106				
	Reach	L_{comp} (m)	E_L (%)		Reach	L_{comp} (m)	E_L (%)
Channel 6	1	100.0651	0.0651	Channel 7	1	99.8942	-0.1058
	2	100.0660	0.0660		2	100.0180	0.0180
	3	99.6338	-0.3662		3	99.9364	-0.0636
	4	100.0845	0.0845		4	100.0642	0.0642
	5	100.1008	0.1008		5	99.9868	-0.0132
	total	499.9502	-0.0100		total	499.8995	-0.0201
	Reach	L_{comp} (m)	E_L (%)		Reach	L_{comp} (m)	E_L (%)
Channel 8	1	99.9702	-0.0298	Channel 9	1	100.0409	0.0409
	2	99.9401	-0.0599		2	100.0315	0.0315
	3	99.9108	-0.0892		3	100.0223	0.0223
	4	100.0849	0.0849		4	99.8125	-0.1875
	5	100.0571	0.0571		5	100.4063	0.4063
	total	499.9631	-0.0074		total	500.3136	0.0627

The series channel system shown in Figure 7.1 took 0.326 seconds in reaching a final solution using a laptop PC with a 2.4 Ghz processor for the BiCGSTAB numerical solver. In a similar manner, the same parallel channel system took 0.736 seconds in reaching a final solution using the same PC laptop for the GEM numerical solver. To reach the final solution the NRSM needed 3 iterations to converge to the specified tolerance. This number of iterations was the same for both numerical solvers, BiCGSTAB and GEM.

8.3 Results for Parallel Channel System

The results for the parallel channel system were compared using WSE profiles and the percent errors of the reach lengths in each channel and reach. Table 8.5 presents the computed WSE at each channel section in the parallel channel system using the SSM, while Table 8.6 presents the computed WSE for the HEC-RAS model (StdSM).

Table 8.5. Computed water surface elevation and water depth for each channel of the parallel channel system using the Simultaneous Solution Method.

	Section	Distance (m)	Depth (m)	WSE (m)		Section	Distance (m)	Depth (m)	WSE (m)
Channel 1	1	0	5.0000	104.8700	Channel 2	1	0	5.0135	104.8735
Q=250	2	50	5.0041	104.8691	Q=212.5	2	50	5.0177	104.8727
m^3/s	3	100	5.0083	104.8683	m^3/s	3	100	5.0220	104.8720
	Section	Distance (m)	Depth (m)	WSE (m)		Section	Distance (m)	Depth (m)	WSE (m)
Channel 3	1	0	5.0417	104.8917	Channel 4	1	0	5.1402	104.8902
Q=96.7202	2	50	5.0666	104.8916	Q=87.0482	2	50	5.1651	104.8901
m^3/s	3	100	5.0915	104.8915	m^3/s	3	100	5.1899	104.8899
	4	150	5.1163	104.8913					
	5	200	5.1412	104.8912					
	Section	Distance (m)	Depth (m)	WSE (m)		Section	Distance (m)	Depth (m)	WSE (m)
Channel 5	1	0	5.1850	104.8850	Channel 6	1	0	5.2386	104.8886
Q=86.0952	2	50	5.2098	104.8848	Q=75.7638	2	50	5.2633	104.8883
m^3/s	3	100	5.2346	104.8846	m^3/s	3	100	5.2881	104.8881
	Section	Distance (m)	Depth (m)	WSE (m)		Section	Distance (m)	Depth (m)	WSE (m)
Channel 7	1	0	5.0432	104.8932	Channel 8	1	0	5.1397	104.8897
Q=115.7798	2	40	5.0630	104.8930	Q=115.7798	2	50	5.1645	104.8895
m^3/s	3	80	5.0829	104.8929	m^3/s	3	100	5.1892	104.8892
	4	120	5.1028	104.8928		4	150	5.2140	104.8890
	5	160	5.1227	104.8927		5	200	5.2387	104.8887
	6	200	5.1425	104.8925					
	Section	Distance (m)	Depth (m)	WSE (m)		Section	Distance (m)	Depth (m)	WSE (m)
Channel 9	1	0	5.2385	104.8885	Channel 10	1	0	5.2244	104.8244
Q=103.0440	2	50	5.2633	104.8883	Q=178.8078	2	50	5.2266	104.8216
m^3/s	3	100	5.2880	104.8880	m^3/s	3	100	5.2287	104.8187

	Section	Distance (m)	Depth (m)	WSE (m)
	1	0	5.2531	104.8431
Channel 11	2	50	5.2561	104.8411
Q=162.7151 m^3/s	3	100	5.2592	104.8392

Table 8.6. Computed water surface elevation and water depth for each channel of the parallel channel system using the Standard Step Method (HEC-RAS model).

	Section	Distance (m)	Depth (m)	WSE (m)		Section	Distance (m)	Depth (m)	WSE (m)
Channel 1	1	0	5.0002	104.8704	Channel 2	1	0	5.0168	104.8769
Q=250	2	50	5.0045	104.8695	Q=201.3328	2	50	5.02128	104.8762
m^3/s	3	100	5.0086	104.8687	m^3/s	3	100	5.02546	104.8755
	Section	Distance (m)	Depth (m)	WSE (m)		Section	Distance (m)	Depth (m)	WSE (m)
Channel 3	1	0	5.0470	104.8970	Channel 4	1	0	5.1465	104.8966
Q=74.56563	2	50	5.0719	104.8969	Q=64.8649	2	50	5.1714	104.8965
m^3/s	3	100	5.0968	104.8969	m^3/s	3	100	5.1964	104.8965
	4	150	5.1217	104.8968					
	5	200	5.1466	104.8967					
	Section	Distance (m)	Depth (m)	WSE (m)		Section	Distance (m)	Depth (m)	WSE (m)
Channel 5	1	0	5.1934	104.8935	Channel 6	1	0	5.2462	104.8963
Q=64.86493	2	50	5.2183	104.8934	Q=54.11041	2	50	5.2711	104.8962
m^3/s	3	100	5.2432	104.8933	m^3/s	3	100	5.2959	104.8960
	Section	Distance (m)	Depth (m)	WSE (m)		Section	Distance (m)	Depth (m)	WSE (m)
Channel 7	1	0	5.0479	104.8979	Channel 8	1	0	5.1458	104.8959
Q=89.26721	2	40	5.0679	104.8978	Q=89.26721	2	50	5.1706	104.8957
m^3/s	3	80	5.0877	104.8978	m^3/s	3	100	5.1955	104.8956
	4	120	5.1077	104.8977		4	150	5.2203	104.8954
	5	160	5.1277	104.8976		5	200	5.2452	104.8953
	6	200	5.1475	104.8976					
	Section	Distance (m)	Depth (m)	WSE (m)		Section	Distance (m)	Depth (m)	WSE (m)
Channel 9	1	0	5.2457	104.8958	Channel 10	1	0	5.2807	104.8808
Q=76.05562	2	50	5.2706	104.8957	Q=96.47379	2	50	5.2851	104.8800
m^3/s	3	100	5.2954	104.8955	m^3/s	3	100	5.2891	104.8792

	Section	Distance (m)	Depth (m)	WSE (m)
Channel 11	1	0	5.2989	104.8889
Q=78.01916	2	50	5.3036	104.8885
m^3/s	3	100	5.3081	104.8881

Two WSE profiles should be plotted, one for the upper branch and another for the lower branch. These profiles are presented in Figure 8.4 and Figure 8.5, respectively. The continuous line represents the results obtained with SSM, while the dotted line refers to the results obtained

with HEC-RAS. The WSE from both methods have similar behavior but are slightly different in magnitude, particularly at the channel branch on the downstream end of the loop (Channel IDs: C10, and C11). Similar to the series channel system, the water surface increase at the locations of the lateral weirs and the WSE decrease at the junctions due to changes in geometry of the two channels and local energy losses, are observed.

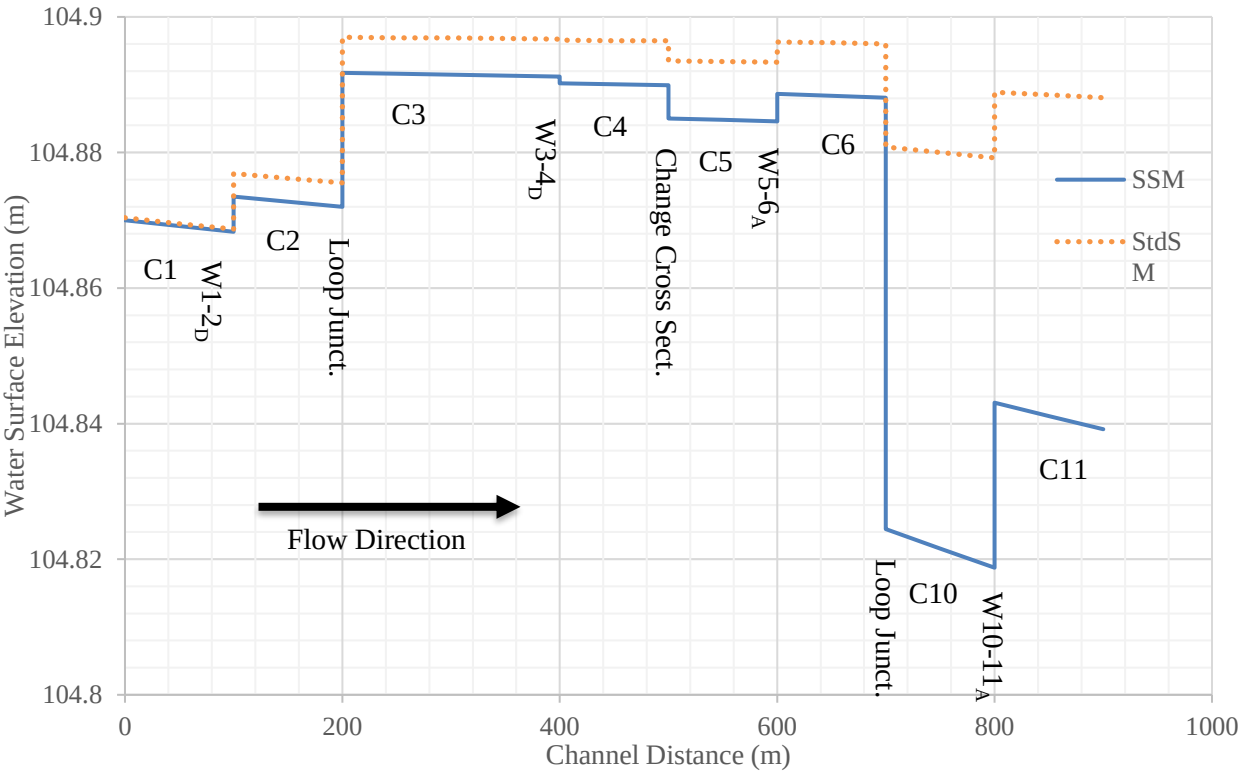

Figure 8.4. Water surface elevation profile at the upper branch of the parallel channel system.

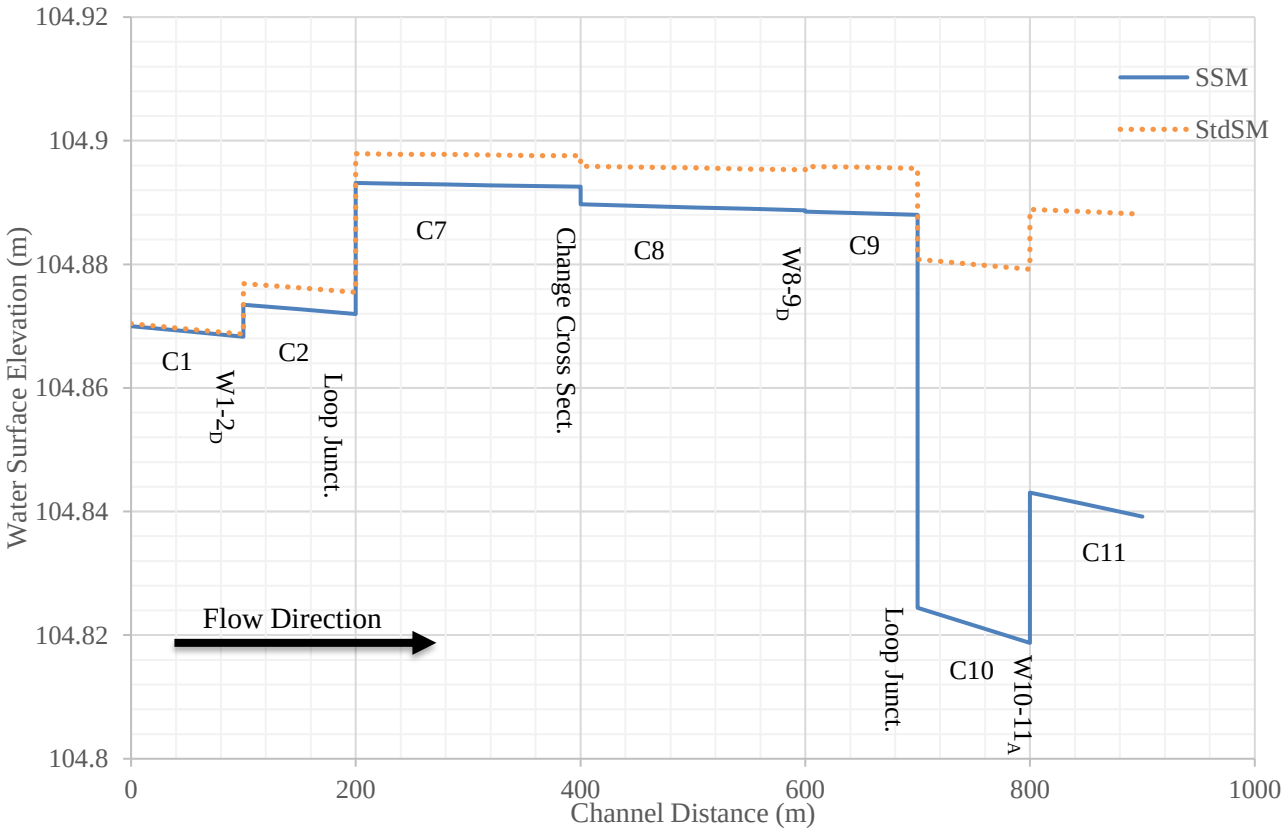

Figure 8.5. Water surface elevation profile at the lower branch of the parallel channel system.

The relative error in reach lengths obtained with this comparison is shown in Figure 8.6 for both models. This relative error in reach lengths was computed using Equation 8.1. The values of relative error for each reach and the entire channel for the SSM are presented in Table 8.7, while the values for the HEC-RAS model are illustrated in Table 8.8. The SSM had a significant lower percent error for each reach length than HEC-RAS (StdSM). SSM underestimated the reach length computed using the DSM for the water depth and discharge calculated (negative values on Figure 8.6). On the other hand, HEC-RAS model overestimated the reach length computed (positive values on Figure 8.6). The maximum percent error for the reach lengths for both models (SSM and StdSM) were found on the channels located before the upstream loop junction

(Channel ID: C1 and C2) and after the downstream loop junction (Channel ID: C10 and C11), which was 1.2% for HEC-RAS model at Channel C11 and 0.06% for the SSM at Channel C10. The difference between errors for each channel can be as much as three orders of magnitude and can be as small as one order of magnitude.

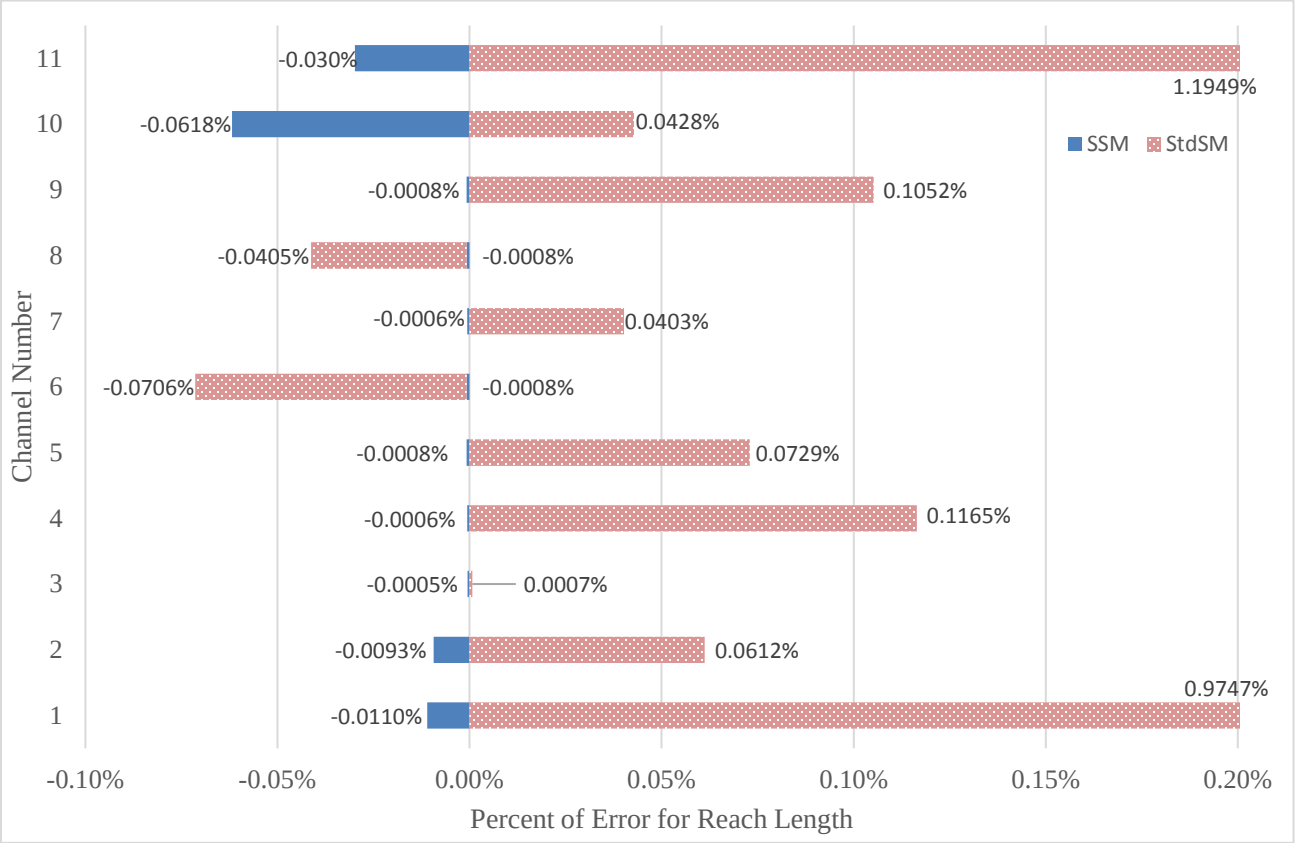

Figure 8.6. Percent error for the reach lengths of both methods for the parallel channel system.

Table 8.7. Percent error for the reach lengths of each channel for the parallel channel system using the Simultaneous Solution Method.

	Reach	L_{comp} (m)	E_L (%)		Reach	L_{comp} (m)	E_L (%)
	1	49.9945	-0.0110		1	49.9953	-0.9316
Channel 1	2	49.9945	-0.0110	Channel 2	2	49.9954	-0.9289
	total	99.9890	-0.0110		total	99.9907	-0.9303
	Reach	L_{comp} (m)	E_L (%)		Reach	L_{comp} (m)	E_L (%)
	1	49.9997	-0.0006		1	49.9997	-0.0006
	2	49.9997	-0.0005	Channel 4	2	49.9997	0.0006
Channel 3	3	49.9997	-0.0005		total	99.9994	-0.0006
	4	49.9997	-0.0005				
	total	199.9989	-0.0005				
	Reach	L_{comp} (m)	E_L (%)		Reach	L_{comp} (m)	E_L (%)
	1	49.9996	-0.0008		1	49.9996	-0.0008
Channel 5	2	49.9996	-0.0008	Channel 6	2	49.9996	0.0008
	total	99.9992	-0.0008		total	99.9992	-0.0008
	Reach	L_{comp} (m)	E_L (%)		Reach	L_{comp} (m)	E_L (%)
	1	39.9998	-0.0006		1	49.9996	-0.0008
	2	39.9998	-0.0006		2	49.9996	-0.0008
Channel 7	3	39.9998	-0.0006	Channel 8	3	49.9996	-0.0008
	4	39.9998	-0.0005		4	49.9996	-0.0008
	5	39.9998	-0.000543		total	199.9984	-0.0008
	total	199.9989	-0.0006				
	Reach	L_{comp} (m)	E_L (%)		Reach	L_{comp} (m)	E_L (%)
	1	49.9996	-0.0008		1	49.9690	-0.0619
Channel 9	2	49.9996	-0.0008	Channel 10	2	49.9691	-0.0617
	total	99.9992	-0.0008		total	99.9382	-0.0618

		Reach	L_{comp} (m)	E_L (%)
		1	49.9851	-0.0299
	Channel 11	2	49.9851	-0.0298
		total	99.9702	-0.0298

Table 8.8. Percent error for the reach lengths of each channel for the parallel channel system using the Standard Step Method from the HEC-RAS model.

	Reach	L_{comp} (m)	E_L (%)		Reach	L_{comp} (m)	E_L (%)
	1	51.8313	3.6625		1	51.7755	3.5510
Channel 1	2	49.1434	-1.7132	Channel 2	2	48.2857	-3.4285
	total	100.9747	0.9747		total	100.0612	0.0612
	Reach	L_{comp} (m)	E_L (%)		Reach	L_{comp} (m)	E_L (%)
	1	49.9498	-0.1004		1	49.9695	-0.0610
	2	50.1474	0.2947	Channel 4	2	50.1470	0.2940
Channel 3	3	49.9637	-0.0726		total	99.9907	0.1165
	4	49.9406	-0.1187				
	total	200.0015	0.0007				
	Reach	L_{comp} (m)	E_L (%)		Reach	L_{comp} (m)	E_L (%)
	1	50.0287	0.0574		1	50.0678	0.1356
Channel 5	2	50.04423	0.0885	Channel 6	2	49.8616	-0.2768
	total	100.0729	0.0729		total	99.9294	-0.0706
	Reach	L_{comp} (m)	E_L (%)		Reach	L_{comp} (m)	E_L (%)
	1	40.1730	0.4325		1	49.8969	-0.2062
	2	39.7894	-0.5266		2	50.0728	0.1455
Channel 7	3	40.1887	0.4718	Channel 8	3	49.8665	-0.2669
	4	40.1665	0.4163		4	50.0828	0.1656
	5	39.7630	-0.5926		total	199.9190	-0.0405
	total	200.0805	0.0403				
	Reach	L_{comp} (m)	E_L (%)		Reach	L_{comp} (m)	E_L (%)
	1	50.0503	0.1005		1	51.9269	3.8538
Channel 9	2	49.8445	-0.3109	Channel 10	2	48.1159	-3.7682
	total	99.8948	0.1052		total	100.0428	0.0428

	Reach	L_{comp} (m)	E_L (%)
	1	52.3538	4.7075
Channel 11	2	48.8412	-2.3177
	total	101.1949	1.1949

The parallel channel system shown in Figure 7.2 took 0.903 seconds in reaching a final solution using a laptop PC with a 2.4 Ghz processor for the BiCGSTAB numerical solver. In a similar manner, the same parallel channel system took 3.367 seconds in reaching a final solution using the same PC laptop for the GEM numerical solver. To reach the final solution, the NRSM

needed 14 iterations to converge to the specified tolerance. This number of iterations was the same for both numerical solvers, BiCGSTAB and GEM.

8.4 Results for Complex Channel Network System

The results presented for the complex channel network system using the SSM method are WSE profiles and percent errors of the reach lengths in each channel and reach. Table 8.9 presents the computed WSE at each channel section in the complex channel network system using the SSM.

Table 8.9. Computed water surface elevation and water depth for each channel of the complex channel network system using the Simultaneous Solution Method.

	Section	Distance (m)	Q (m^3/s)	Depth (m)	WSE (m)
Channel 1	1	0	400.00	7.0000	107.0000
	2	120	400.00	7.0097	106.9977
	3	240	400.00	7.0195	106.9955
	4	360	360.00	7.0382	107.0022
	5	480	360.00	7.0484	107.0004
	6	600	360.00	7.0586	106.9986

	Section	Distance (m)	Q (m^3/s)	Depth (m)	WSE (m)
Channel 2	1	0	144.40	7.0819	107.0219
	2	80	144.40	7.1217	107.0217
	3	160	117.40	7.1658	107.0258
	4	240	117.40	7.2057	107.0257
	5	320	117.40	7.2456	107.0256
	6	400	117.40	7.2854	107.0254

	Section	Distance (m)	Q (m^3/s)	Depth (m)	WSE (m)
Channel 3	1	0	215.60	7.0763	107.0163
	2	40	215.60	7.0961	107.0161
	3	80	215.60	7.1159	107.0159
	4	120	194.00	7.1392	107.0192
	5	160	194.00	7.1591	107.0191
	6	200	194.00	7.1790	107.0190

	Section	Distance (m)	Q (m^3/s)	Depth (m)	WSE (m)
Channel 4	1	0	45.86	7.1918	107.0318
	2	20	45.86	7.2018	107.0318
	3	40	45.86	7.2118	107.0318
	4	60	45.86	7.2218	107.0318
	5	80	45.86	7.2318	107.0318
	6	100	45.86	7.2417	107.0317

	Section	Distance (m)	Q (m^3/s)	Depth (m)	WSE (m)
Channel 5	1	0	50.71	7.2407	107.0307
	2	40	50.71	7.2607	107.0307
	3	80	50.71	7.2807	107.0307
	4	120	50.71	7.3006	107.0306
	5	160	50.71	7.3206	107.0306
	6	200	50.71	7.3406	107.0306

	Section	Distance (m)	Q (m^3/s)	Depth (m)	WSE (m)
Channel 6	1	0	-4.85	7.2434	107.0334
	2	20	-4.85	7.2534	107.0334
	3	40	-4.85	7.2634	107.0334
	4	60	-4.85	7.2734	107.0334
	5	80	-4.85	7.2834	107.0334
	6	100	-4.85	7.2934	107.0334

	Section	Distance (m)	Q (m^3/s)	Depth (m)	WSE (m)
Channel 7	1	0	112.55	7.2861	107.0261
	2	20	112.55	7.2961	107.0261
	3	40	95.65	7.3080	107.0280
	4	60	95.65	7.3180	107.0280
	5	80	95.65	7.3280	107.0280
	6	100	95.65	7.3380	107.0280

	Section	Distance (m)	Q (m^3/s)	Depth (m)	WSE (m)
Channel 8	1	0	146.36	7.3219	107.0119
	2	40	146.36	7.3417	107.0117
	3	80	146.36	7.3616	107.0116
	4	120	146.36	7.3814	107.0114
	5	160	122.23	7.4075	107.0175
	6	200	122.23	7.4274	107.0174

	Section	Distance (m)	Q (m^3/s)	Depth (m)	WSE (m)
Channel 9	1	0	148.14	7.1831	107.0231
	2	100	142.33	7.2336	107.0236
	3	200	142.33	7.2834	107.0234
	4	300	142.33	7.3332	107.0232
	5	400	135.68	7.3838	107.0238
	6	500	135.68	7.4337	107.0237

	Section	Distance (m)	Q (m^3/s)	Depth (m)	WSE (m)
Channel 10	1	0	257.91	7.4252	107.0152
	2	120	257.91	7.4364	107.0144
	3	240	216.64	7.4526	107.0186
	4	360	216.64	7.4641	107.0181
	5	480	216.64	7.4756	107.0176
	6	600	216.64	7.4870	107.0170

Two WSE profiles were plotted, one for the upper branch and another for the lower branch. These profiles are presented in Figure 8.7 and Figure 8.8, respectively. The continuous line shows the results obtained with SSM. Similar to the series and parallel channel systems, the water surface increased upstream from the locations of the lateral weirs. This behavior was observed on both WSE profiles and downstream from the location of the sluice gates. In addition, the WSE decreased at the junction between two channels due to changes in geometry of the two channels, and to local energy losses. Similar to the parallel channel system, the WSE increased downstream from the loop junction, in which three or more channels join in a single point.

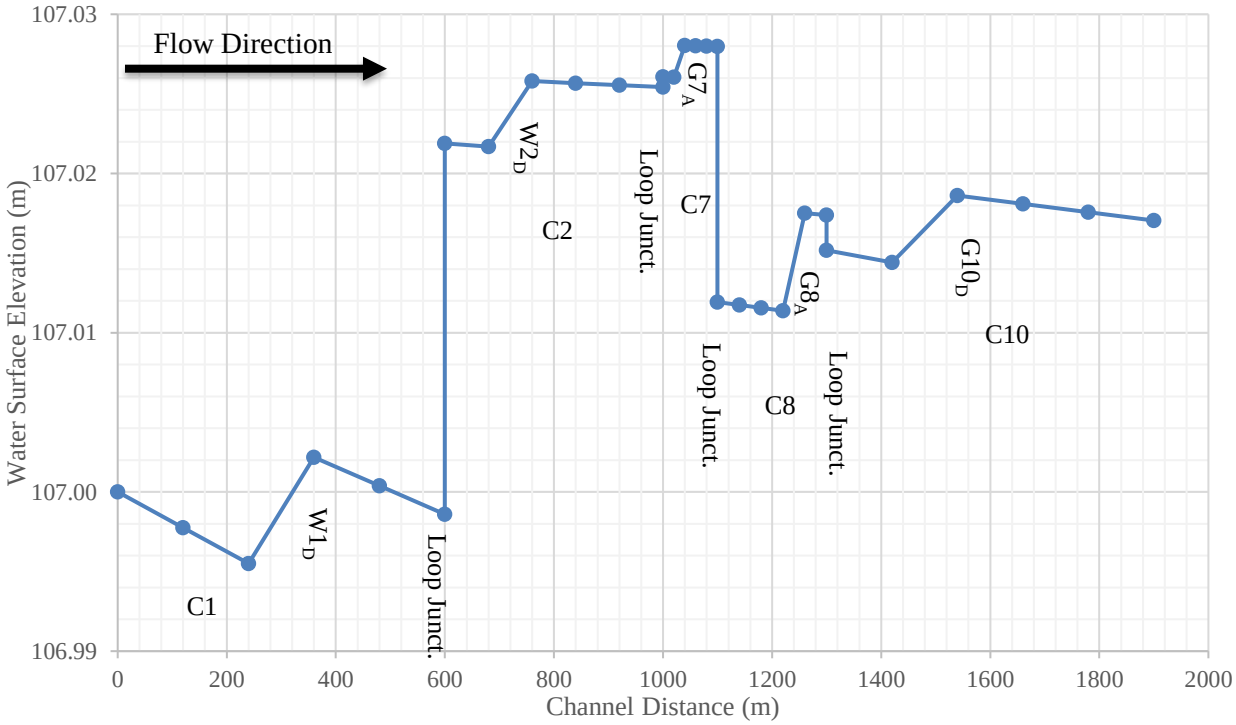

Figure 8.7. Water surface elevation profile at the upper branch of the complex channel network system.

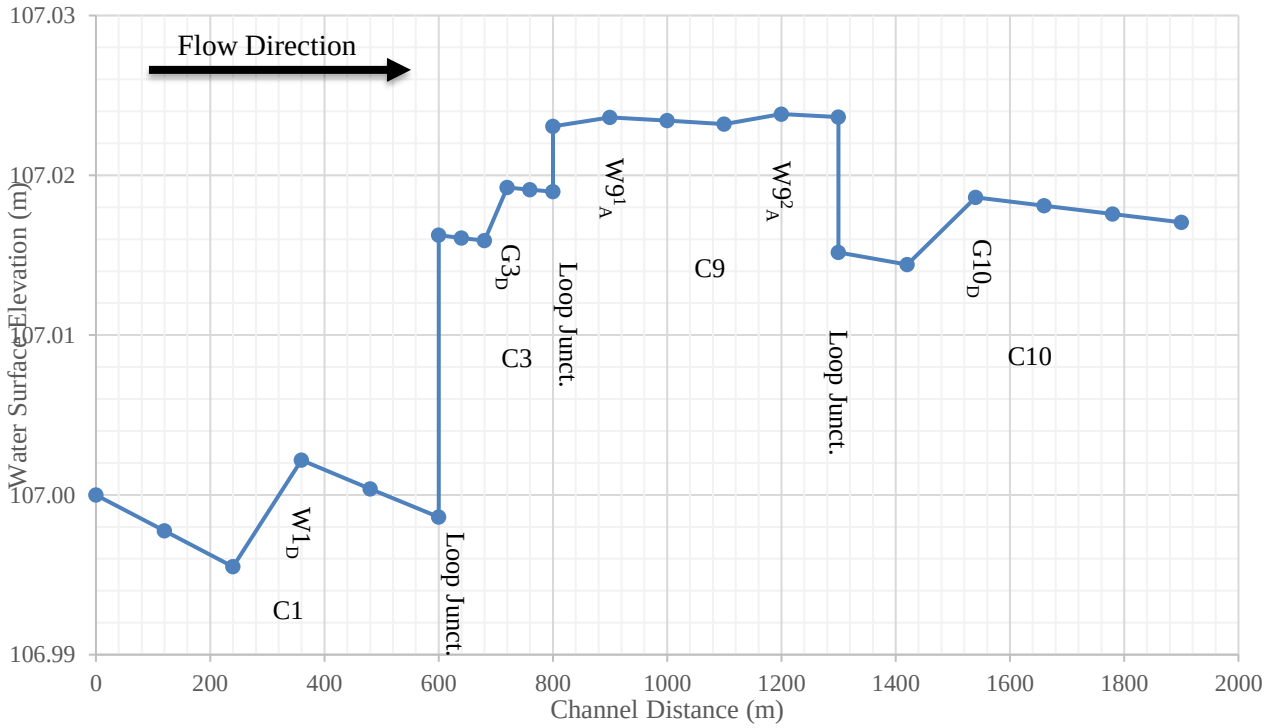

Figure 8.8. Water surface elevation profile at the lower branch of the complex channel network system.

The percent error in reach lengths obtained with this comparison is shown in Figure 8.9 for the SSM model. This relative error in reach lengths was computed using Equation 8.1. The values of relative error for each reach and the entire channel for the SSM are presented in Table 8.10. The SSM underestimated the reach length computed using the DSM for the water depth and discharge calculated (negative values on Figure 8.9). The two highest percent errors for the reach lengths was found on the first channel before the upstream loop junction (Channel ID: C1) and after the downstream loop junction (Channel ID: C10); which were -0.0126% and -0.0033%, respectively. This behavior is similar for the parallel channel system case study, in which the two maximum percent errors for the SSM occurred at the channels located upstream and downstream of the loop junction. On the other hand, the minimum percent error for the reach lengths occurred

at the channels that connects the upper and lower branch (Channel ID: C4 and C5), both with a value of -0.0001%.

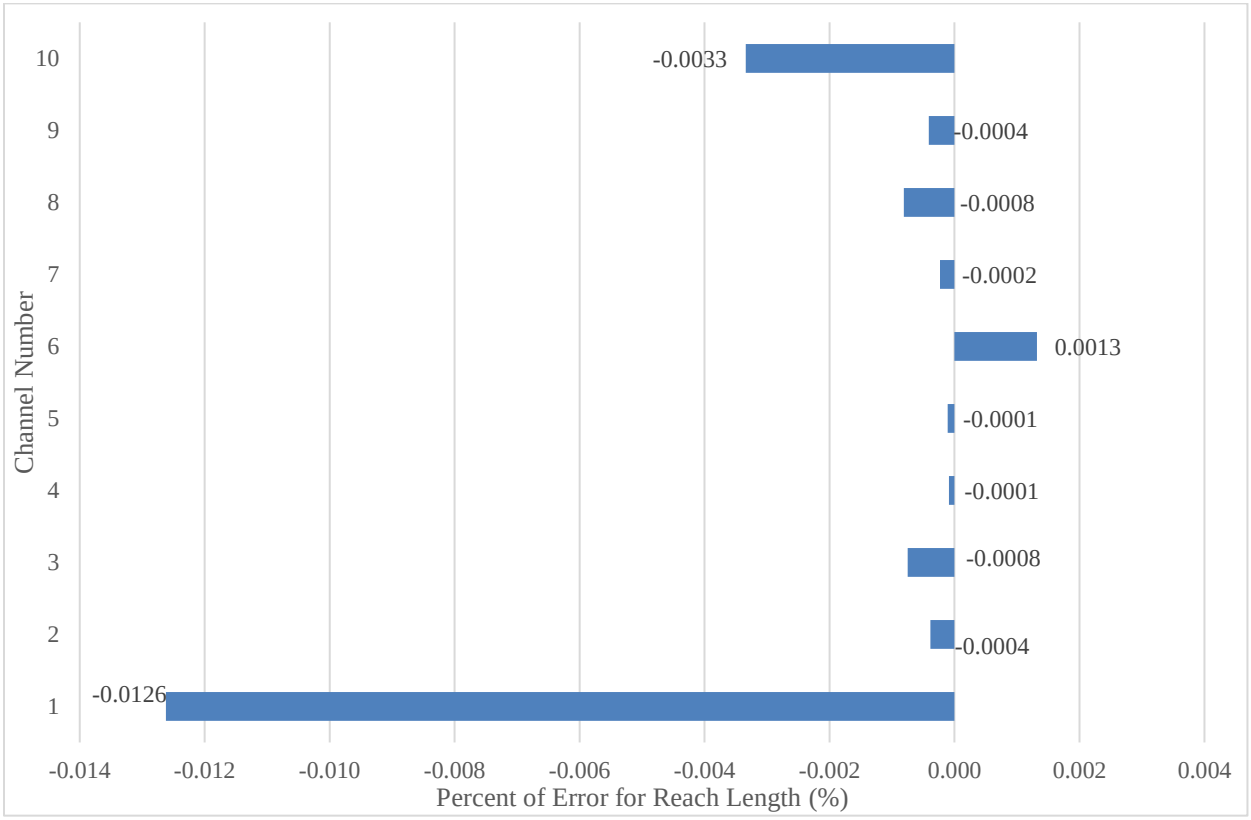

Figure 8.9. Percent error for each reach length of the Simultaneous Solution Method results for the complex channel network system.

Table 8.10. Percent error for the reach length of each channel for the complex channel network system using the Simultaneous Solution Method.

	Reach	L_{comp} (m)	E_L (%)		Reach	L_{comp} (m)	E_L (%)
Channel 1	1	119.9827	-0.0144	Channel 2	1	79.9996	-0.0005
	2	119.9828	-0.0143		2	79.9997	-0.0004
	3	119.9849	-0.0126		3	79.9997	-0.0003
	4	119.9869	-0.0109		4	79.9997	-0.0003
	5	119.9870	-0.0109		5	79.9997	-0.0003
	total	599.9243	-0.0126		total	399.9985	-0.0004
	Reach	L_{comp} (m)	E_L (%)		Reach	L_{comp} (m)	E_L (%)
Channel 3	1	39.9997	-0.0008	Channel 4	1	20.0000	-0.0001
	2	39.9997	-0.0008		2	20.0000	-0.0001
	3	39.9997	-0.0007		3	20.0000	-0.0001
	4	39.9997	-0.0007		4	20.0000	-0.0001
	5	39.9997	-0.0007		5	20.0000	-0.0001
	total	199.9985	-0.0008		total	99.9999	-0.0001
	Reach	L_{comp} (m)	E_L (%)		Reach	L_{comp} (m)	E_L (%)
Channel 5	1	40.0000	-0.0001	Channel 6	1	20.0003	0.0013
	2	40.0000	-0.0001		2	20.0003	0.0013
	3	40.0000	-0.0001		3	20.0003	0.0013
	4	40.0000	-0.0001		4	20.0003	0.0013
	5	40.0000	-0.0001		5	20.0003	0.0013
	total	199.9998	-0.0001		total	100.0013	0.0013
	Reach	L_{comp} (m)	E_L (%)		Reach	L_{comp} (m)	E_L (%)
Channel 7	1	19.9999	-0.0003	Channel 8	1	39.9996	-0.0009
	2	20.0000	-0.0002		2	39.9996	-0.0009
	3	20.0000	-0.0002		3	39.9996	-0.0009
	4	20.0000	-0.0002		4	39.9997	-0.0007
	5	20.0000	-0.0002		5	39.9998	-0.0006
	total	99.9998	-0.0002		total	199.9984	-0.0008
	Reach	L_{comp} (m)	E_L (%)		Reach	L_{comp} (m)	E_L (%)
Channel 9	1	99.9995	-0.0005	Channel 10	1	119.9948	-0.0043
	2	99.9996	-0.0004		2	119.9957	-0.0036
	3	99.9996	-0.0004		3	119.9965	-0.0029
	4	99.9996	-0.0004		4	119.9965	-0.0029
	5	99.9996	-0.0004		5	119.9965	-0.0029
	total	499.9980	-0.0004		total	599.9800	-0.0033

The complex channel network system shown in Figure 7.3 took 0.904 seconds in reaching a final solution using a laptop PC with a 2.4 Ghz processor for the BiCGSTAB numerical solver.

To reach a final solution, the NRSM needed 10 iterations to converge to the specified tolerance. The GEM numerical solver could not solve the nonlinear system of equations.

8.5 Results for Lajas Valley Irrigation District Channel System

The results for the LVIDS case study using the SSM method includes WSE profiles, percent error of the reach lengths in each channel and reach, and calibration results for water depth. Table 8.11 presents the computed WSE at each channel section in the LVIDS using the SSM.

Table 8.11. Computed water surface elevation and water depth for each channel of the numerical model of the Lajas Valley Irrigation District System case study using the Simultaneous Solution Method.

	Section	Distance (m)	Depth (m)	WSE (m)		Section	Distance (m)	Depth (m)	WSE (m)
Channel 1	1	0	0.6100	47.9350	Channel 2	1	0	0.3851	47.5921
Q= 0.329	2	11.22	0.6142	47.9313	Q= 0.2255	2	20.72	0.3869	47.5649
m^3/s	3	22.45	0.6185	47.9278	m^3/s	3	41.45	0.3890	47.5525
	4	33.67	0.6229	47.9243		4	62.17	0.3913	47.5403
	5	44.90	0.6274	47.9209		5	82.89	0.3940	47.5284
	6	56.12	0.6319	47.9177		6	103.61	0.3969	47.5168
	7	67.34	0.6366	47.9145		7	124.34	0.4001	47.5056
	8	78.57	0.6414	47.9114		8	145.06	0.4037	47.4947
	9	89.79	0.6463	47.9084		9	165.78	0.4077	47.4842
	10	101.02	0.6512	47.9055		10	186.50	0.4121	47.4740
	11	112.24	0.6562	47.9027		11	207.23	0.4169	47.4643
	12	123.46	0.6614	47.8999		12	227.95	0.4221	47.4550
	13	134.69	0.6666	47.8973		13	248.67	0.4277	47.4461
	14	145.91	0.6719	47.8947		14	269.39	0.4338	47.4377
	15	157.14	0.6772	47.8923		15	290.12	0.4403	47.4297
	16	168.36	0.6827	47.8898		16	310.84	0.4473	47.4222

WSE profiles were plotted for the entire main channel length, which was 479.20-m. This profile is presented in Figure 8.10. The continuous line represents the results obtained with SSM. At the junction, between the main channel and the lateral channel M-63, a decrease on the WSE occurred due to changes in geometry of the two channels, and to local energy losses. The increase in WSE due to a lateral weir cannot be appreciated at the profile, since it occurs at the same location of the junction. Therefore, the losses due to the change in channel geometry are greater than the increment due to a lateral weir. In addition, between the first two cross-sections of the channel downstream from the junction (Channel ID: C2), a stepper slope (i.e., one order of magnitude bigger) can be observed. This can be attributed to the inline weir that is located at the beginning of the channel.

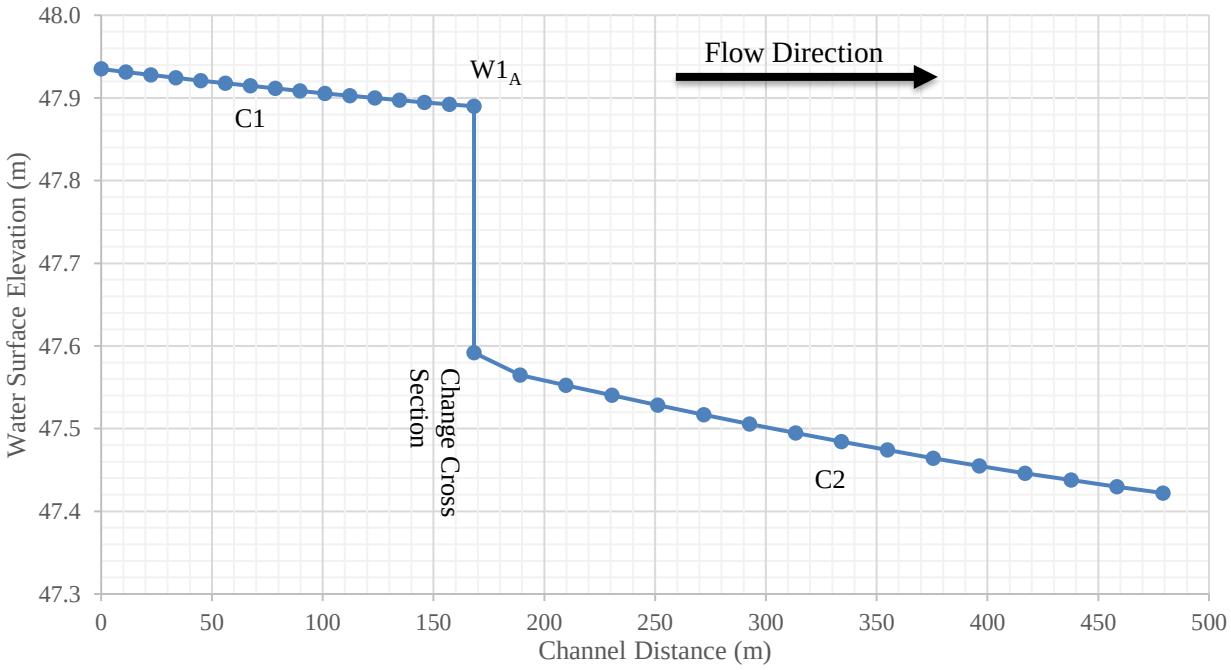

Figure 8.10. Water surface elevation profile of the Lajas Valley Irrigation District System case study using the Simultaneous Solution Method.

The values of relative error for each reach and the entire channel for the SSM are presented in Table 8.12. For this case study, the SSM model overestimated the reach length computed using the DSM for the water depth and discharge calculated (positive values on Table 8.12)The highest percent error for the reach lengths was found on the first upstream cross-section of each channel, in which the channel downstream from the junction had the greatest value (Channel ID: C2). This can be attributed to the fact that the inline weir was located just upstream this cross-section. As the distance along the channel increases, the percent error for reach length decreases. This was found at both channels. The minimum percent error for the reach lengths was found at the last cross-section of each channel, in which the channel upstream from the junction had the least value (Channel ID: C1). The percent errors for the reach lengths for the entire channel

downstream from the junction (Channel ID: C2) were at least 3 times greater than for the entire channel upstream from the junction (Channel ID: C1).

Table 8.12. Percent error for the reach lengths of each channel for the Lajas Valley Irrigation District System case study using the Simultaneous Solution Method.

	Reach	L_{comp} (m)	E_L (%)		Reach	L_{comp} (m)	E_L (%)
	1	11.2488	0.2213		1	21.1129	1.8829
	2	11.2481	0.2148		2	20.8880	0.7980
	3	11.2474	0.2084		3	20.8738	0.7295
	4	11.2467	0.2021		4	20.8613	0.6688
	5	11.2460	0.1961		5	20.8501	0.6149
	6	11.2453	0.1901		6	20.8401	0.5666
	7	11.2447	0.1843		7	20.8311	0.5231
Channel 1	8	11.2440	0.1786	Channel 2	8	20.8229	0.4837
	9	11.2434	0.1731		9	20.8155	0.4479
	10	11.2428	0.1677		10	20.8087	0.4152
	11	11.2422	0.1624		11	20.8025	0.3851
	12	11.2417	0.1573		12	20.7967	0.3573
	13	11.2411	0.1523		13	20.7914	0.3315
	14	11.2405	0.1474		14	20.7864	0.3076
	15	11.2400	0.1427		15	20.7818	0.2854
	total	168.6629	0.1799		total	312.6631	0.5865

The results for the calibration results for water depth at different locations for this case study are summarized in Table 8.13. This table presents the distance from the beginning of the channel to the location were the cross-section was obtained. The “Unadjusted SSM” column refers to the values obtained from the SSM using the initial estimates of the calibration parameters. In a similar manner, the “Adjusted SSM” column refers to the values obtained from the SSM using the best combination of calibration parameters that produced the lowest percent error for the selected water depth. Linear interpolation was used to obtain the water depth at specific locations. The percent error computed was based in Equation 8.1, but instead of L_{comp}, the unadjusted or adjusted water depth from the SSM was used, and instead of L_{given}, the field

surveyed water depth was used. The "Percent Decreased" column was computed as one minus the ratio between the percent error for the Adjusted SSM and the percent error for the Unadjusted SSM. A visualization of the calibration results is presented in the correlation diagram shown in Figure 8.11. The triangles represent the correlation between the field surveyed and the Unadjusted SSM water depths, while the red circles represent the correlation between the field surveyed and the Adjusted SSM water depths. The solid line represents a perfect correlation. The best combination of the calibration parameters that were used to compute the Adjusted SSM water depths were: an effective discharge coefficient for the inline weir of 3.14, and an equivalent Manning's roughness coefficient of 0.41. This represents a decrease of the initial estimates of the effective discharge coefficient and the equivalent Manning's roughness coefficient of 6.7% and 12.8%, respectively. These values are within the errors expected in field applications.

For both SSM water depths, there were three overestimated water depths and one underestimated water depth. The maximum percent error of overestimating at both SSM water depth occurred at almost 65 m from the beginning of the channel that is downstream from the junction (cross-section ID: MC-BD). As the distance from the beginning of the channel increased, the percent error for both SSM water depths decreased. Water depth at the surveyed cross-section closest to the inline weir at the channel downstream from the junction is underestimated by both SSM models (cross-section ID: MC-BU). As the calibration process decreased, the percent error for the overestimated water depths at cross-sections (cross-section ID: MC-BD, MC-CU, and MC-CD), as well as the percent of error for the underestimated water depths at cross-sections (cross-section ID: MC-BU) increased. The calibration process reduced the percent

error for the water depth, as much as 95% for the overestimated water depths, but it also increased the percent error for the underestimated water depth by almost 73%. This can be visualized when the circles on the correlation diagram (Figure 8.11) get closer to the perfect correlation line.

Table 8.13. Calibration results for water depth at different locations for the Lajas Valley Irrigation District System case study using the Simultaneous Solution Method.

		Water depth (m)			Percent of Error (%)		
Cross Section ID	Distance (m)	Field Surveyed	Unadjusted SSM	Adjusted SSM	Unadjusted SSM	Adjusted SSM	Percent Decreased (%)*
MC-BU	40.73	0.4572	0.4177	0.3889	-8.6253	-14.9270	-73.1
MC-BD	64.76	0.3810	0.4202	0.3917	10.3026	2.8053	72.8
MC-CU	230.83	0.4191	0.4481	0.4229	6.9229	0.9006	87.0
MC-CD	266.90	0.4318	0.4572	0.4330	5.8803	0.2938	95.0

* A positive value represents a percent of decreased and a negative value a percent of increased with respect of the Unadjusted value of percent of error.

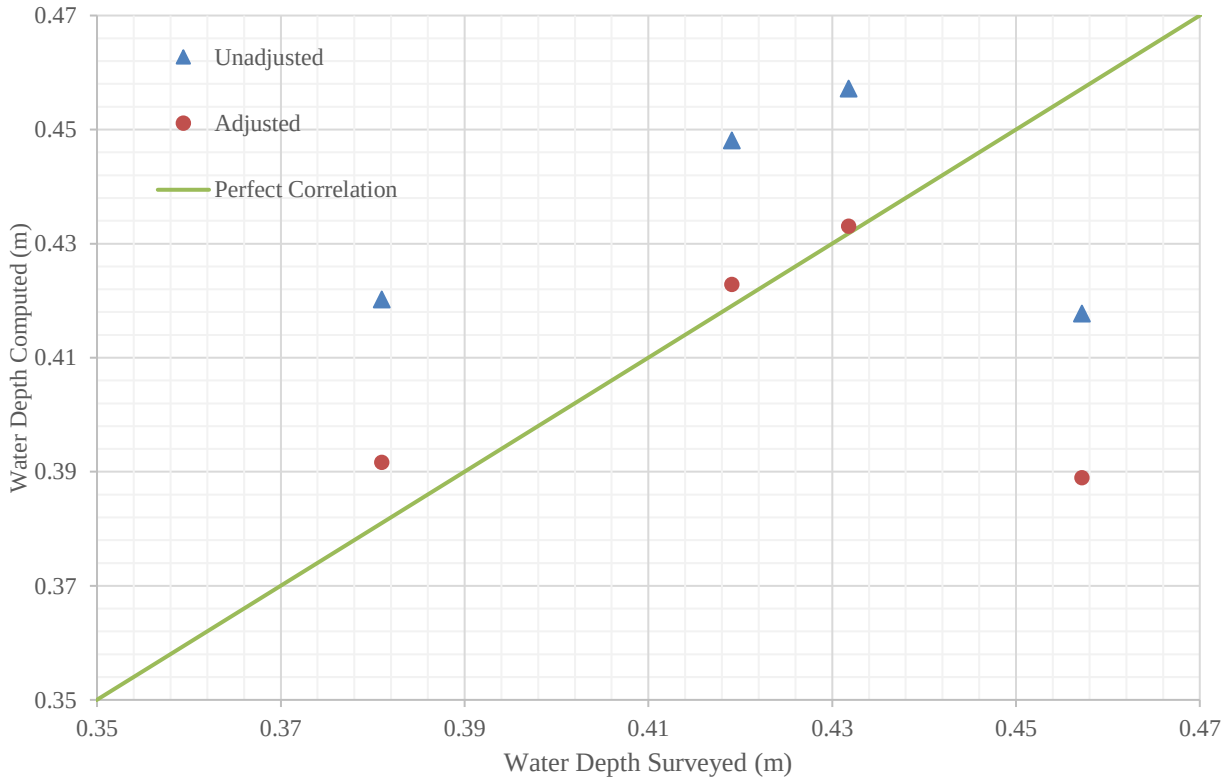

Figure 8.11. Correlation diagram of the calibration results for water depth at different channel locations for the Lajas Valley Irrigation District System case study using the Simultaneous Solution Method.

The numerical model of the LVIDS series channel system shown in Figure 7.4 took 0.211 seconds in reaching a final solution using a laptop PC with a 2.4 Ghz processor for the BiCGSTAB numerical solver. In a similar manner, the same numerical model took 0.186 seconds in reaching a final solution using the same PC laptop for the GEM numerical solver. To reach the final solution, the NRSM needed 5 iterations to converge to the specified tolerance. This number of iterations was the same for both numerical solvers, BiCGSTAB and GEM.

9 CHAPTER – CONCLUSIONS

The proposed algorithm, Simultaneous Solution Method (SSM), proved to be excellent for determining water depths, flow velocity and diverted lateral flow through weirs, sluice gates and inverted siphons in complex channel systems. The percent error computed for the reach length of the SSM where smaller than the ones obtained from the StdSM. This was observed at the series and parallel channel system case studies. In addition, the proposed algorithm was capable of analyzing and designing different hydraulic structures within a channel system, such as lateral weirs, sluice gates and inverted siphons. Water surface profiles followed the theoretical behavior and assumptions established on the literature on all the modeled cases, especially downstream from a lateral weir or a sluice gate, and when a change in channel cross-section occurred. The SSM underestimated the reach length computed using the DSM for the water depth and discharge calculated. The HEC-RAS model overestimated the reach length computed. In systems with loop channels, the maximum percent error for the reach length was found on the channels upstream from the upstream loop junction and downstream from the downstream loop junction. In channels that have inline weirs, the greatest percent of error for the reach length occurred downstream the inline weir. In general, as the distance along the channel increased, the percent error for the reach length decreased. Therefore, it can be established that the distance along the channel is inversely proportional to the percent error for the reach length. The calibration process conducted at the LVIDS case study demonstrates that the percent error for water depth can decrease dramatically after calibration.

The BiCGSTAB solved the numerical system faster than the GEM and converged successfully in all the examples, with exception of the LVIDS case study. But for both numerical solvers used (BiCGSTAB and GEM), the NRSM converged to a solution in the same amount of iterations for a specified tolerance of convergence. The series channel system converged with the least number of iterations, namely 3s. On the other hand, the model that converged with the highest amount of iterations was the parallel channel system with a total of 14 iterations.

The model can be widely applied for series, looped and branched channels networks in irrigation channels with different hydraulic structures. Many of these applications are beyond the capability of the well-known software HEC-RAS. The iterative GUI provides easy input parameters and visualization of the results. The SSM is comparatively easier to use, understand, learn and to setup than other available models for solving series, looped and network channel systems.

REFERENCES

Ankum, P. (2002). "Design of Open-Channel and Hydraulic Structures." TU Delft.

Babaoğlu, B. (2003). "Application of BiConjugate Gradient Stabilized Method with Spectral Acceleration for Propagation over Terrain Profiles." M.S. Thesis, Bilkent University, Ankara, Turkey.

Burden, R. L., and Faires, J. D. (2005). *Numerical Analysis*, 8th Ed., Thomson Brooks/Cole.

Brunner, G.W. (2016). "HEC-RAS River Analysis System Hydraulic Reference Manual, Ver. 5.0." U.S. Army Corps of Engineers, Vicksburg, MS.

Chaudhry, H. M. (2008). *Open-Channel Flow*, 2nd Ed., Springer Science, New York, NY, 150-197.

Chaudhry, M. H., and Schulte, A. M. (1986). "Computation of steady-state, gradually varied flow in parallel channels." Can. J. Civil Eng., 13(1), 39-45.

Chaudhry, M. H., and Schulte, A. M. (1987). "Gradually-varied flows in open-channel network." J. Hydraul. Res., 25(3), 357-371.

Chow, V. T. (1959). "Development of Uniform Flow and its Formulas." *Open Channel Hydraulics*, 1st Ed., McGraw-Hill Book Company, New York, NY.

Dalrymple, T., and Benson, M. A. (1967). "Measurements of Peak Discharge by the Slope-Area Method." Techniques of Water-Resources Investigation 3-A2, U. S. Geological Survey, U. S. Department of Interior, Denver, CO.

Das, B. M., and Sobhan, K. (2014). "Origin of Soil and Grain Size." *Principle of Geotechnical Engineering*, 8th Ed., Cengage Learning, Stamford, CT.

Gerald, C. F., and Wheatley, P. O. (1992). "Solving Sets of Equations." *Applied Numerical Analysis*, 4th Ed., Addison-Wesley Publishing Company, New York, NY.

Gupta, R. S. (2008). "Conveyance Systems: Open Channel Flow." *Hydrology and Hydraulic Systems*, 3th Ed., Waveland Press, Inc., Long Grove, IL.

Hager, W. H. (1986). "Lateral Outflow Over Side Weirs." J. Hydraul. Eng, 113.

Hoffman, J. D. (2001). “Systems of Linear Algebraic Equations.” *Numerical Methods for Engineers and Scientist*, 2nd Ed., Marcel Dekker, Inc., New York, NY>

Houghtalen, R. J., Osman, A., and Hwang, N. H. (2013). “Water Flow in Open Channels.” *Fundamentals of Hydraulic Engineering Systems*, 4th Ed., Person Education, Inc.

Islam, A., Raghuwanshi, N. S., Singh, R., and Sen, D. J. (2005). “Comparison of Gradually Varied Flow Computation Algorithms for Open-Channel Network.” J. Irrig. Drain. E., 10.1061/(ASCE)0733-9437(2005)131:5(457).

Islam, A., Raghuwanshi, N. S., and Singh, R. (2008). “Development and Application of Hydraulic Simulation Model for Irrigation Canal Networks.” J. Irrig. Drain. E., 10.1061/(ASCE)0733-943(2008)134:1(49).

Irrigation Museum. (2015). “Irrigation Timeline.” <http://www.irrigationmuseum.org/exhibit2.aspx> (Mar. 22, 2016).

May, R. W. P., Bromwich, B. C., Gasowski, Y., and Rickard, C. E. (2003). “Design Considerations.” *Hydraulic Design of Side Weirs*, 1st Ed., Thomas Telford Publishing, Reston, VA, 15-23.

Michael, A. M. (2008). “Utilization of Water Resources and Irrigation Development.” *Irrigation: Theory and Principles*, 2nd Ed., Vikas Publishing House, Jangpura, India.

Moler, C. (2004). “The Origins of MATLAB.” Technical Articles and Newsletters, MathWorks. < https://www.mathworks.com/company/newsletters/articles/the-origins-of-matlab.html> (Oct. 26, 2017).

Naidu, B. J., Bhallamudi, S. M., and Narasimhan, S. (1997). “GVF Computation in Tree-type Channel Networks.” J. Hydraul. Eng., 0733-9429/97/0008·0700-0708.

Puerto Rico Department of Natural Resources (PRDNR). (2008). “Plan Integral de Aguas de Puerto Rico.” <http://www.recursosaguapuertorico.com/Cuencas-Principales-en-PR.html> (March 22, 2016).

Reddy, H. P., and Bhallamudi, S. M. (2004). “Gradually Varied Flow Computations in Cyclic Looped Channel Networks.” J. Irrig. Drain. E., 10.1061/(ASCE)0733-9437(2004)130:5(424).

Saad, Y. (2003). “Krylov Subspace Methods part II.” *Iterative Methods for Sparse Linear System*, 2nd Ed., SIAM, Philadelphia, PA, 229-258.

Sen, D. J., and Garg, N. K. (2002). “Efficient Algorithm for Gradually Varied Flows in Channel Networks.”, J. Irrig. Drain. E., 10.1061/(ASCE)0733-9437(2002)128:6(351).

Silva-Araya, W.F., and Vargas, V. M. (2014). “Computer Design of Lateral Weirs System for Irrigation on Vegetative Strips.” World Conference on Computers in Agriculture and Natural Resources, San Jose, Costa Rica.

Swamee, P.K. (1992). “Sluice-Gate Discharge Equations.” J. Irrig. Drain. E., 118, 56-60.

United Nations Sustainable Development (1992). “Agenda 21.” *United Nations Conference on Environmental and Development*, Rio de Janeiro, Brazil.

U. S. Bureau of Reclamation (USBR). (2001). “Weirs.” *Water Measurement Manual*, 3rd Ed., U.S. Government Printing Office, Washington, DC, 7.1-7.30.

Utah Department of Transportation (UDT) (2004). “Manual of Instruction: Roadway Drainage.” <https://www.udot.utah.gov/main/f?p=100:pg:0:::1:T,V:826> (July 10, 2016).

Water Resources of Puerto Rico (WRPR) (2017). “Distritos de Riego Valle de Lajas.” <https://m.recursosaguapuertorico.com/?url=http://www%2Erecursosaguapuertorico%2Ecom%2Fdistritos%2Driego%2Ehtml#2764> (Oct. 12, 2017).

Yuvashankar, V., Nejad, M. S., and Lui, A. (2016). “Understanding the Bi-Conjugate Gradient Stabilized Method (Bi-CGSTAB).” <https://static1.squarespace.com/static/55ade5ebe4b0d3eba632821b/t/576ebb166a4963e8802f5d67/1466874648553/Yuvashankar_Nejad_Liu.pdf> (Sept. 10, 2017).

Zhu, D., Chen, Y., Wang, Z., and Liu, Z. (2011). “Simple, Robust, and Efficient Algorithm for Gradually Varied Subcritical Flow Simulation in General Channel Networks.” J. Hydraul. Eng., 10.1061/(ASCE)HY .1943-7900.0000356.

APPENDIX 1

Jacobian Matrix for the parallel channel system proposed as a case study

The following notation is used on the Jacobian matrix for the first case study:

- Y_{ups} and Q_{ups} = are the upstream boundary condition equation for the water depth and the discharge at the first section of the first channel, respectively (Equation 3.6).
- *dE/ dy i,j* = first derivative of the energy equation with respect to the water depth on the reach *j* from channel *i* (Equation 3.4).
- *dE/ dQ i,j* = first derivative of the energy equation with respect to the discharge on the reach *j* from channel *i* (Equation 3.4).
- *dC/ dQ i,j* = first derivative of the continuity equation with respect to the discharge on the reach *j* from channel *i* (Equation 3.5).
- The first number next to the derivative term (*i*) is the channel number. The second number (j) refers to the reach number on the channel of the first number. For example, *dE/ dQ 2,3* refers to the first derivative of the energy equation with respect to the discharge on the third reach from the second channel.
- The derivative terms in color red represents the boundary conditions at the upstream joint of the loop (enclosed by a solid red rectangle). The derivative terms in color green represents the boundary conditions at the downstream joint of the loop (enclosed by a dashed green rectangle).

row/column	1	2	3	4	5	6	7	8	9	10	11	12	13	14	15	16	17	18	19	20	21	22	23	24	25	26
1	Yupst 1,1																									
2		Qupst 1,1																								
3	dE/dY 1,1	dE/dQ 1,1	dE/dY 1,2	dE/dQ 1,2																						
4		dC/dQ 1,1		dC/dQ 1,2																						
5			dE/dY 1,2	dE/dQ 1,2	dE/dY 1,3	dE/dQ 1,3																				
6				dC/dQ 1,2		dC/dQ 1,3																				
7					dE/dY 1,3	dE/dQ 1,3	dE/dY 1,4	dE/dQ 1,4																		
8						dC/dQ 1,3		dC/dQ 1,4																		
9							dE/dY 1,4	dE/dQ 1,4	dE/dY 1,5	dE/dQ 1,5																
10								dC/dQ 1,4		dC/dQ 1,5																
11									dE/dY 1,5	dE/dQ 1,5	dE/dY 1,6	dE/dQ 1,6														
12										dC/dQ 1,5		dC/dQ 1,6														
13												dC/dQ 1,6	dC/dQ 2,1	dC/dQ 3,1												
14											dE/dY 1,6	dE/dQ 1,6	dE/dQ 2,1		dE/dY 2,1											
15											dE/dY 1,6	dE/dQ 1,6		dE/dQ 3,1		dE/dY 3,1										
16													dE/dQ 2,1		dE/dY 2,1		dE/dY 2,2	dE/dQ 2,2								
17														dE/dQ 3,1		dE/dY 3,1			dE/dY 3,2	dE/dQ 3,2						
18													dC/dQ 2,1					dC/dQ 2,2								
19														dC/dQ 3,1						dC/dQ 3,2						
20																	dE/dY 2,2	dE/dQ 2,2			dE/dY 2,3	dE/dQ 2,3				
21																			dE/dY 3,2	dE/dQ 3,2			dE/dY 3,3	dE/dQ 3,3		
22																		dC/dQ 2,2				dC/dQ 2,3				
23																				dC/dQ 3,2				dC/dQ 3,3		
24																					dE/dY 2,3	dE/dQ 2,3			dE/dY 2,4	dE/dQ 2,4
25																							dE/dY 3,3	dE/dQ 3,3		
26																						dC/dQ 2,3				dC/dQ 2,4
27																								dC/dQ 3,3		
28																									dE/dY 2,4	dE/dQ 2,4
29																										
30																										dC/dQ 2,4
31																										
32																										

row/column	27	28	29	30	31	32	33	34	35	36	37	38	39	40	41	42	43	44	45	46	47	48	49	50	51	52	53
1																											
2																											
3																											
4																											
5																											
6																											
7																											
8																											
9																											
10																											
11																											
12																											
13																											
14																											
15																											
16																											
17																											
18																											
19																											
20																											
21																											
22																											
23																											
24																											
25	dE/dY 3,4	dE/dQ 3,4																									
26																											
27		dC/dQ 3,4																									
28			dE/dY 2,5	dE/dQ 2,5																							
29	dE/dY 3,4	dE/dQ 3,4			dE/dY 3,5	dE/dQ 3,5																					
30				dC/dQ 2,5																							
31		dC/dQ 3,4				dC/dQ 3,5																					
32			dE/dY 2,5	dE/dQ 2,5			dE/dY	dE/dQ 2,6																			
33					dE/dY 3,5	dE/dQ 3,5			dE/dY 3,6	dE/dQ 3,6																	
34				dC/dQ 2,5				dC/dQ 2,6																			
35						dC/dQ 3,5				dC/dQ 3,6																	
36							dE/dY	dE/dQ 2,6			dE/dY 2,7	dE/dQ 2,7															
37									dE/dY 3,6	dE/dQ 3,6			dE/dY 3,7	dE/dQ 3,7													
38								dC/dQ 2,6				dC/dQ 2,7															
39										dC/dQ 3,6				dC/dQ 3,7													
40											dE/dY 2,7	dE/dQ 2,7			dE/dY 2,8	dE/dQ 2,8											
41													dE/dY 3,7	dE/dQ 3,7			dE/dY 3,8	dE/dQ 3,8									
42												dC/dQ 2,7				dC/dQ 2,8											
43														dC/dQ 3,7				dC/dQ 3,8									
44															dE/dY 2,8	dE/dQ 2,8			dE/dY 2,9	dE/dQ 2,9							
45																	dE/dY 3,8	dE/dQ 3,8			dE/dY 3,9	dE/dQ 3,9					
46																dC/dQ 2,8				dC/dQ 2,9							
47																		dC/dQ 3,8				dC/dQ 3,9					
48																			dE/dY 2,9	dE/dQ 2,9			dE/dY 2,10	dE/dQ 2,10			
49																					dE/dY 3,9	dE/dQ 3,9			dE/dY 3,10	dE/dQ 3,10	
50																				dC/dQ 2,9				dC/dQ 2,10			
51																						dC/dQ 3,9				dC/dQ 3,10	
52																							dE/dY 2,10	dE/dQ 2,10			dE/dY 2,11
53																									dE/dY 3,10	dE/dQ 3,10	
54																								dC/dQ 2,10			
55																										dC/dQ 3,10	
56																											dE/dY 2,11
57																											
58																											
59																											
60																											
61																											
62																											
63																											
64																											
65																											

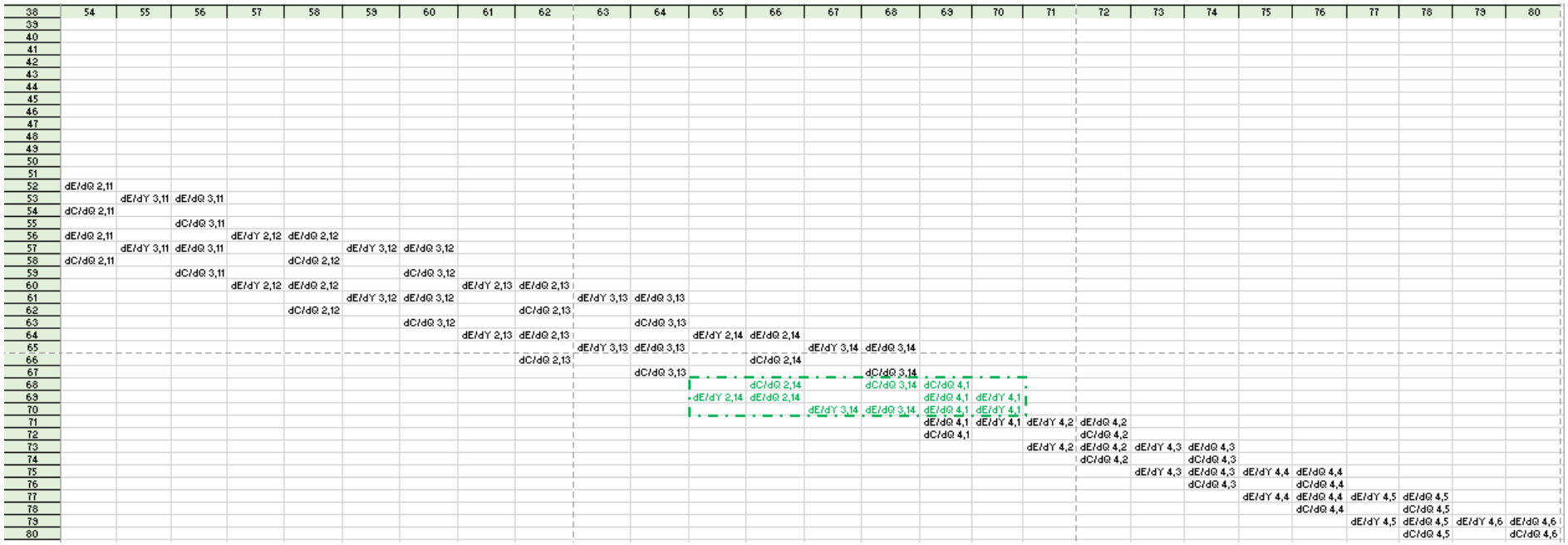
38 54 55 56 57 58 59 60 61 62 63 64 65 66 67 68 69 70 71 72 73 74 75 76 77 78 79 80
52 dE/dQ 2,11
53 dE/dY 3,11 dE/dQ 3,11
54 dC/dQ 2,11
55 dC/dQ 3,11
56 dE/dQ 2,11 dE/dY 2,12 dE/dQ 2,12
57 dE/dY 3,11 dE/dQ 3,11 dE/dY 3,12 dE/dQ 3,12
58 dC/dQ 2,11 dC/dQ 2,12
59 dC/dQ 3,11 dC/dQ 3,12
60 dE/dY 2,12 dE/dQ 2,12 dE/dY 2,13 dE/dQ 2,13
61 dE/dY 3,12 dE/dQ 3,12 dE/dY 3,13 dE/dQ 3,13
62 dC/dQ 2,12 dC/dQ 2,13
63 dC/dQ 3,12 dC/dQ 3,13
64 dE/dY 2,13 dE/dQ 2,13 dE/dY 2,14 dE/dQ 2,14
65 dE/dY 3,13 dE/dQ 3,13 dE/dY 3,14 dE/dQ 3,14
66 dC/dQ 2,13 dC/dQ 2,14
67 dC/dQ 3,13 dC/dQ 3,14
68 dC/dQ 2,14 dC/dQ 3,14 dC/dQ 4,1
69 dE/dY 2,14 dE/dQ 2,14 dE/dQ 4,1 dE/dY 4,1
70 dE/dY 3,14 dE/dQ 3,14 dE/dQ 4,1 dE/dY 4,1
71 dE/dQ 4,1 dE/dY 4,1 dE/dY 4,2 dE/dQ 4,2
72 dC/dQ 4,1 dC/dQ 4,2
73 dE/dY 4,2 dE/dQ 4,2 dE/dY 4,3 dE/dQ 4,3
74 dC/dQ 4,2 dC/dQ 4,3
75 dE/dY 4,3 dE/dQ 4,3 dE/dY 4,4 dE/dQ 4,4
76 dC/dQ 4,3 dC/dQ 4,4
77 dE/dY 4,4 dE/dQ 4,4 dE/dY 4,5 dE/dQ 4,5
78 dC/dQ 4,4 dC/dQ 4,5
79 dE/dY 4,5 dE/dQ 4,5 dE/dY 4,6 dE/dQ 4,6
80 dC/dQ 4,5 dC/dQ 4,6